Supporting information

Synthesis and Properties of Quinoidal (Di-)Anionic Coupled Polymethine-Oxonol Dyes and Their Aromatic Counterparts

Benjamin Mourot,[a,‡] Carmelo Naim,[b,‡] Olivier Siri,[a] Denis Jacquemin*[,b,c] and Simon Pascal*[,a,b]

[a] *Aix Marseille Univ, CNRS UMR 7325, Centre Interdisciplinaire de Nanoscience de Marseille (CINaM), Campus de Luminy, case 913, Marseille cedex 09 13288, France*

[b] *Nantes Université, CEISAM UMR 6230, CNRS, Nantes F-44000, France*

[c] *Institut Universitaire de France (IUF), Paris F-75005, France*

TABLE OF CONTENT

I. GENERAL REMARKS AND ANALYSIS CONDITIONS

Reagents and solvents. All reagents and solvents were purchased from Merck and were used as received. 4,6-Dihydroxy-5-methylisophthalaldehyde (**4**) was synthesized using a published procedure.[1] When heating was required, oil bathes were used. Column chromatography was performed on silica gel 60 (230–400 mesh). Optical properties were recorded in spectrophotometric grade solvents.

Analytical methods and apparatus. Melting points (M.P.) were measured in open capillary tubes with a STUART SMP30 melting points apparatus and are uncorrected. NMR spectra were recorded with a Jeol 400 MHz NMR. NMR chemical shifts are given in ppm (δ) relative to Me_4Si with solvent resonances used as internal standards ($CDCl_3$: 7.26 ppm for ^1H and 77.2 for ^{13}C; DMSO-d_6: 2.50 ppm for ^1H and 39.5 for ^{13}C). NMR peak assignments were confirmed using COSY, DEPT-135, HMQC and HMBC methods. The following abbreviations are used for multiplicity of NMR signals: s = singlet, d = doublet, t = triplet, q = quadruplet, m = multiplet, br = broad signal, app = apparent multiplicity. FTIR spectra were recorded on an Agilent Cary 630 FTIR equipped with an attenuated total reflectance (ATR) sampling. UV-Vis-NIR absorption spectra were recorded on a Cary 50 Scan UV-Visible-NIR spectrophotometer at room temperature with a 300 nm/min scan rate. HRMS analyses were performed on a QStar Elite (Applied Biosystems SCIEX) or a SYNAPT G2 HDMS (Waters) spectrometers by the “Spectropole” of the Aix-Marseille University. These two instruments are equipped with an ESI or MALDI source and a TOF mass analyzer.

Fluorescence. Emission spectra were measured using a Horiba-Jobin Yvon Fluorolog-3 spectrofluorometer equipped with a three-slit double-grating excitation and a spectrograph emission monochromator with dispersions of 2.1 nm mm^{-1} (1200 grooves per mm). A 450 W xenon continuous wave lamp provided excitation. The luminescence of diluted solutions was detected at right angle using 10 mm quartz cuvettes. Fluorescence at 77 K was measured with the same apparatus, using a quartz Dewar flask filled with liquid nitrogen. Fluorescence quantum yields Φ were measured in diluted dichloromethane solution with an optical density lower than 0.1 using the following equation (eq. 1):

$$\frac{\Phi_x}{\Phi_r} = \left(\frac{A_r(\lambda)}{A_x(\lambda)}\right)\left(\frac{n_x^2}{n_r^2}\right)\left(\frac{D_x}{D_r}\right) \quad (eq.1)$$

where A is the absorbance at the excitation wavelength (λ), n the refractive index and D the integrated intensity. The letters “r” and “x” stand for reference and sample. The fluorescence quantum yields of the chromophores **1–3** were measured relative to Anthracene (Φ = 28% in EtOH), Coumarin 153 (Φ = 38% in EtOH) or Cresyl Violet (Φ = 56% in EtOH), respectively.[2]

Short luminescence decay was monitored using a Horiba DeltaFlex modular fluorescence lifetime system equipped with a TC-SPC. Excitation was performed using a DeltaDiode (Model: DD-440L; peak wavelength: 438 nm) and Ludox in distilled water was used to determine the instrumental response

function used for deconvolution, which was performed using the EzTime software. All the measurements were fitted with single exponential decays.

Theoretical calculations. DFT and TD-DFT calculations were performed using Gaussian 16[3] with the M06-2X exchange-correlation functional.[4] Initial conformational analysis employed the 6-31G(d) atomic basis set to identify the most stable isomers and tautomers. Structures with Gibbs free energy differences smaller than 2 kcal mol^{-1} relative to the most stable structure were retained for further study. The geometries of these selected structures were re-optimized and using the larger 6-311G(d,p) atomic basis set, confirming them as true minima through frequency calculations. Excitation energies and oscillator strengths were then computed with the 6-311+G(2d,p) atomic basis set and the same functional. Some of the standard settings of Gaussian were tuned for improving the accuracy: SCF convergence was set to 10^{-10} a.u., geometry optimizations used the "tight" option, and the "superfine" (for energy) and "ultrafine" (for derivatives) integration grids were chosen. Solvent effects were modeled using the PCM approach[5] choosing DMSO as solvent; geometry optimizations used equilibrium solvation with the LR aporoach, while vertical excitations have been determined in in the non-equilibrium limit using the cLR² protocol,[6] that accounts for both state-specific and linear-response solvation effects. The electronic density difference (EDD) plots were computed as the difference between the excited- and ground-state electronic densities obtained at TD-DFT and DFT levels, respectively, and visualized using the Chemcraft software.[7] For neutral and anionic species, CC2 corrections[8,9] were applied to TD-DFT vertical excitation energies by calculating the gas-phase excitation energy difference between the two methods using the DFT geometries. However, for the dianionic structures, it was not possible to reliably establish the correspondence between the excited states determined at CC2 and TD-DFT levels due to the highly diffuse nature of the electronic density and the significant mixing of the electronic states in these systems. CC2 calculations were performed using the aug-cc-pVDZ atomic basis set along with the corresponding auxiliary basis set in the Turbomole software,[10] applying the frozen-core approximation. The Nuclear-Independent Chemical Shift (NICS)[11,12] was evaluated at B3LYP/6-311+G(2d,p) in the center of the core ring to estimate the aromatic character of each molecule. The activation free energies (ΔG‡) for the single and double excited-state proton transfer processes in molecule 1b•2H were estimated by locating the corresponding transition state tautomers using the standard algorithms implemented in Gaussian. Vibrationally resolved absorption and emission spectra were simulated using FCClasses3[13] with the Vertical Hessian (VH) vibronic model under the Franck–Condon approximation, neglecting Herzberg–Teller effects.[14] Geometries, gradients, and Hessians were obtained at the (TD-)DFT level, and excitation energies were refined using the combined cLR² and CC2 protocol (or simply the cLR^2 when CC2 energies were not available). A Gaussian broadening of 0.10 eV was applied to all spectra. For absorption spectra, the first two, three or four more relevant excited states — depending on the molecule — were included to ensure an accurate representation of the experimental spectral features.

II. SYNTHETICS PROTOCOLS AND CHARACTERIZATION

2-(3-cyano-4,5,5-trimethylfuran-2(5*H*)-ylidene) malononitrile (5)

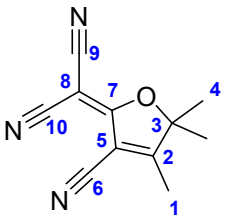

This procedure was adapted from the literature.[15] Magnesium turnings (412.0 mg, 17.0 mmol, 1.13 equiv.) were added to 15 mL of absolute ethanol. Then, 3-hydroxy-3-methylbutan-2-one (1.53 g, 15 mmol, 1.0 equiv.) and malononitrile (3 g, 45 mmol, 3.0 equiv.) were added to the mixture and the resulting solution was stirred at 60 °C for 8 hours. Then, the mixture was concentrated under reduced pressure, acidified with HCl (6 M, aqueous), the resulting precipitate was collected by filtration and then recrystallized with ethanol (about 125 mL for 3.0 g of crude product) to yield **5** as a yellow powder (1.8145 g, 9.11 mmol, 61%).

R*f* = 0.31 (SiO_2, pure CH_2Cl_2). **M. P.:** 197 – 199 °C. **^{1}H NMR (400 MHz, $CDCl_3$):** δ (ppm) = 2.36 (s, 3H, *H*-1), 1.62 (s, 6H, *H*-4). **^{13}C{^{1}H} NMR (101 MHz, $CDCl_3$):** δ (ppm) = 182.6 (*C*-7), 175.3 (*C*-2), 111.1 (*C*-10 or *C*-9), 110.5 (*C*-10 or *C*-9), 109.1 (*C*-6), 104.9 (*C*-3), 99.9 (*C*-5), 58.7 (*C*-8), 24.5 (*C*-4), 14.3 (*C*-1). **IR (neat):** ν (cm^{-1}) = 3750, 3650, 2996, 2876, 2835, 2313, 2223, 1612, 1560, 1426, 1389, 1362, 1318, 1211, 1155, 1106, 1080, 1030, 1002, 957, 934, 900, 858, 788, 749, 726, 659.

5-(benzo[*d*]thiazol-2-yl)-2,4-dihydroxy-3-methylbenzaldehyde (1a)

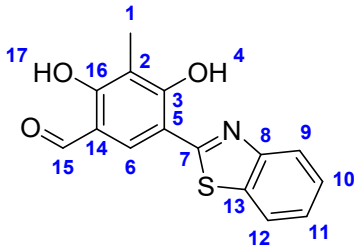

A solution of 4,6-dihydroxy-5-methylisophthalaldehyde **4** (23.7 mg, 0.132 mmol, 1.0 equiv.) and 2-aminothiophenol (16.5 mg, 0.132 mmol, 1.0 equiv.) in 200 µL of absolute EtOH was stirred at room temperature overnight. The resulting precipitate was collected by filtration and washed with petroleum ether to afford **1a** as a pale-yellow powder (26.2 mg, 91.83 µmol, 70% yield).

R*f* = 0.39 (SiO_2, CH_2Cl_2:acetone, 98:2). **M. P.:** 208 – 210 °C. **^{1}H NMR (400 MHz, $CDCl_3$):** δ (ppm) = 11.86 (s, 1H, *H*-17), 9.74 (s, 1H, *H*-15), 8.57 (s, 1H, *H*-4), 7.66 (dd, $^3J_{9,10}$ = 7.5 Hz, $^4J_{9,11}$ = 1.7 Hz, 1H, *H*-9), 7.51 (s, 1H, *H*-6), 7.27 (m, 1H, *H*-10), 8.05 (d, $^3J_{9,10}$ = 8.3 Hz, 2H, *H*-9), 7.21 (dt, $^3J_{11,10}$ = 7.6 Hz, $^3J_{11,12}$ = 7.3 Hz, $^4J_{11,9}$ = 1.5 Hz, 1H, *H*-11), 7.15 (dd, $^3J_{12,11}$ = 7.6 Hz, $^4J_{12;10}$ = 1.3 Hz, 1H, *H*-12), 2.19 (s, 3H, *H*-1). **^{13}C{^{1}H} NMR (101 MHz, $CDCl_3$):** δ (ppm) = 194.2 (*C*-15), 166.6 (*C*-7), 164.3 (*C*-16 or *C*-3), 161.3 (*C*-16 or *C*-3), 146.0 (*C*-8), 138.1 (*C*-6), 131.7 (*C*-13), 128.1 (*C*-12), 128.0 (*C*-11 or *C*-10), 127.9 (*C*-11 or *C*-10), 117.8 (*C*-14), 114.8 (*C*-5), 113.3 (*C*-2), 7.2 (*C*-1). **IR (neat):** ν (cm^{-1}) = 2922, 2851, 1625, 1596, 1565, 1469, 1440, 1361, 1307, 1267, 1209, 1160, 1053, 1017, 973, 859, 750, 722, 680, 541, 497. **HRMS (ESI-TOF):** calculated for $[M-H]^-$ ($C_{15}H_{10}NO_3S^-$) 284.0387, found 284.0388.

4,6-bis(benzo[d]thiazol-2-yl)-2-methylbenzene-1,3-diol (1b)

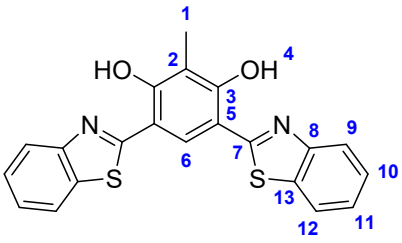

A solution of 4,6-dihydroxy-5-methylisophthalaldehyde **4** (21.7 mg, 0.120 mmol, 1.0 equiv.) and 2-aminothiophenol (31.7 mg, 0.253 mmol, 2.1 equiv.) in 200 µL of DMSO was heated to reflux for 30 minutes. It was then cooled down to room temperature, diluted with H_2O and the resulting precipitate was collected by filtration and dried with Et_2O to afford **1b** as a white powder (38.3 mg, 98.09 µmol, 81% yield).

R*f* = 0.97 (SiO_2, CH_2Cl_2:acetone, 99:1). **M. P.:** 305 – 306 °C. **^{1}H NMR (400 MHz, $CDCl_3$):** δ (ppm) = 7.95 (d, $^3J_{12,11}$ = 7.8 Hz, 2H, *H*-12), 7.91 (d, $^3J_{9,10}$ = 7.9 Hz, 2H, *H*-9), 7.90 (s, 1H, *H*-6), 7.51 (t, $^3J_{10,9}$ = 8.0 Hz, $^3J_{10,11}$ = 7.3 Hz, 2H, *H*-10), 7.41 (t, $^3J_{11,12}$ = 7.8 Hz, $^3J_{11;10}$ = 7.3 Hz, 2H, *H*-11), 2.34 (s, 3H, *H*-1). **^{13}C{^{1}H} NMR (101 MHz, $CDCl_3$):** δ (ppm) = 169.1 (*C*-7), 160.1 (*C*-3), 151.8 (*C*-8), 132.3 (*C*-13), 126.9 (*C*-10), 126.4 (*C*-6), 125.5 (*C*-11), 122.0 (*C*-12), 121.6 (*C*-9), 113.5 (*C*-2), 110.2 (*C*-5), 8.32 (*C*-1). **IR (neat):** ν (cm^{-1}) = 3049, 1931, 1899, 1620, 1525, 1502, 1476, 1461, 1431, 1380, 1367, 1328, 1315, 1270, 1247, 1227, 1192, 1161, 1131, 1090, 1051, 929, 903, 884, 854, 785, 746, 718. **HRMS (ESI-TOF):** calculated for $[M\text{-}H]^-$ ($C_{21}H_{13}N_2O_2S_2^-$) 389.0424, found 389.0424.

5-((1,3-dioxo-1,3-dihydro-2H-inden-2-ylidene)methyl)-2,4-dihydroxy-3-methylbenzaldehyde (2a)

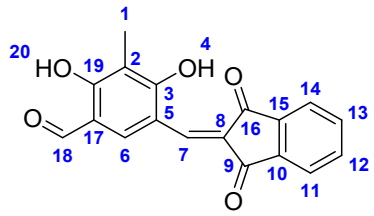

To a solution of 4,6-dihydroxy-5-methylisophthalaldehyde **4** (100.0 mg, 5.551 mmol, 1.0 equiv.) and 1,3-indandione (170.4 mg, 1.166 mmol, 2.1 equiv.) in 10 mL of EtOH was added two drops of pyridine (11.9 mg, 0.15 mmol) and the mixture was heated to reflux for 3 hours. It was then allowed to stir at room temperature for 12 hours. The resulting precipitate was collected by filtration and washed with *n*-pentane to afford **2a** as a pale-yellow powder (93.6 mg, 0.304 mmol, 53%).

R*f* = 0.14 (SiO_2, pure CH_2Cl_2:acetone, 98:2). **M. P.:** 252 – 254 °C (decomp.). **^{1}H NMR (400 MHz, DMSO-*d*$_6$):** δ (ppm) = 11.9 (bs, 1H, *H*-4, exchangeable with D_2O), 9.88 (s, 1H, *H*-18), 9.37 (s, 1H, *H*-7), 8.26 (s, 1H, *H*-6), 8.00 – 7.90 (m, 4H, *H*-14, *H*-13, *H*-12 and *H*-11), 2.10 (s, 3H, *H*-1). **^{13}C{^{1}H} NMR (101 MHz, DMSO-*d*$_6$):** δ (ppm) = 195.4 (*C*-18), 189.9 (*C*-16 or *C*-9), 189.0 (*C*-16 or *C*-9), 164.6 (*C*-19 or *C*-3), 164.4 (*C*-19 or *C*-3), 141.6 (*C*-8), 139.8 (*C*-7), 139.3 (*C*-5), 138.8 (*C*-6), 135.8 (*C*-13 or *C*-12), 135.6 (*C*-13 or *C*-12), 126.2 (*C*-17), 122.9 (*C*-14 or *C*-11), 122.9 (*C*-14 or *C*-11), 114.8 (*C*-15 or *C*-10), 114.7 (*C*-15 or *C*-10), 111.5 (*C*-2), 8.2 (*C*-1). **IR (neat):** ν (cm^{-1}) = 3314, 3294, 3048, 2855, 2320, 2148, 2001, 1707, 1658, 1569, 1451, 1369, 1316, 1228, 1173, 1146, 1053, 1005, 958, 907, 852, 772, 731, 607, 567, 528, 495, 414. **HRMS (ESI-TOF):** calculated for $[M\text{-}H]^-$ ($C_{18}H_{11}O_5^-$) 307.0612, found 307.0613.

2,2'-((4,6-dihydroxy-5-methyl-1,3-phenylene)bis(methaneylylidene))bis(1H-indene-1,3(2H)-dione) (2b)

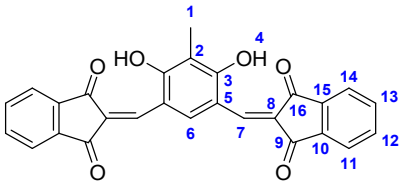

A solution of 4,6-dihydroxy-5-methylisophthalaldehyde **4** (53.9 mg, 299.2 µmol, 1.0 equiv.) and 1,3-indandione (91.8 mg, 628.3 µmol, 2.1 equiv.) in 1 mL of 2,6-lutidine was heated to 95 °C overnight. It was then cooled down to room temperature, diluted with H_2O and the resulting precipitate was collected by filtration to afford **2b** as a brown powder (36.6 mg, 83.89 µmol, 28%).

M. P.: 239 – 241 °C (decomp.). **^{1}H NMR (400 MHz, DMSO-d_6):** δ (ppm) = 9.89 (s, 1H, *H*-4), 8.27 (s, 2H, *H*-7), 9.37 (s, 1H, *H*-7), 7.98–7.88 (m, 9H, *H*-14, *H*-13, *H*-12, *H*-11 and *H*-6), 2.14 (s, 3H, *H*-1). **^{13}C{^{1}H} NMR (101 MHz, DMSO-d_6):** δ (ppm) = 190.6 (*C*-16 or *C*-9), 188.7 (*C*-16 or *C*-9), 164.7 (*C*-3), 142.1 (*C*-15 or *C*-10), 141.8 (*C*-7), 139.8 (*C*-15 or *C*-10), 138.7 (*C*-6), 136.1 (*C*-13 or *C*-12), 135.9 (*C*-13 or *C*-12), 125.89 (*C*-8), 123.4 (*C*-14 or *C*-11), 123.2 (*C*-14 or *C*-11), 115.1 (*C*-5), 112.4 (*C*-2), 10.2 (*C*-1). **IR (neat):** ν (cm^{-1}) = 3317, 3064, 2115, 1767, 1714, 1671, 1593, 1557, 1534, 1443, 1395, 1377, 1352, 1282, 1245, 1194, 1156, 1091, 1032, 1006, 964, 887, 852, 758, 730, 692. **HRMS (ESI-TOF):** calculated for $[M-H]^-$ ($C_{27}H_{15}O_6^-$) 435.0874, found 438.0874.

(E)-2-(3-cyano-4-(5-formyl-2,4-dihydroxy-3-methylstyryl)-5,5-dimethylfuran-2(5H)-ylidene)malononitrile (3a)

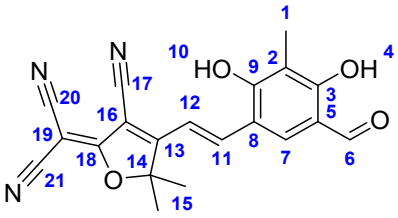

Protocol 1: To a solution of 4,6-dihydroxy-5-methylisophthalaldehyde **4** (9.4 mg, 52.18 µmol, 1.0 equiv.) and **5** (10.39 mg, 52.18 µmol, 1.0 equiv.) in 1.5 mL of absolute EtOH was added a catalytic amount of piperazine and the mixture was allowed to stir at room temperature overnight. It was then diluted with 1,2-dimethoxyethane and *n*-pentane and the resulting precipitate was collected by filtration and washed with EtOH to afford **3a** as a red powder (6.2 mg, 17.16 µmol, 33%).

Protocol 2: To a solution of 4,6-dihydroxy-5-methylisophthalaldehyde **4** (58.4 mg, 3.242 mmol, 1.0 equiv.) and **5** (135.6 mg, 6.807 mmol, 2.1 equiv.) in 5 mL of absolute EtOH was added two drops of pyridine (11.9 mg, 0.15 mmol) and the resulting mixture was heated to reflux overnight. The solution was then cooled down to room temperature, diluted with Et_2O and filtered. The filtrate was evaporated under reduced pressure and the residue was triturated in Et_2O and *n*-pentane and filtered again. The solid was washed with EtOH to remove the excess of **5**, which left **3a** as a red powder (76.9 mg, 212.8 µmol, 66%).

Protocol 3: To a solution of 4,6-dihydroxy-5-methylisophthalaldehyde **4** (57.1 mg, 3.169 mmol, 1.0 equiv.) and **5** (132.6 mg, 6.656 mmol, 2.1 equiv.) in 5 mL of anhydrous MeOH was added two drops of pyridine (11.9 mg, 0.15 mmol) and the resulting mixture was heated to reflux over the week-end. The solution was then cooled down to room temperature, diluted with *n*-pentane and filtered. The resulting

precipitate was further purified by silical gel column chromatography (CH_2Cl_2:MeOH 9:1 as eluent) to afford **3a** as a red powder (95.8 mg, 265.1 µmol, 84%).

R*f* = 0.34 (SiO_2, CH_2Cl_2:MeOH, 98:2). **M. P.:** 323 – 325 °C. **^{1}H NMR (400 MHz, DMSO-*d*$_6$):** δ (ppm) = 11.81 (bs, 1H, *H*-10), 9.85 (s, 1H, *H*-6), 8.32 (s, 1H, *H*-7), 8.22 (d, $^3J_{11,12}$ = 16.6 Hz, 1H, *H*-11), 7.32 (d, $^3J_{12,11}$ = 16.6 Hz, 1H, *H*-12), 2.10 (s, 3H, *H*-1), 1.73 (s, 6H, *H*-15). **^{13}C{^{1}H} NMR (101 MHz, DMSO-*d*$_6$):** δ (ppm) = 195.4 (*C*-6), 177.5 (*C*-18), 176.3 (*C*-13), 163.5 (*C*-9 or *C*-3), 162.9 (*C*-9 or *C*-3), 143.4 (*C*-12), 135.1 (*C*-7), 116.8 (*C*-17), 116.4 (*C*-8), 115.6 (*C*-5), 113.8 (*C*-11), 113.0 (*C*-16), 112.2 (*C*-2), 112.0 (*C*-21 or *C*-20), 111.5 (*C*-21 or *C*-20), 99.2 (*C*-14), (*C*-19), 95.2 (*C*-24), 53.6 (*C*-19), 25.3 (*C*-15), 8.2 (*C*-1). **IR (neat):** ν (cm^{-1}) = 3428, 2235, 2218, 1648, 1568, 1524, 1308, 1217, 1168, 1107, 1013, 977, 915, 873, 810, 778, 718, 679. **HRMS (ESI-TOF):** calculated for $[M-H]^-$ ($C_{20}H_{14}N_3O_4^-$) 360.0990, found 360.0996.

2,6-dimethylpyridin-1-ium 4,6-bis((E)-2-(4-cyano-5-(dicyanomethylene)-2,2-dimethyl-2,5-dihydrofuran-3-yl)vinyl)-2-methylbenzene-1,3-bis(olate) (3b)

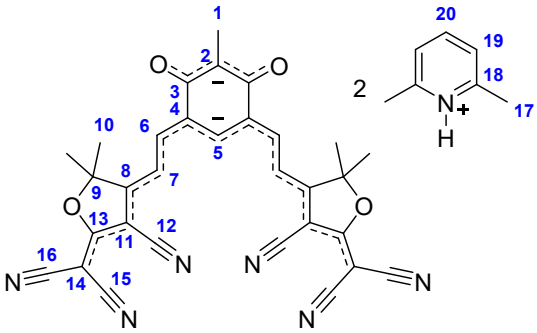

A solution of 4,6-dihydroxy-5-methylisophthalaldehyde **4** (51.3 mg, 284.7 µmol, 1.0 equiv.) and **5** (141.8 mg, 711.9 µmol, 2.5 equiv.) in 4 mL of 2,6-lutidine was stirred at 95 °C overnight. It was then cooled down to room temperature, diluted with Et_2O and the resulting precipitate was collected by filtration to afford **3b** as a black powder (121.4 mg, 160.4 µmol, 56%).

M. P.: > 400 °C. **^{1}H NMR (400 MHz, DMSO-*d*$_6$):** δ (ppm) = 8.18–8.09 (m, 3H, *H*-20 and *H*-5), 8.05 (d, $^3J_{7,6}$ = 17.2 Hz, 2H, *H*-7), 7.53 (d, $^3J_{19,20}$ = 8.2 Hz, 4H, *H*-19), 7.40 (d, $^3J_{6,7}$ = 16.9 Hz, 2H, *H*-6), 2.67 (s, 12H, *H*-17), 2.04 (s, 3H, *H*-1), 1.77 (s, 12H, *H*-10). **^{13}C{^{1}H} NMR (101 MHz, DMSO-*d*$_6$):** δ (ppm) = 177.3 (*C*-13), 175.6 (*C*-8), 153.9 (*C*-18), 145.3 (*C*-7), 143.6 (*C*-5), 123.6 (*C*-19), 117.8 (*C*-12), 113.5 (*C*-15 or *C*-16), 112.9 (*C*-15 or *C*-16), 112.7 (*C*-2), 112.0 (*C*-6), 98.1 (*C*-9), 51.3 (*C*-14), 25.9 (*C*-10), 20.4 (*C*-17), 9.4 (*C*-1); 4 C missing (*C*-3, *C*-4, *C*-11 and *C*-20). **IR (neat):** ν (cm^{-1}) = 3750, 2983, 2929, 2205, 2172, 2002, 1735, 1622, 1558, 1489, 1457, 1366, 1231, 1189, 1146, 1102, 1046, 966, 853, 783, 650, 540, 511, 471, 431. **HRMS (ESI-TOF):** calculated for $[M-2(C_7H_{10}N)]^{2-}$ ($C_{31}H_{20}N_6O_4^{2-}$) 270.0779, found 270.0779; calculated for $[M-2(C_7H_{10}N)+H]^-$ 541.1630, found 541.1630.

III. NMR SPECTRA

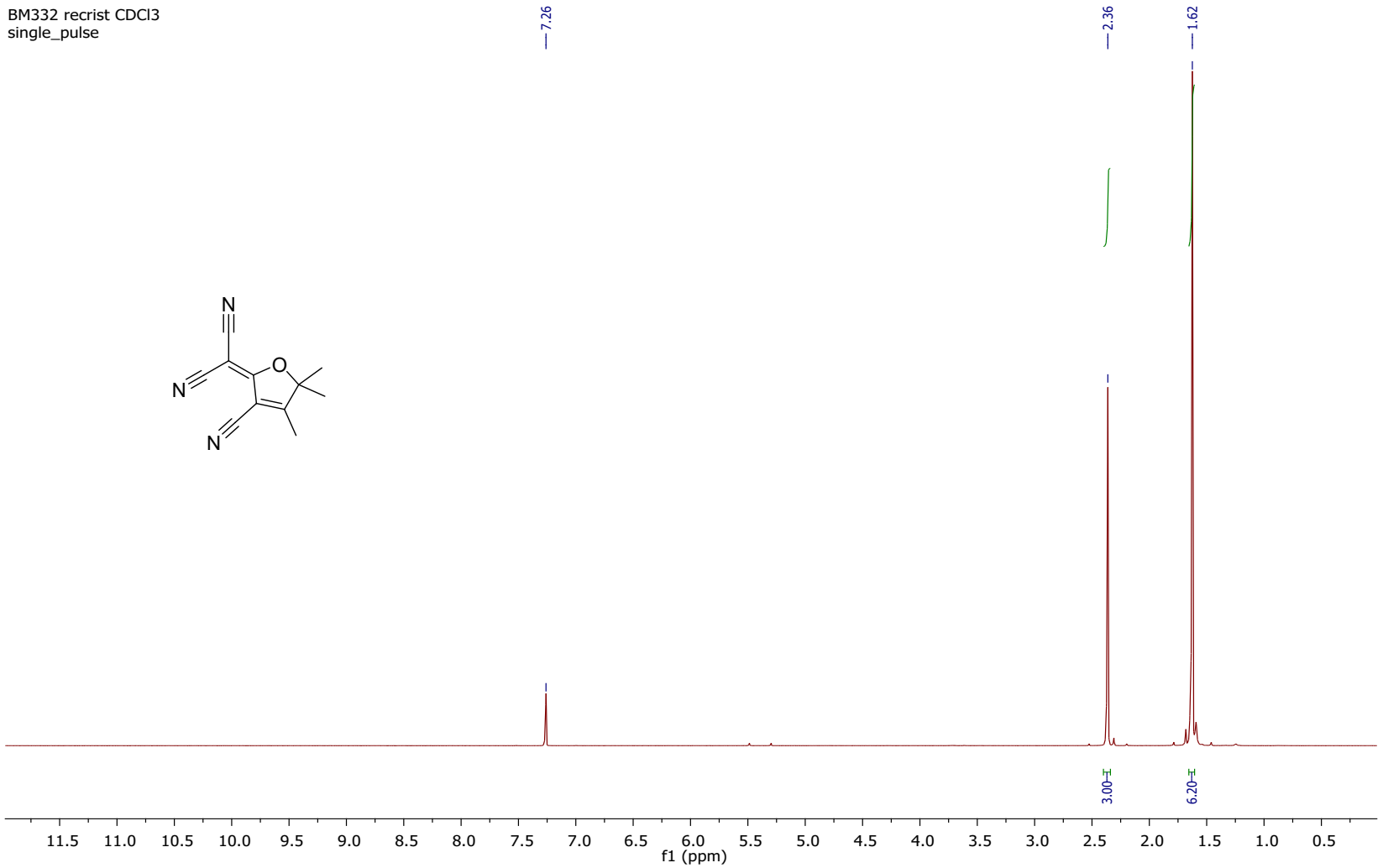

Figure S 1. ^{1}H NMR (400 MHz, $CDCl_3$) of compound **5**.

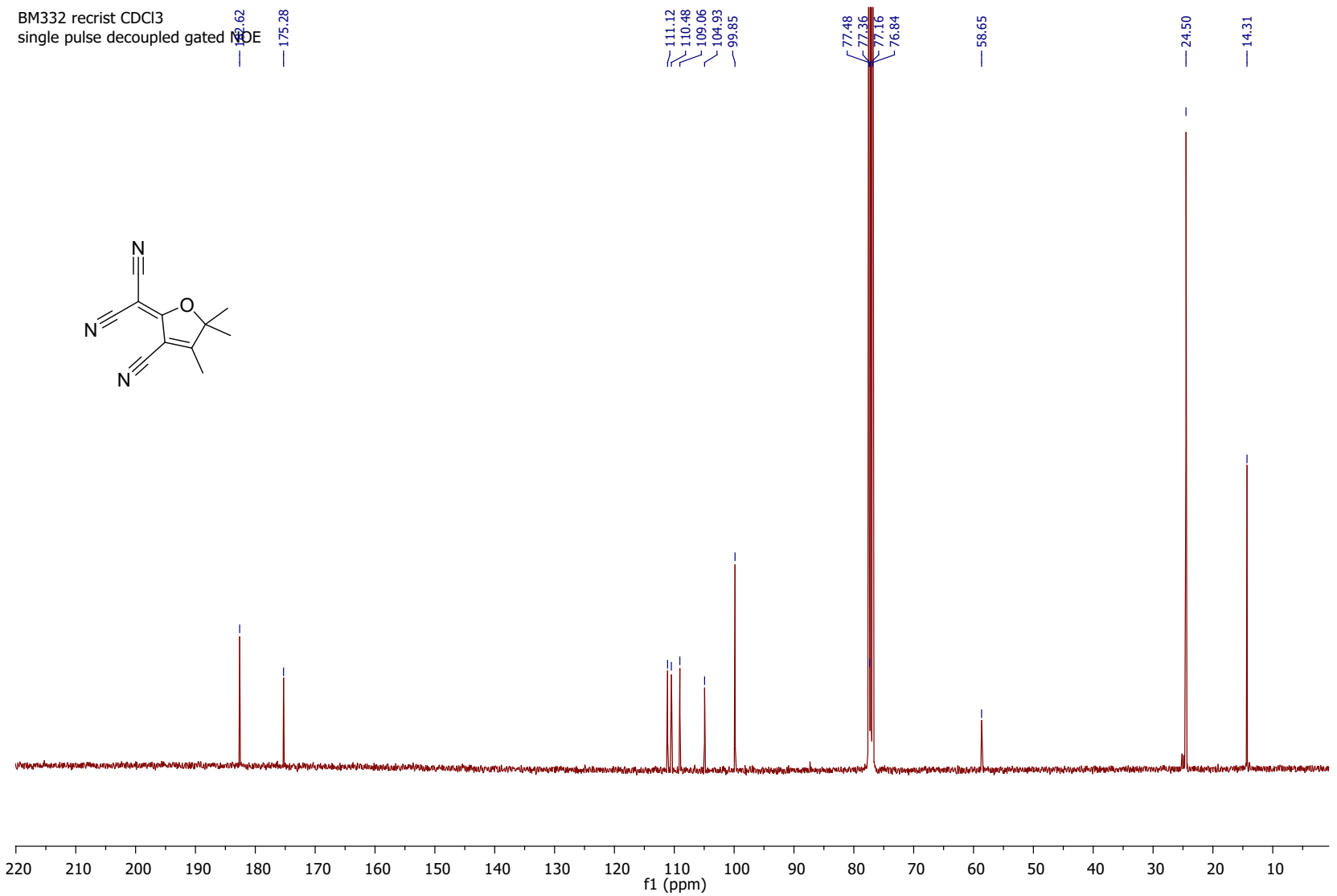

Figure S 2. ^{13}C NMR (101 MHz, $CDCl_3$) of compound **5**.

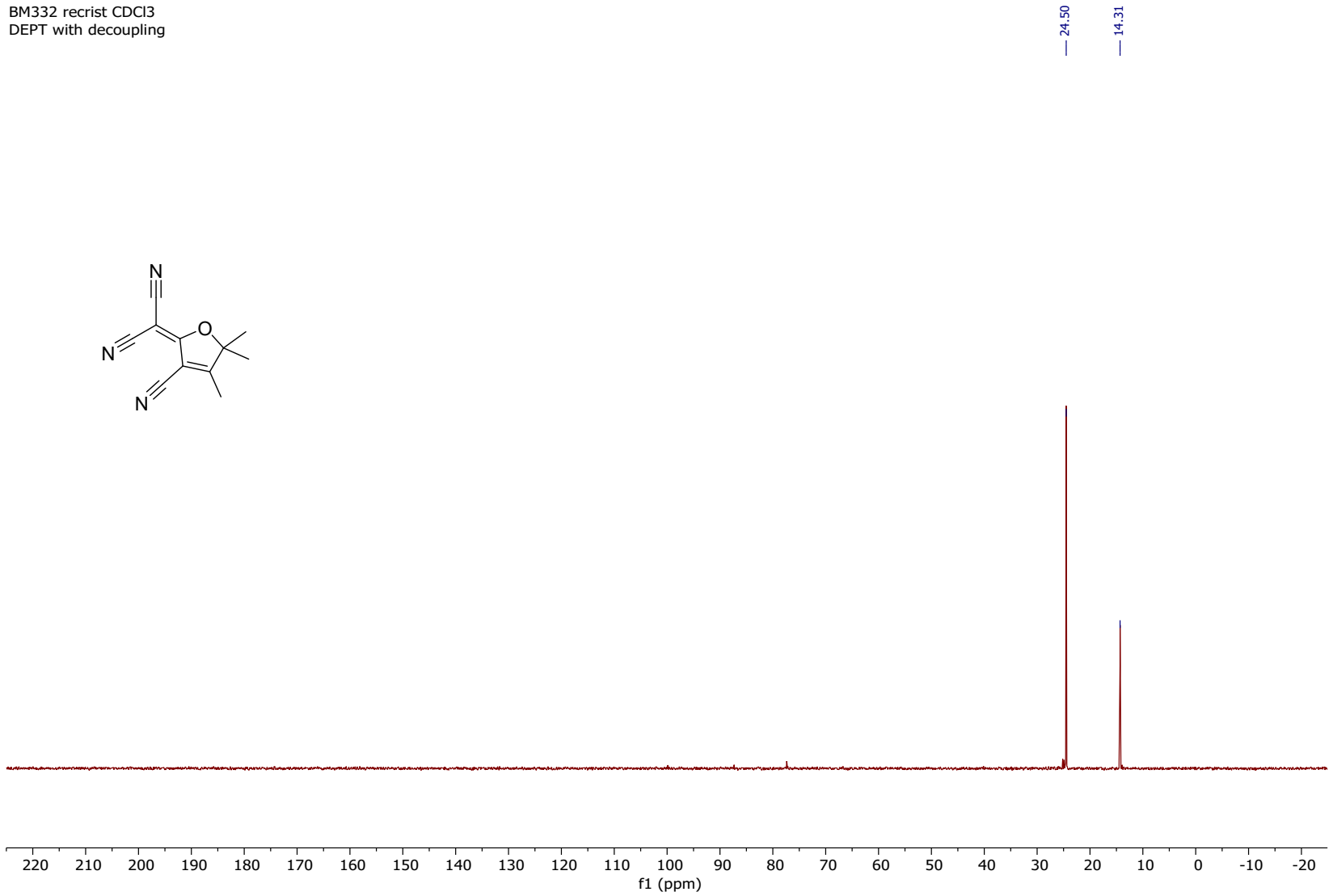

Figure S 3. DEPT ^{13}C NMR (101 MHz, $CDCl_3$) of compound **5**.

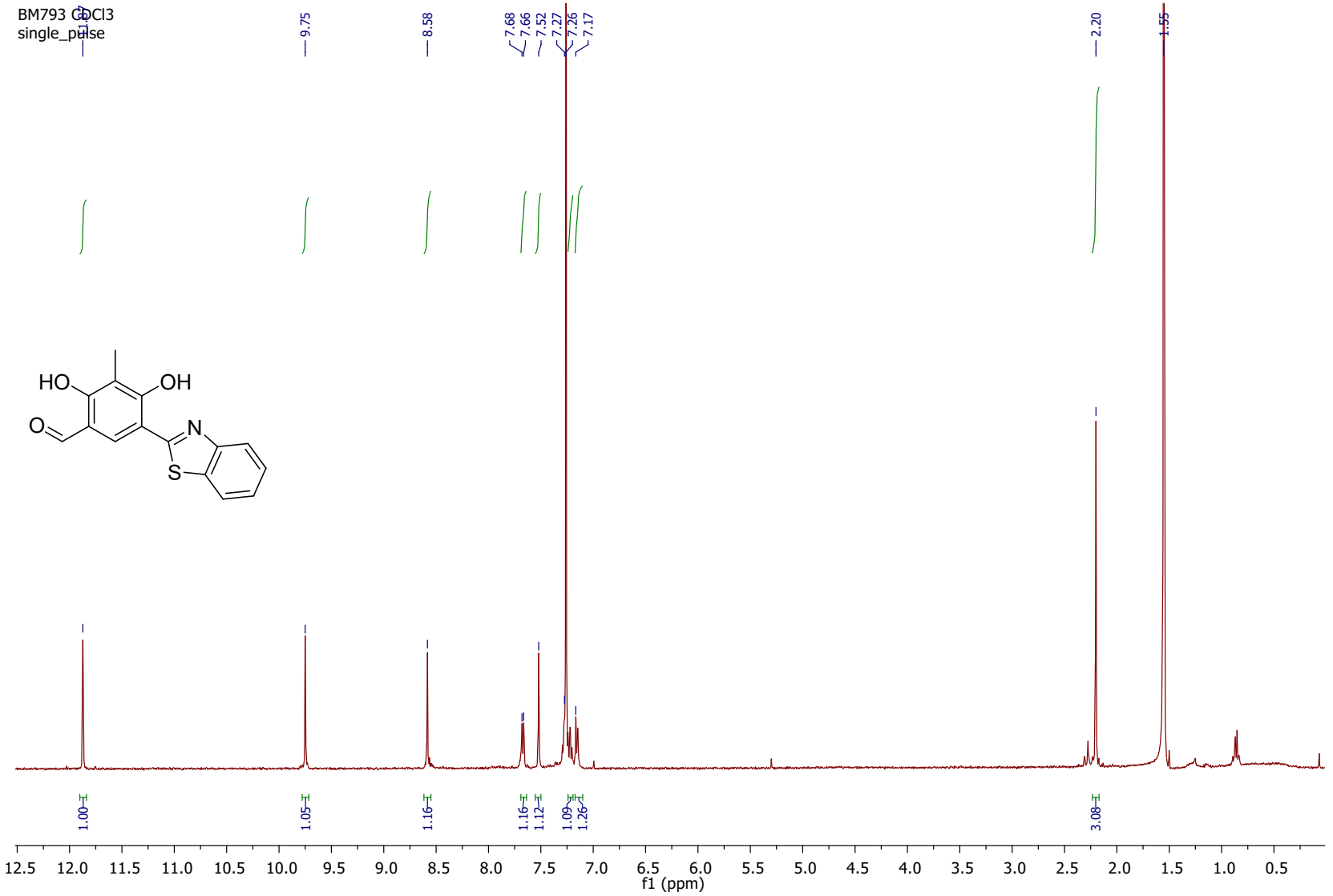

Figure S 4. ^{1}H NMR (400 MHz, $CDCl_3$) of compound **1a**.

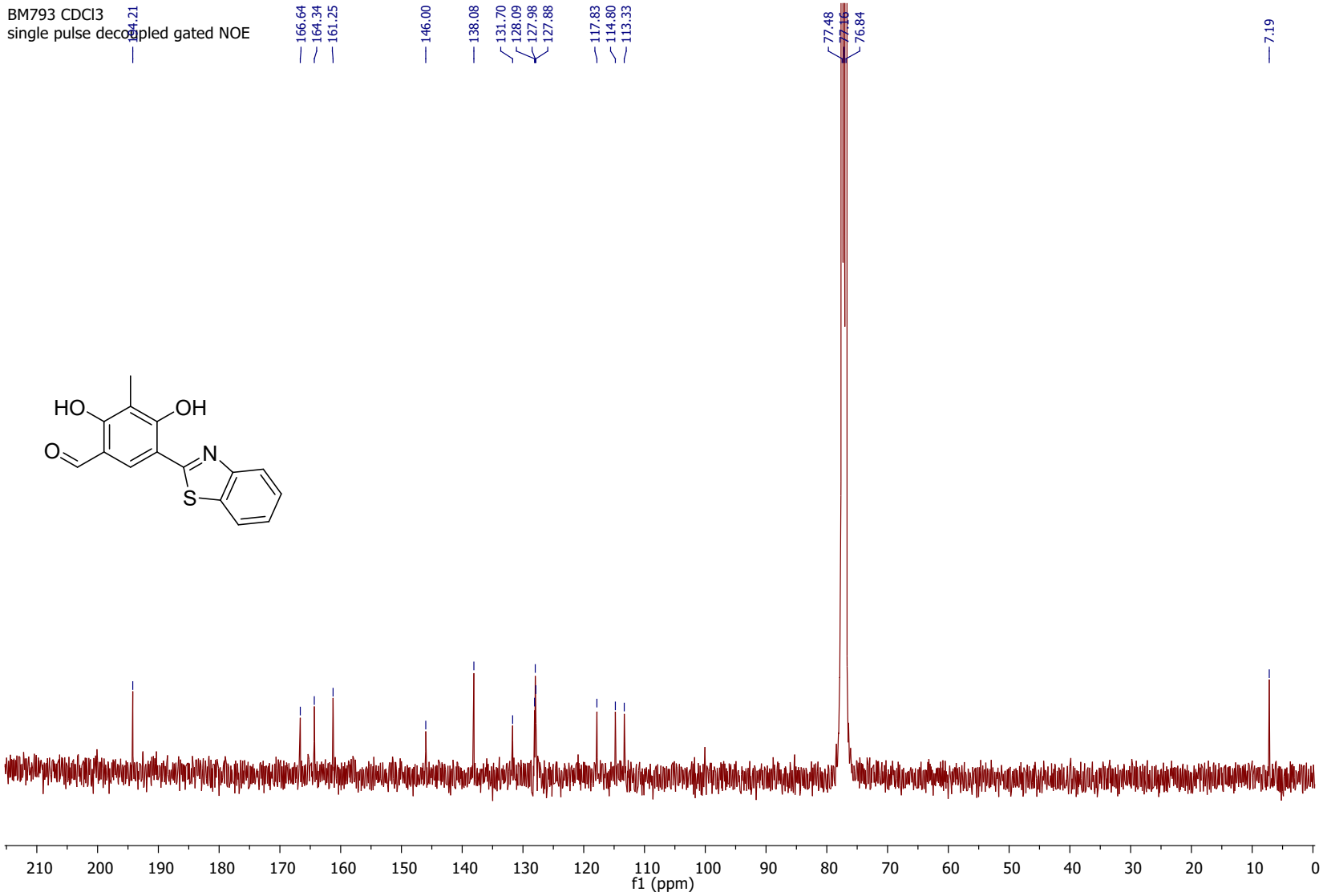

Figure S 5. ^{13}C NMR (101 MHz, $CDCl_3$) of compound **1a**.

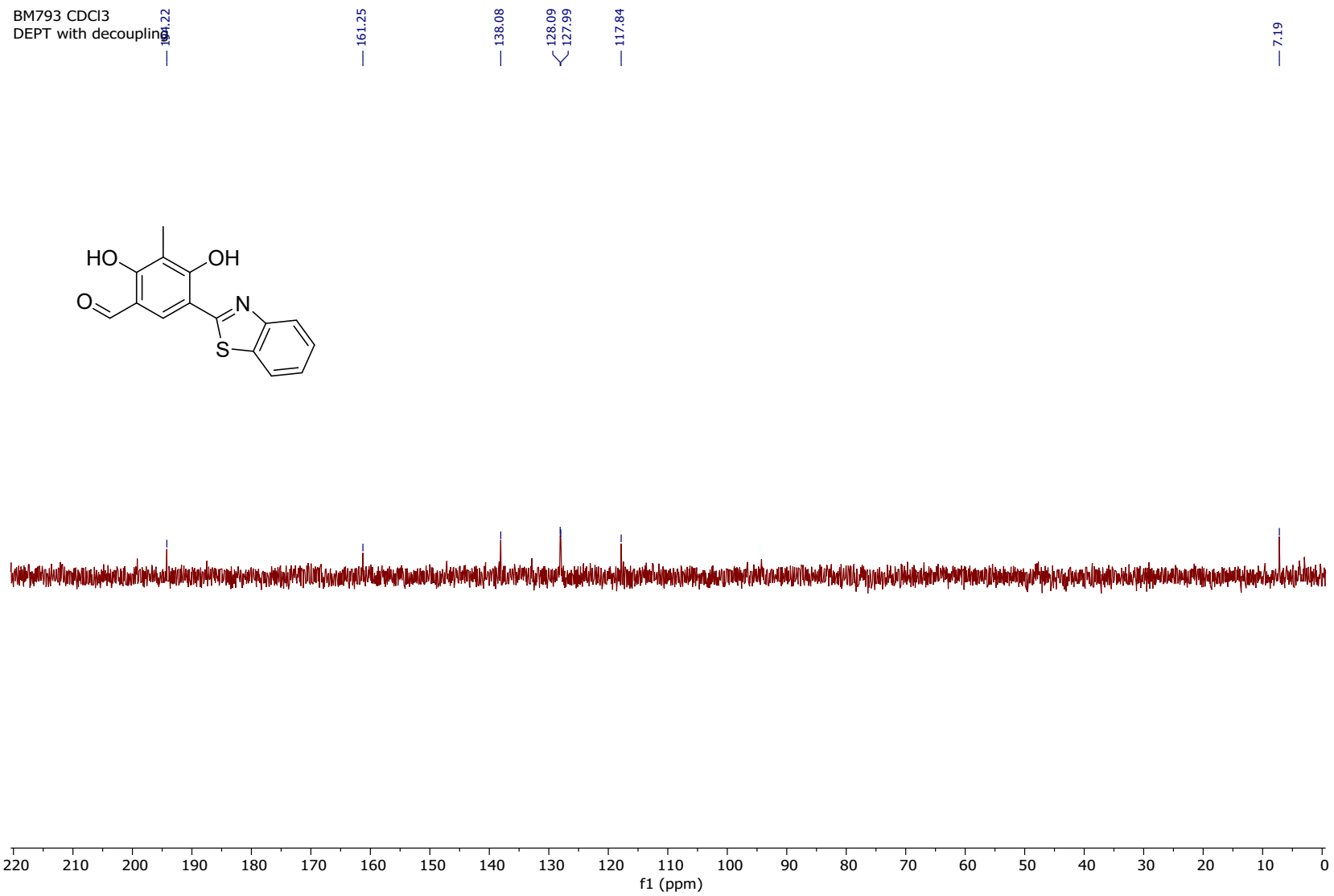

Figure S 6. DEPT ^{13}C NMR (101 MHz, $CDCl_3$) of compound **1a**.

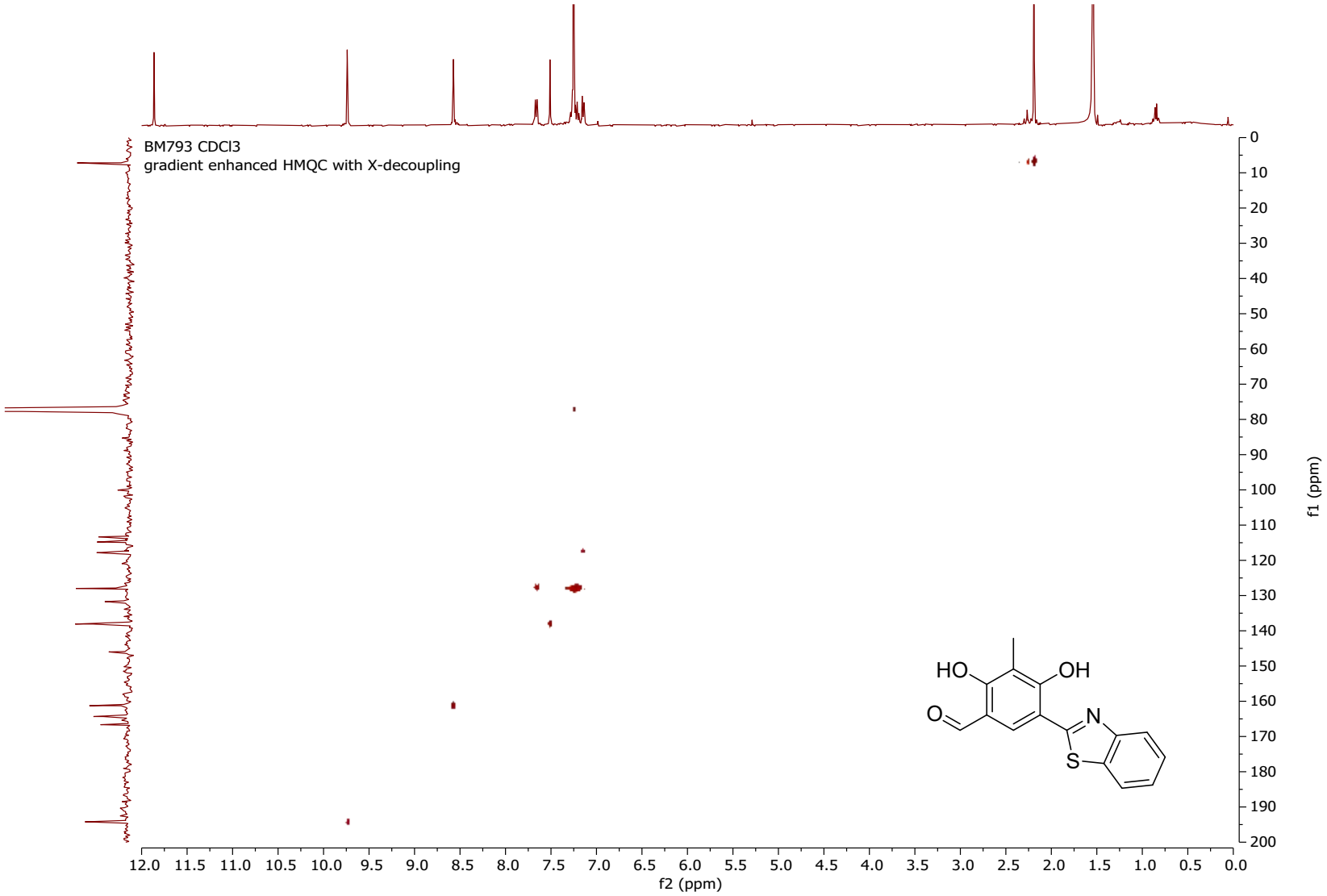

Figure S 7. HMQC NMR ($CDCl_3$) of compound **1a**.

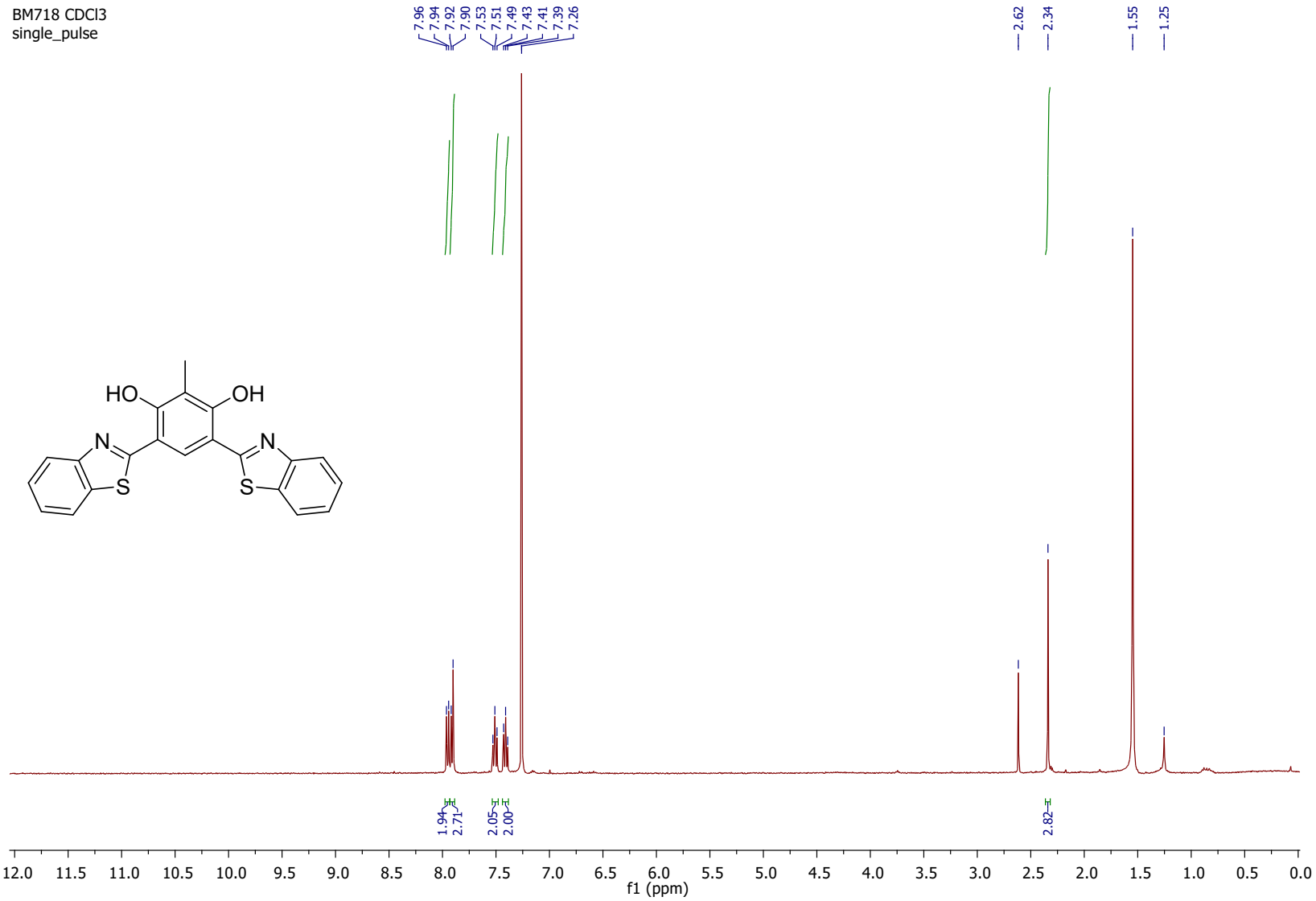

Figure S 8. ^{1}H NMR (400 MHz, $CDCl_3$) of compound **1b**.

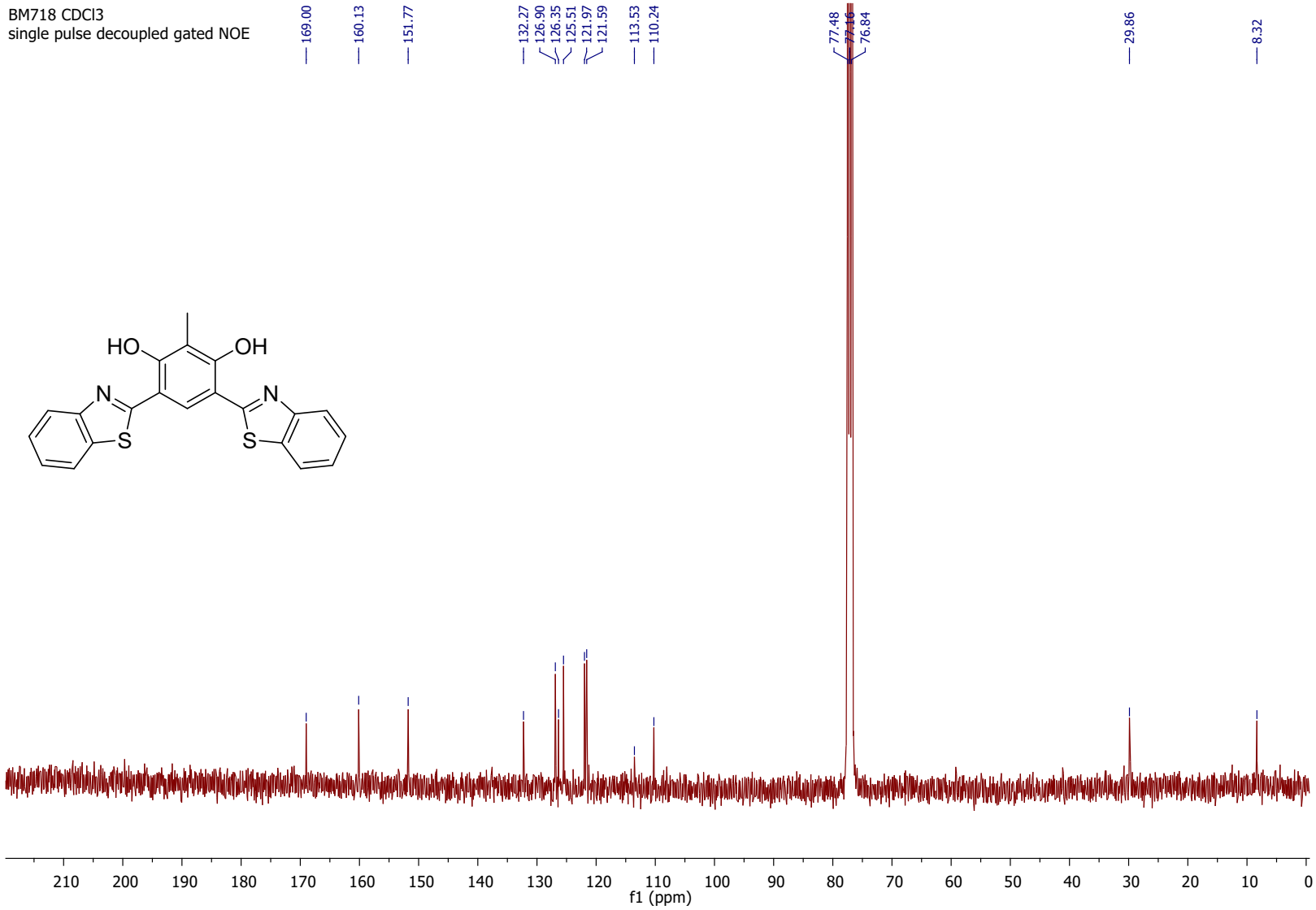

Figure S 9. ^{13}C NMR (101 MHz, $CDCl_3$) of compound **1b**.

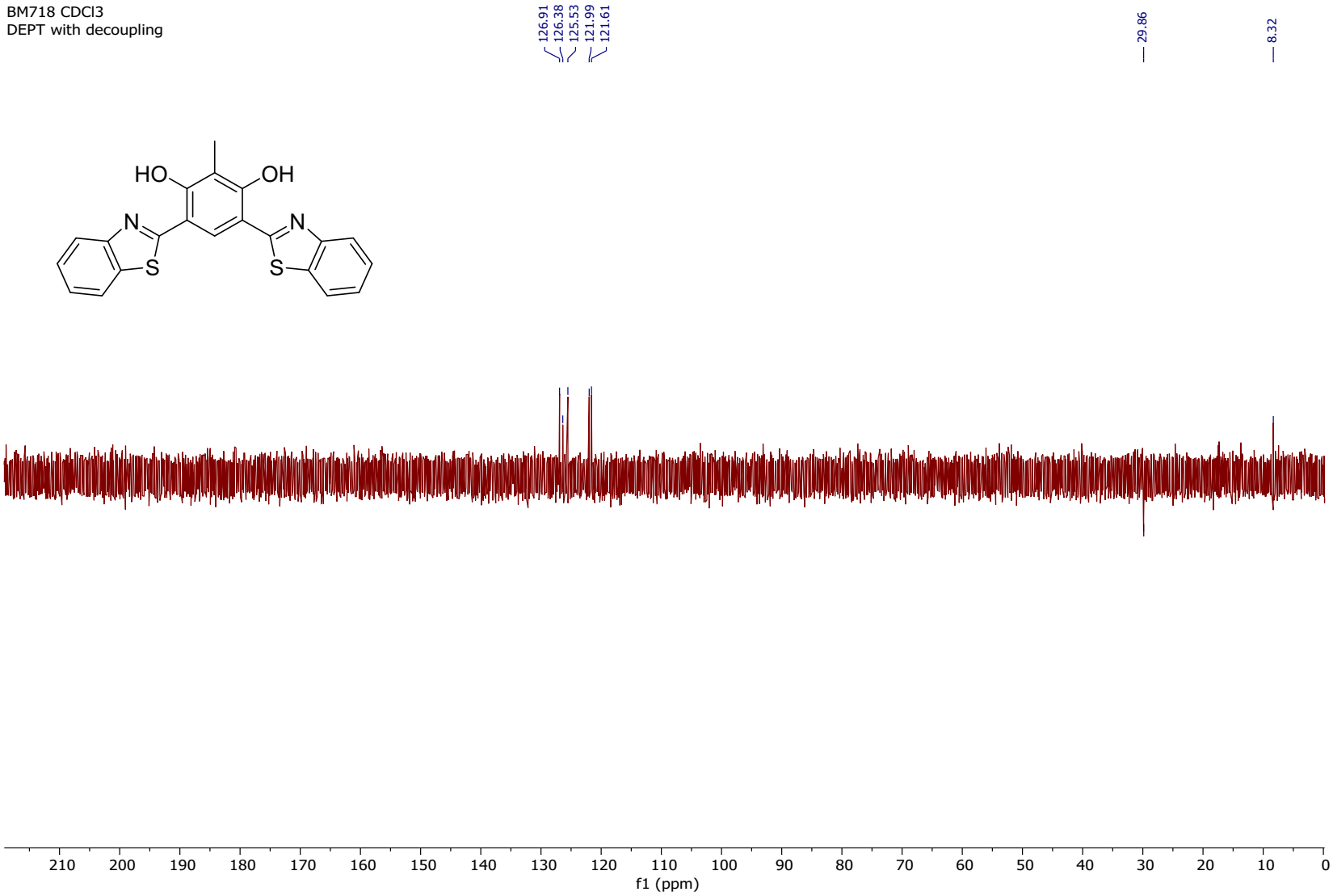

Figure S 10. DEPT ^{13}C NMR (101 MHz, $CDCl_3$) of compound **1b**.

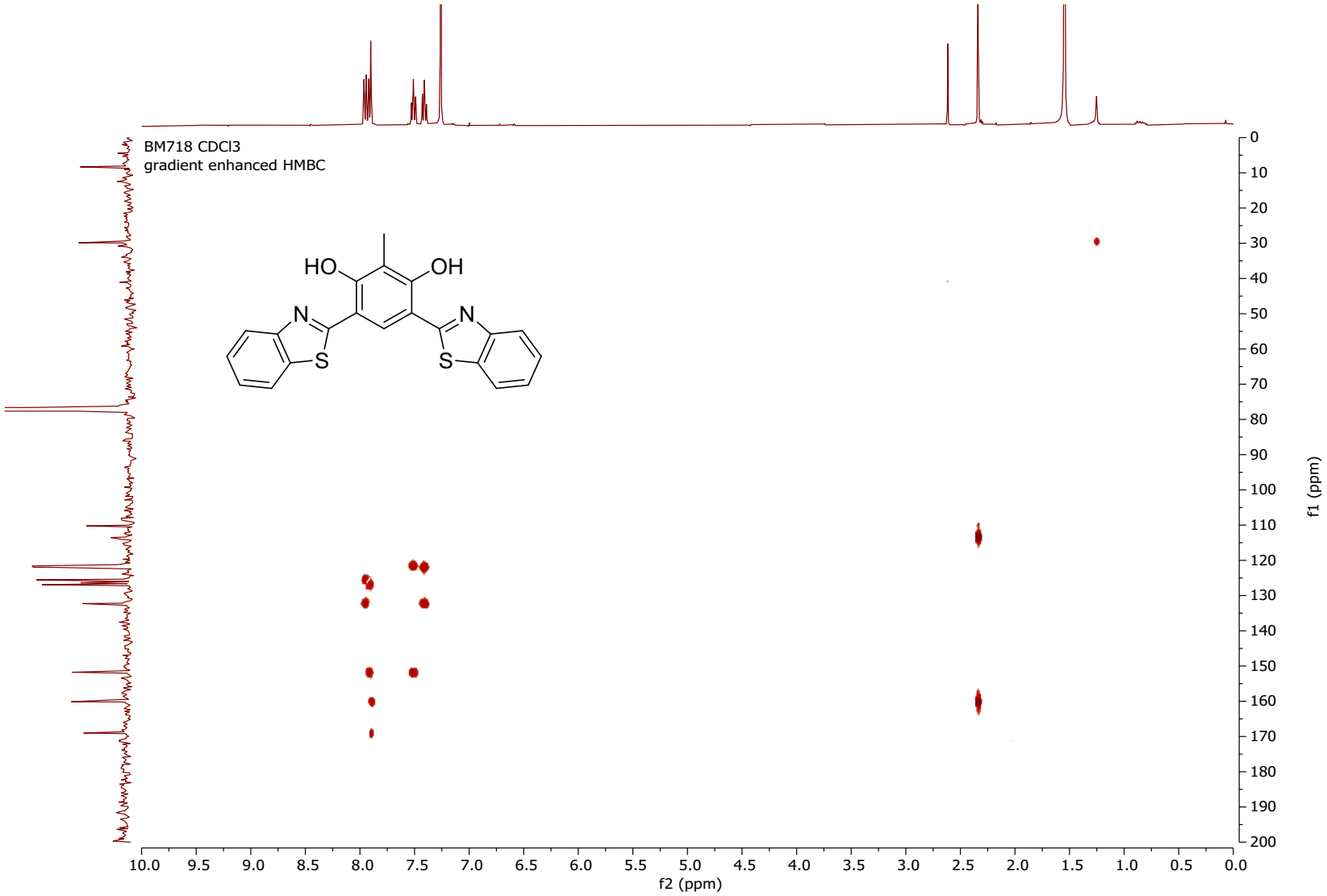

Figure S 11. HMBC NMR ($CDCl_3$) of compound **1b**.

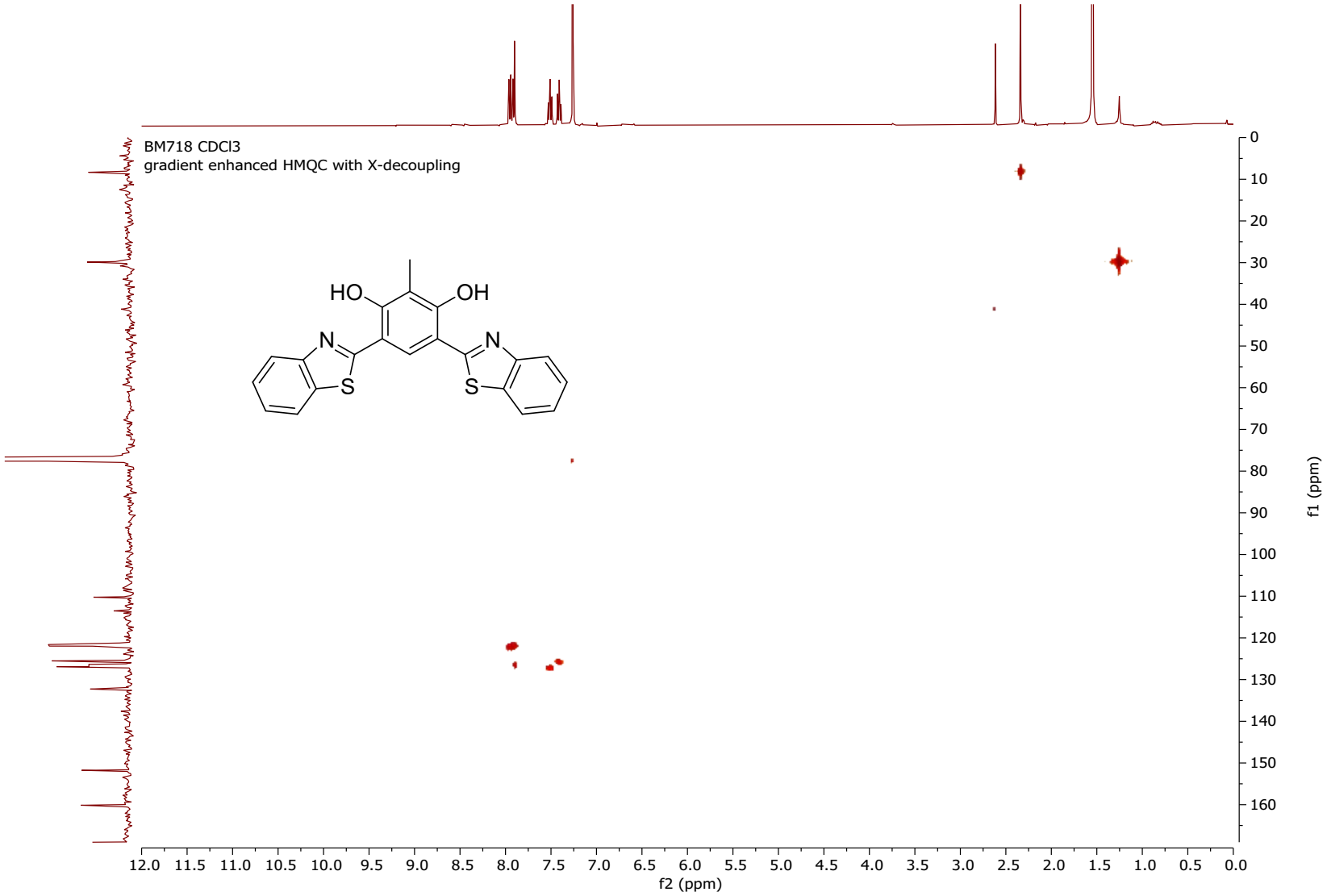

Figure S 12. HMQC NMR ($CDCl_3$) of compound **1b**.

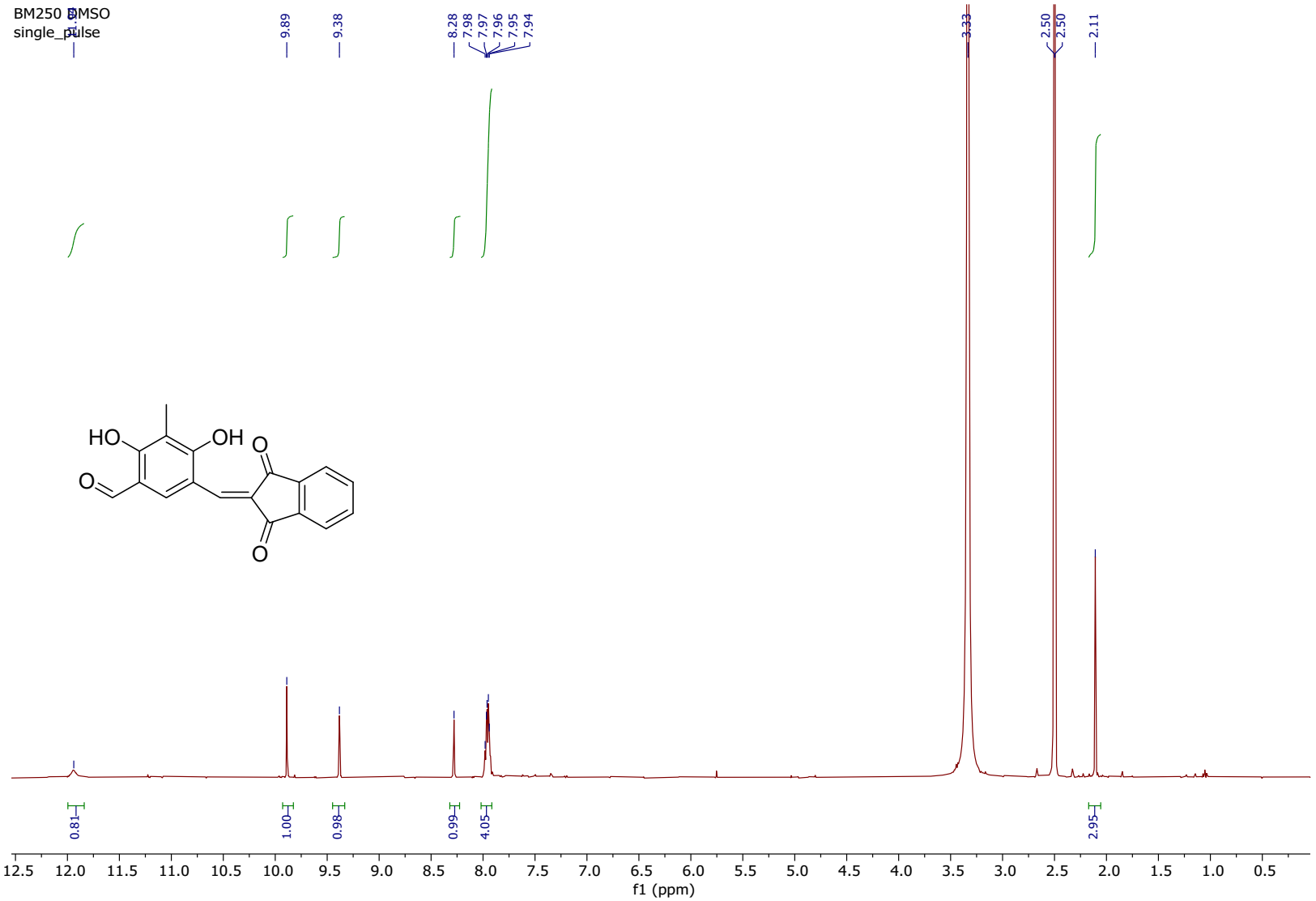

Figure S 13. ^{1}H NMR (400 MHz, DMSO-d_6) of compound **2a**.

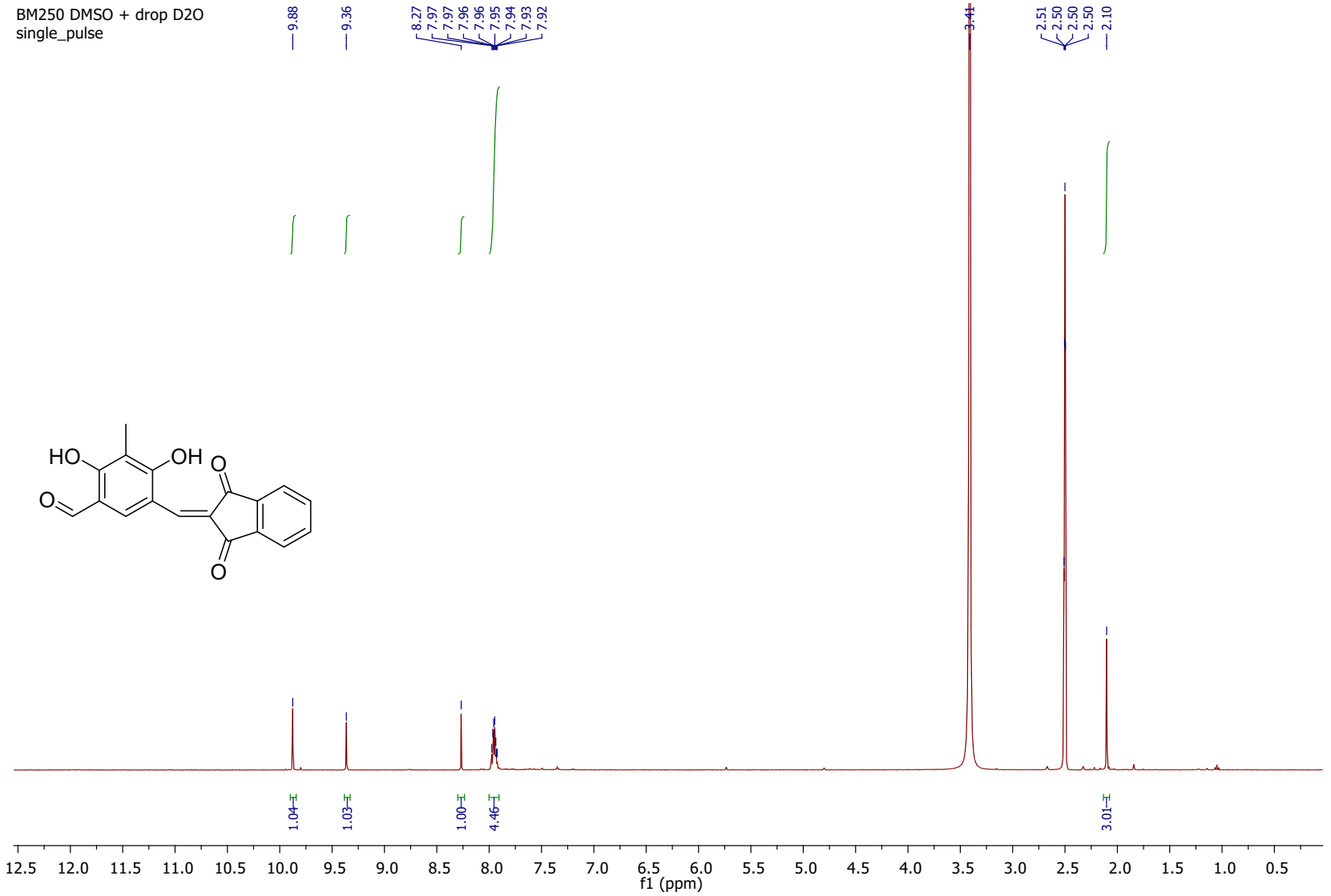

Figure S 14. ^{1}H NMR (400 MHz, DMSO-d_6 + drop of D_2O) of compound **2a**.

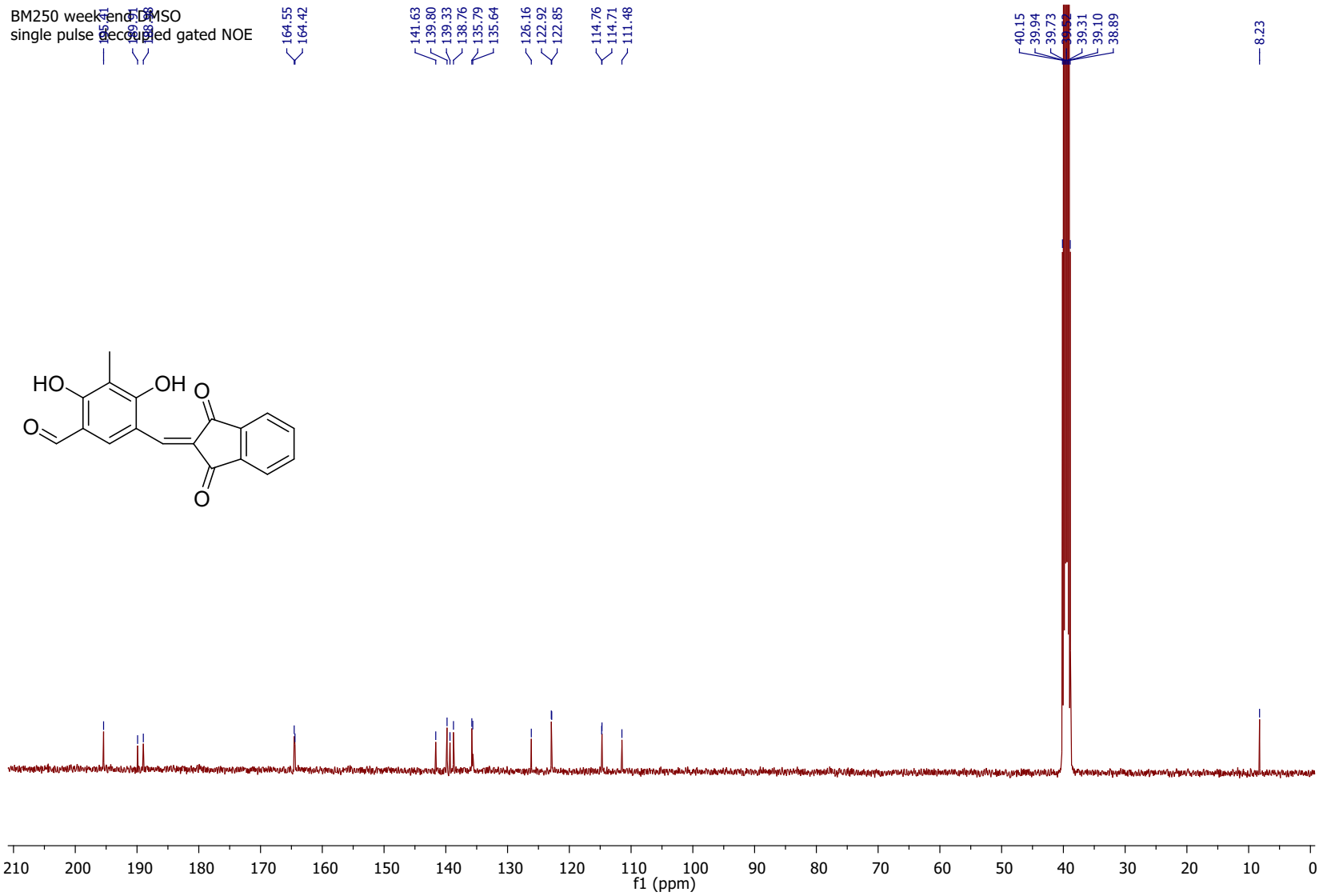

Figure S 15. ^{13}C NMR (101 MHz, DMSO-d_6) of compound **2a**.

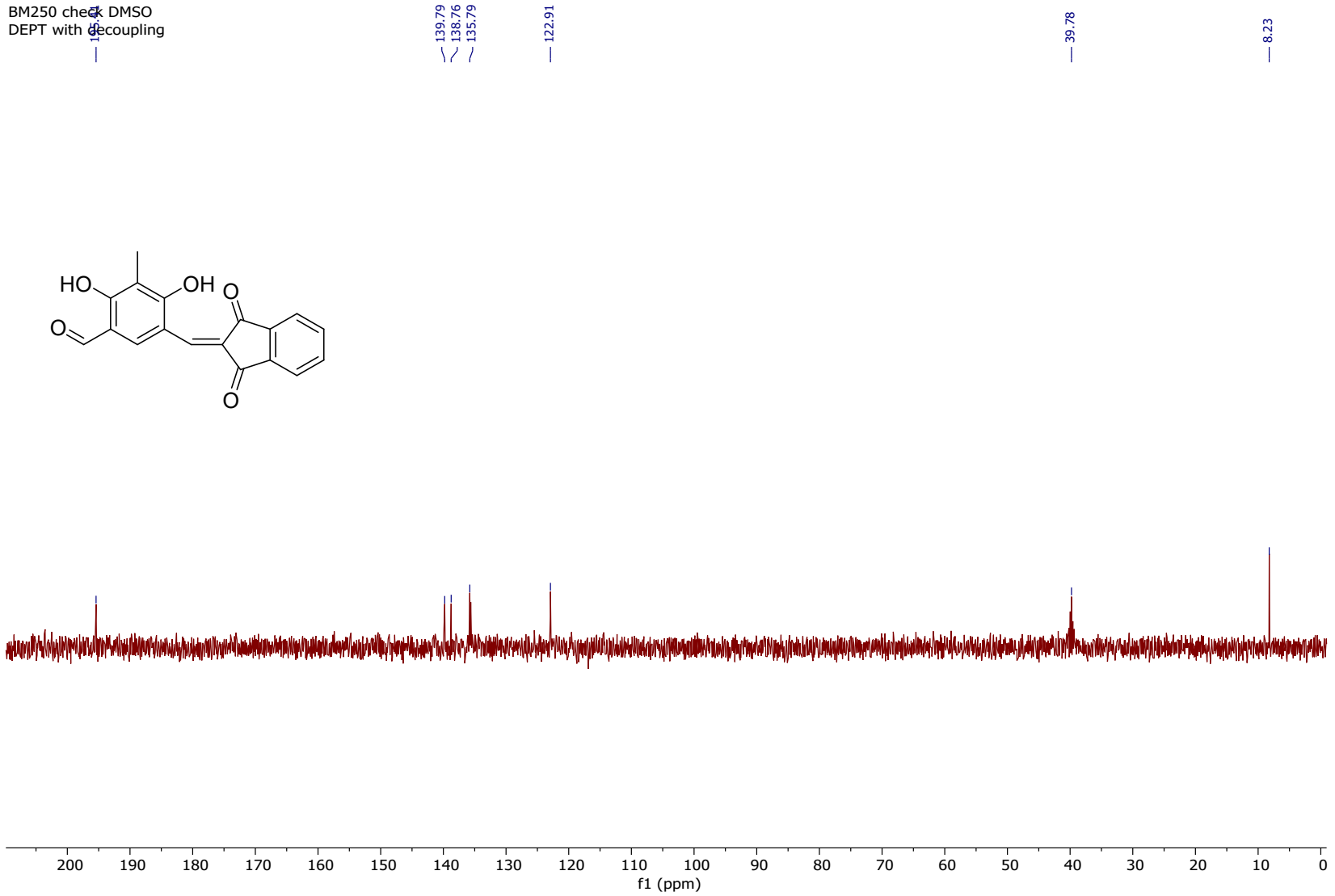

Figure S 16. DEPT ^{13}C NMR (101 MHz, DMSO-d_6) of compound **2a**.

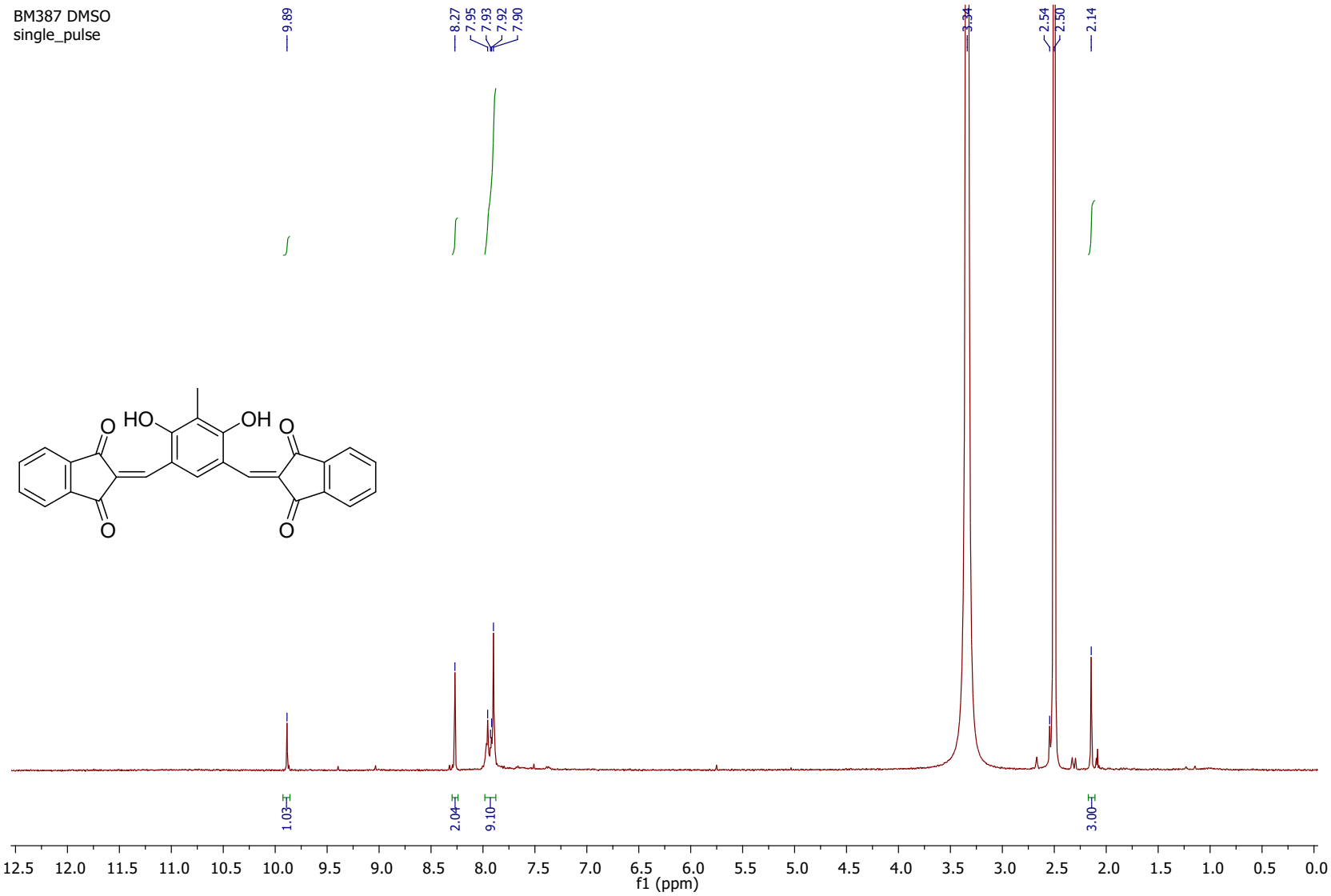

Figure S 17. ^{1}H NMR (400 MHz, DMSO-d_6) of compound **2b**.

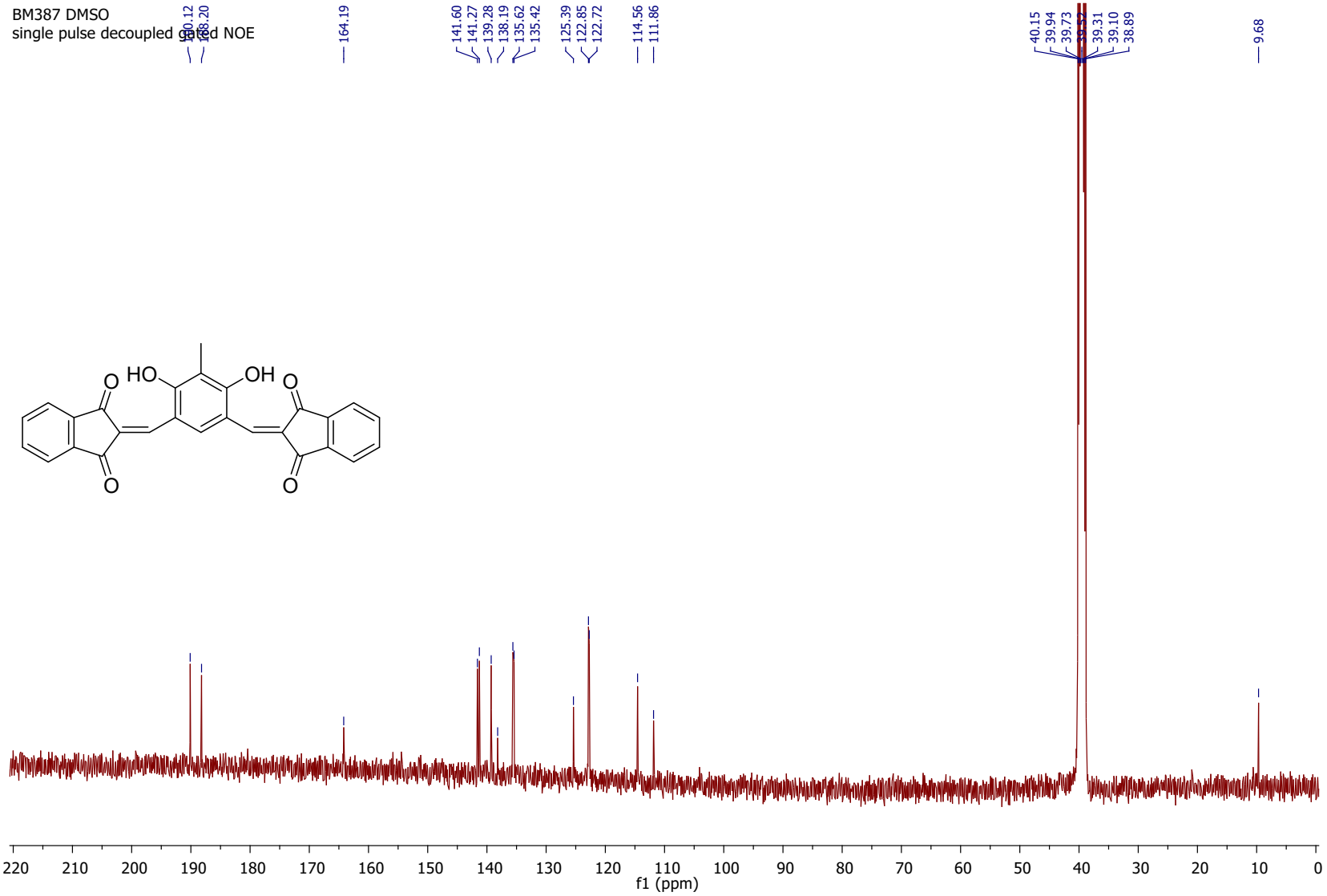

Figure S 18. ^{13}C NMR (101 MHz, DMSO-d_6) of compound **2b**.

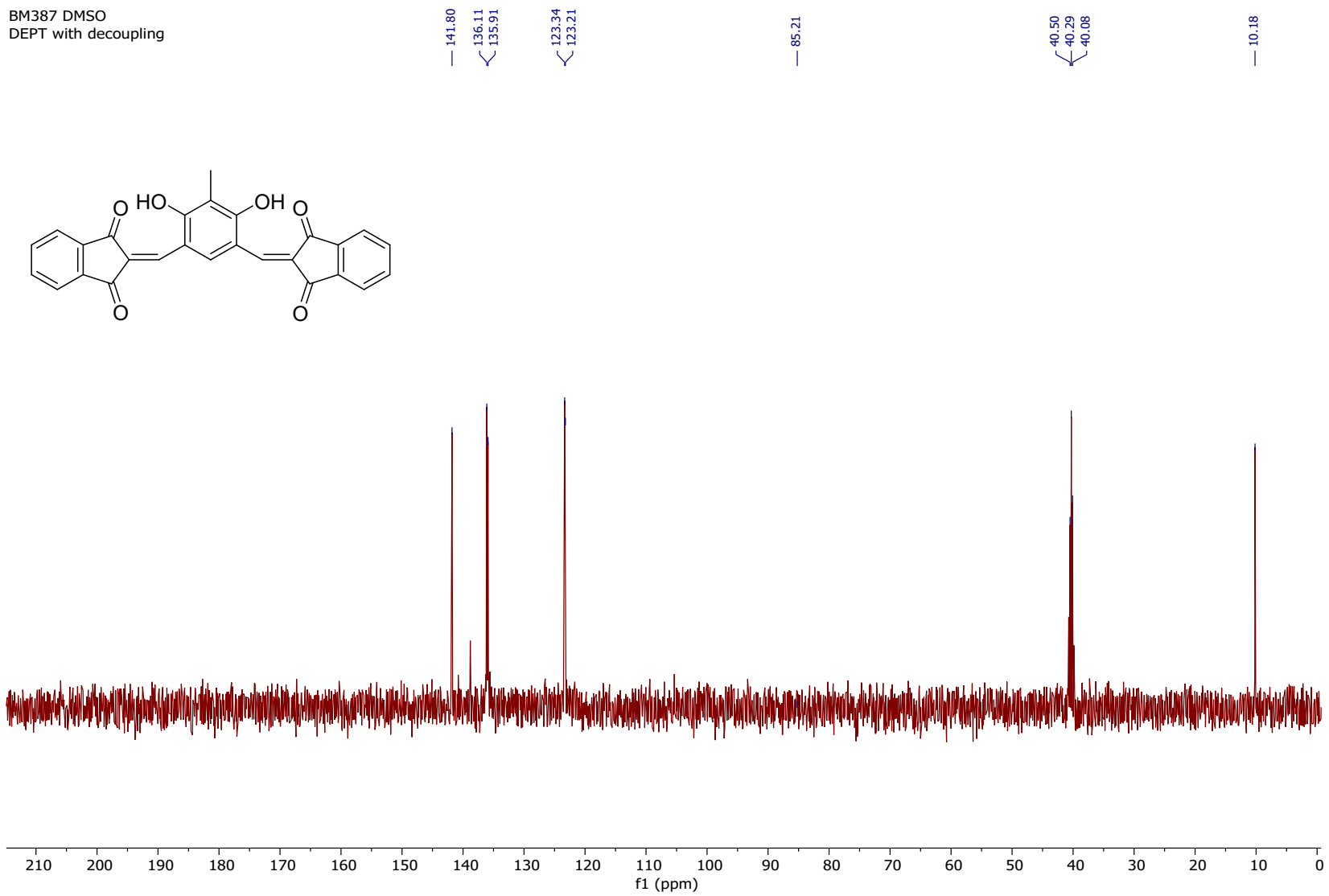

Figure S 19. DEPT ^{13}C NMR (101 MHz, DMSO-d_6) of compound **2b**.

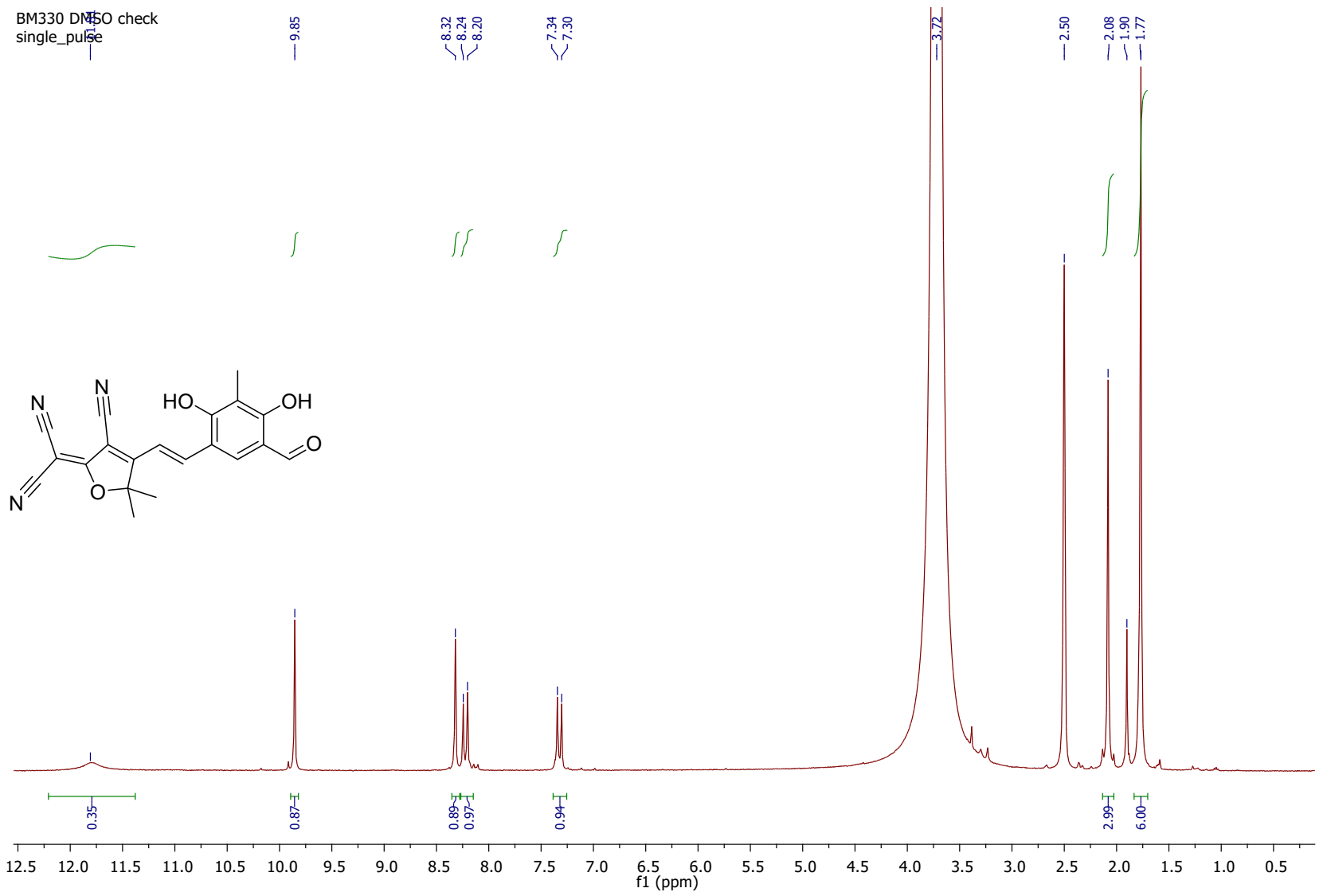

Figure S 20. ^{1}H NMR (400 MHz, DMSO-d_6) of compound **3a**.

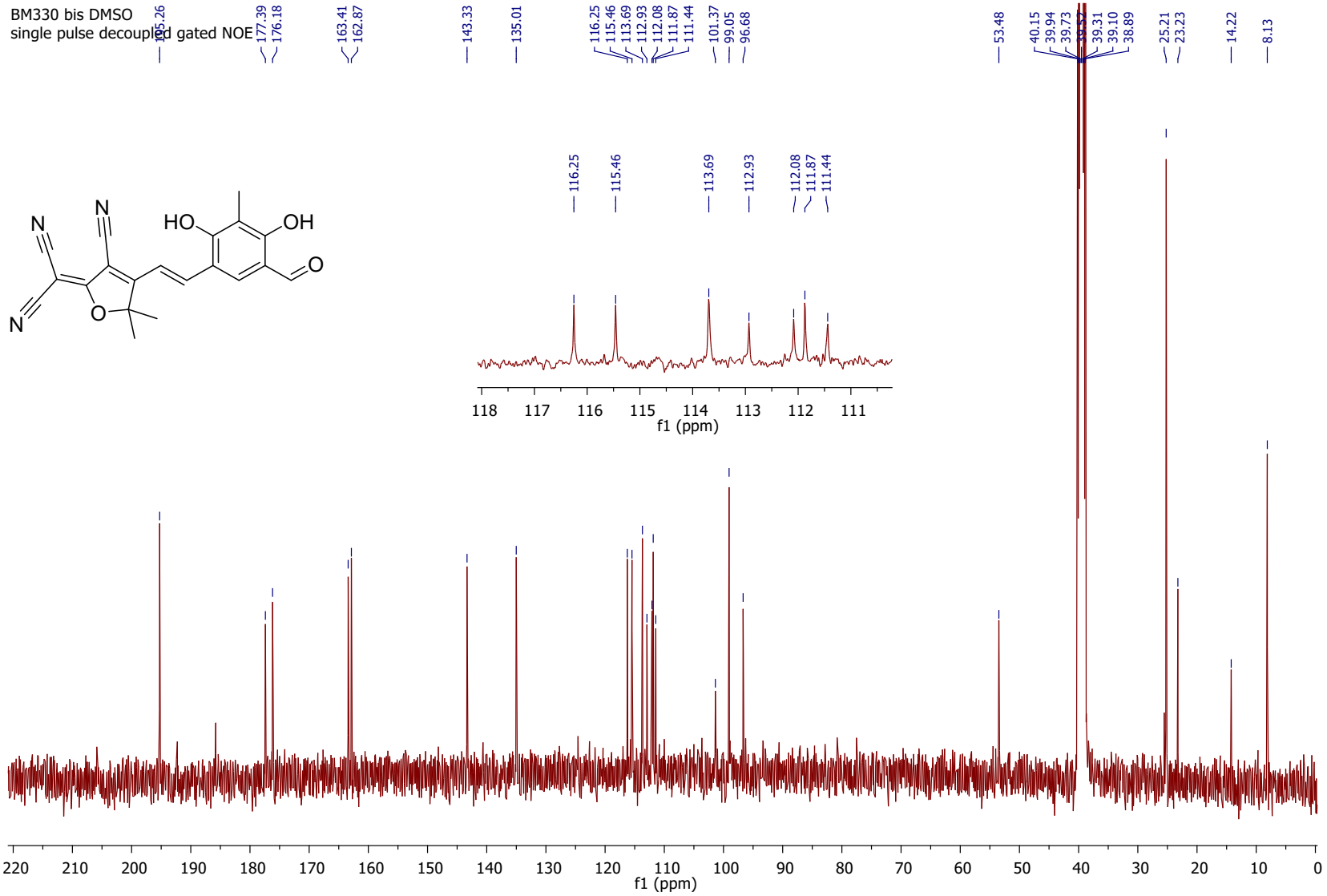

Figure S 21. ^{13}C NMR (101 MHz, DMSO-d_6) of compound **3a**.

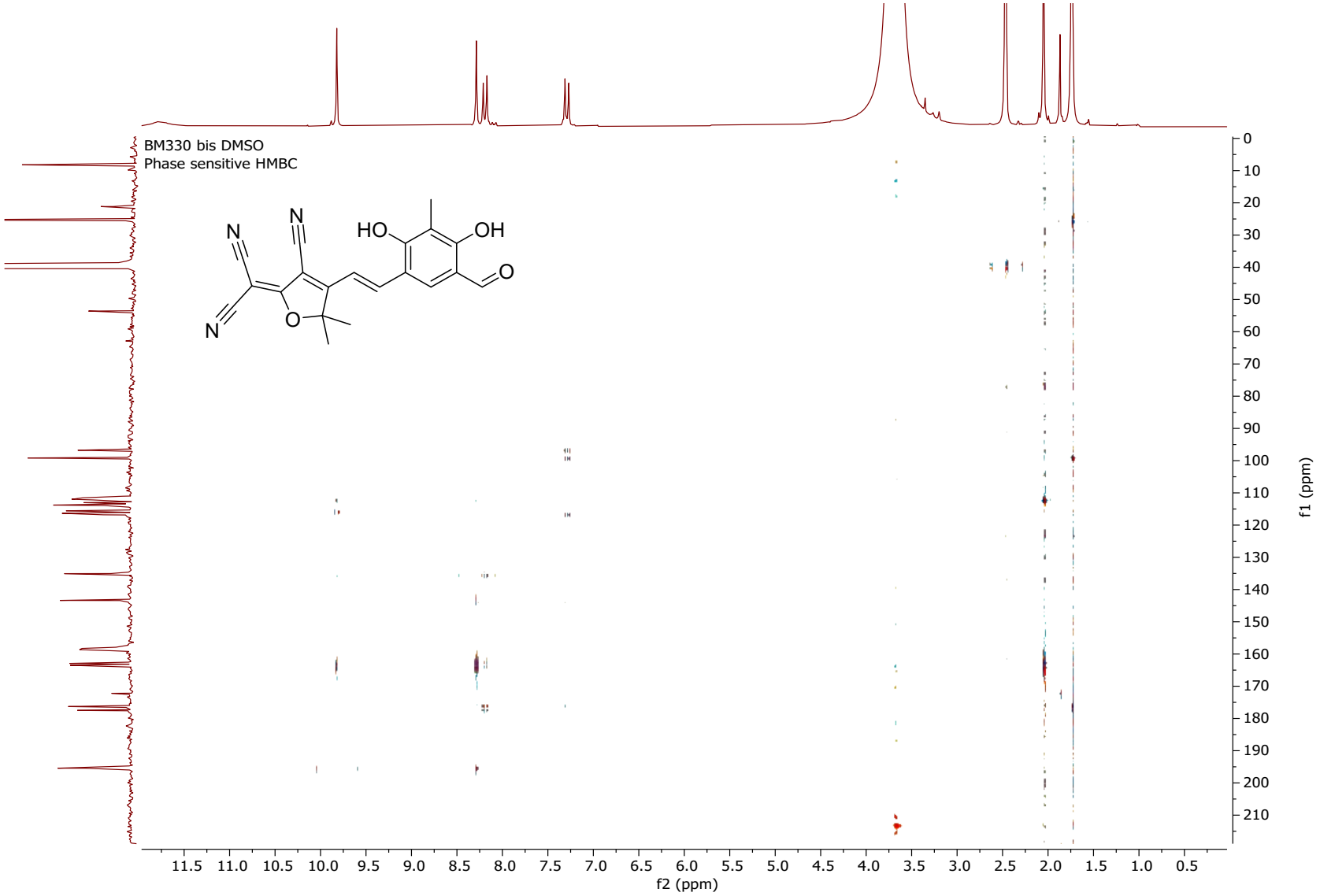

Figure S 22. HMBC NMR (DMSO-d_6) of compound **3a**.

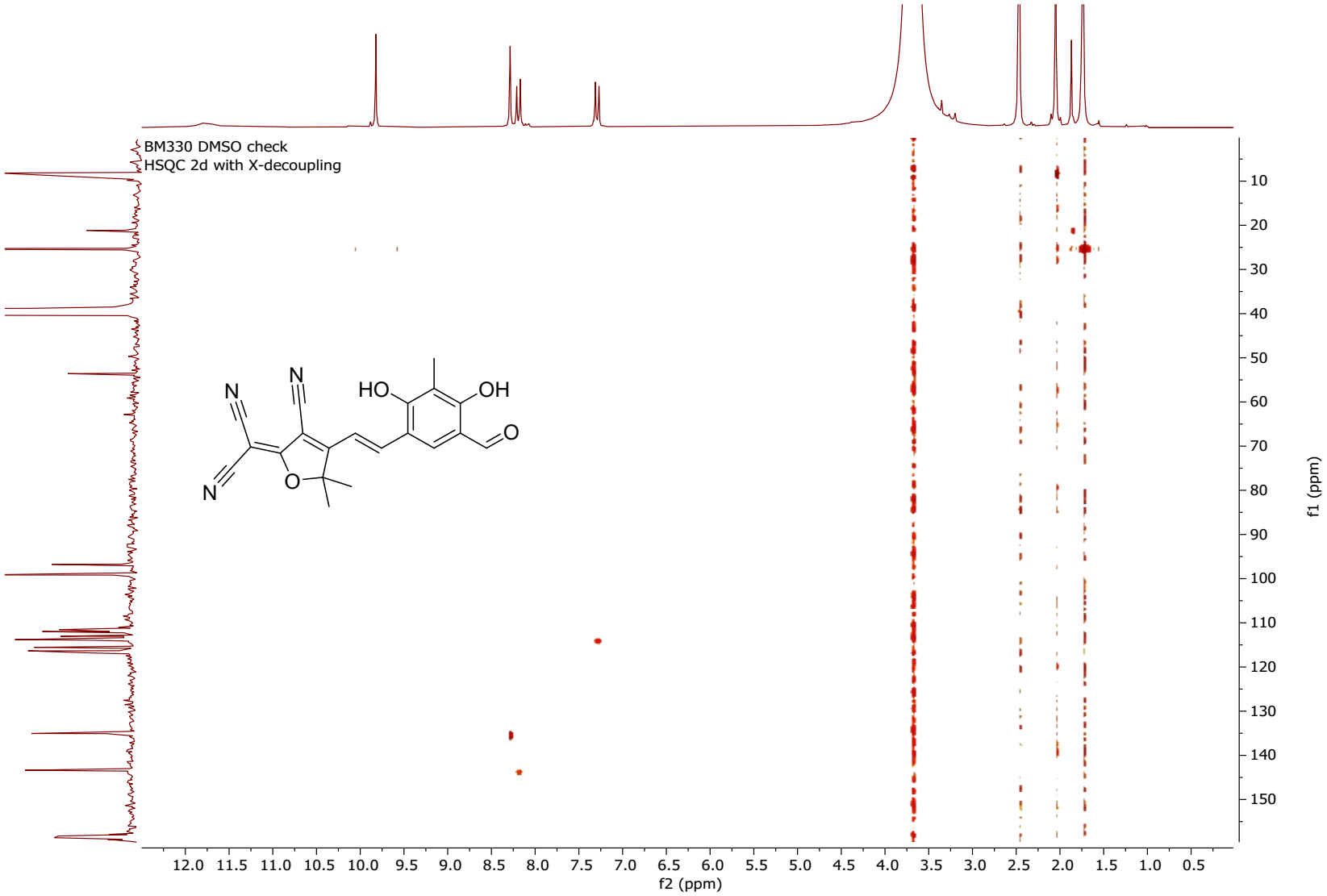

Figure S 23. HSQC NMR (DMSO-d_6) of compound **3a**.

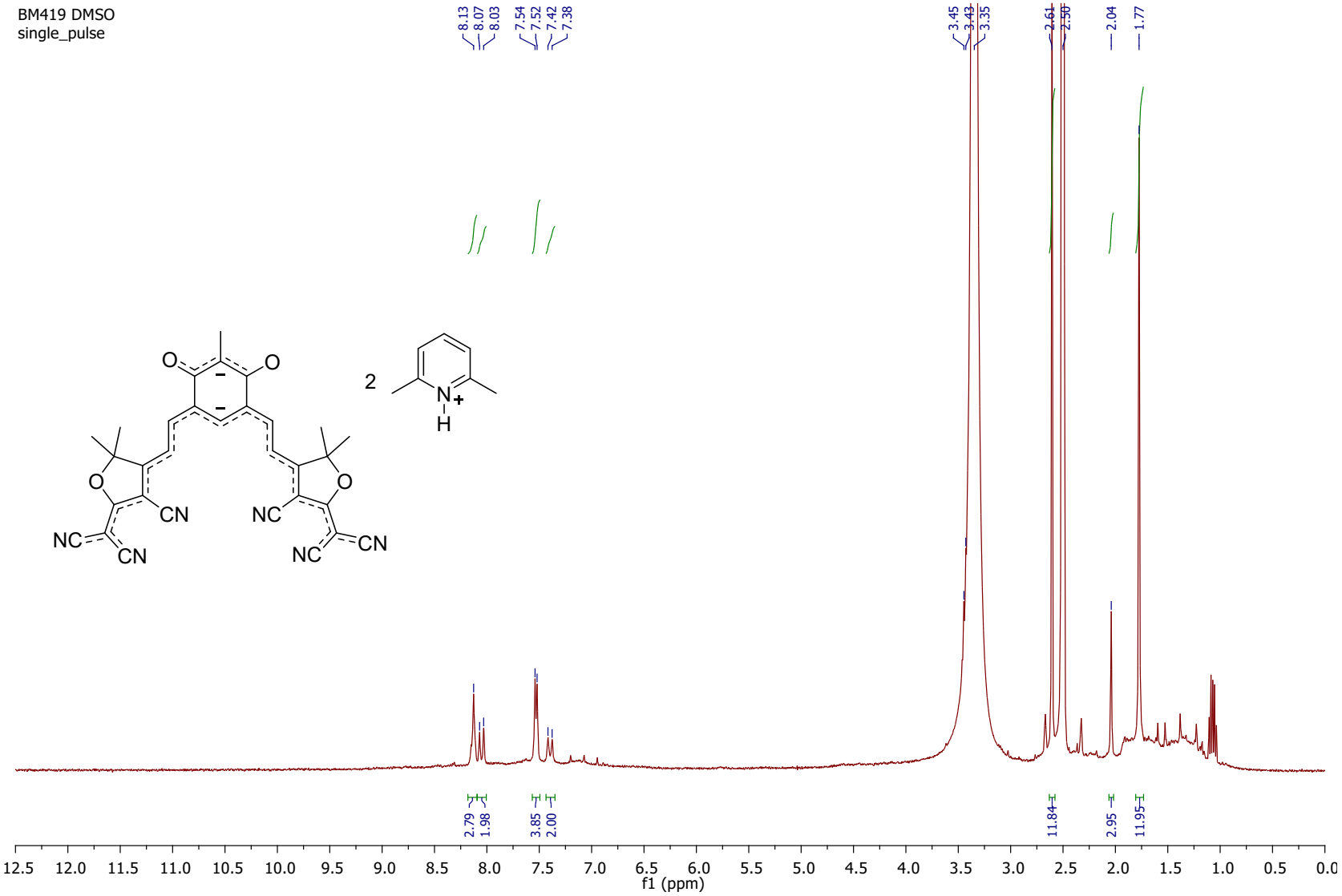

Figure S 24. ^{1}H NMR (400 MHz, DMSO-d_6) of compound **3b**.

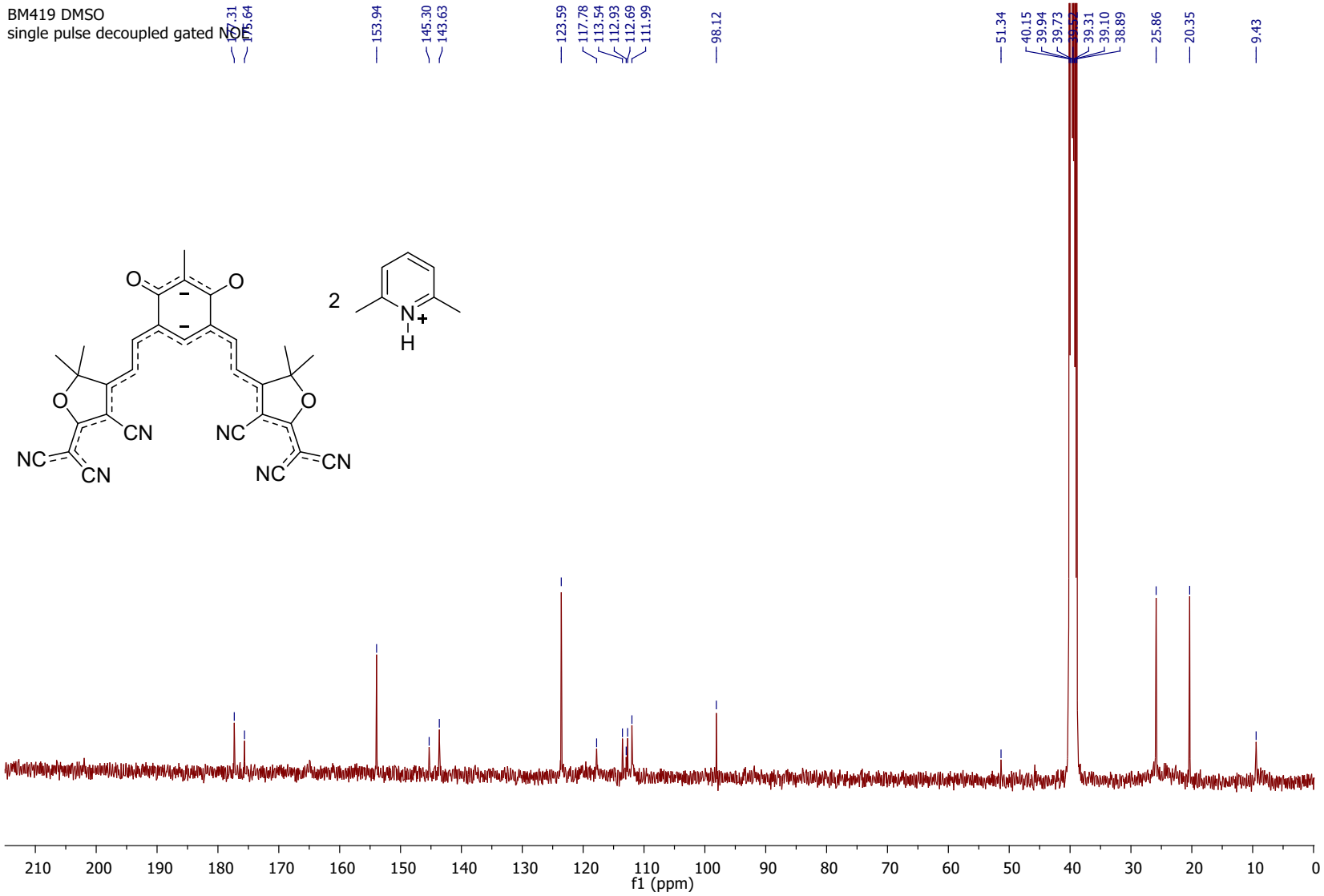

Figure S 25. ^{13}C NMR (101 MHz, DMSO-d_6) of compound **3b**.

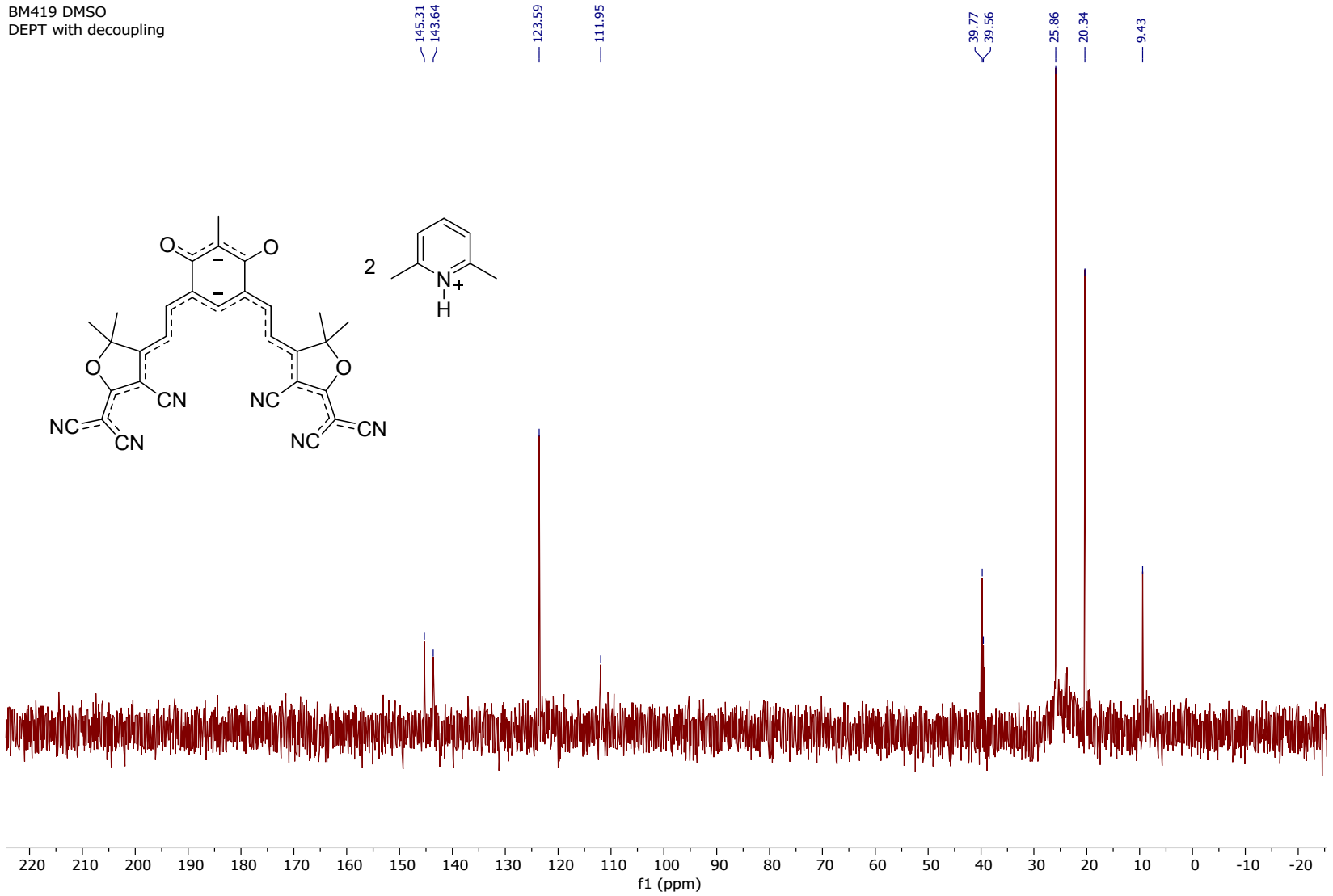

Figure S 26. DEPT ^{13}C NMR (101 MHz, DMSO-d_6) of compound **3b**.

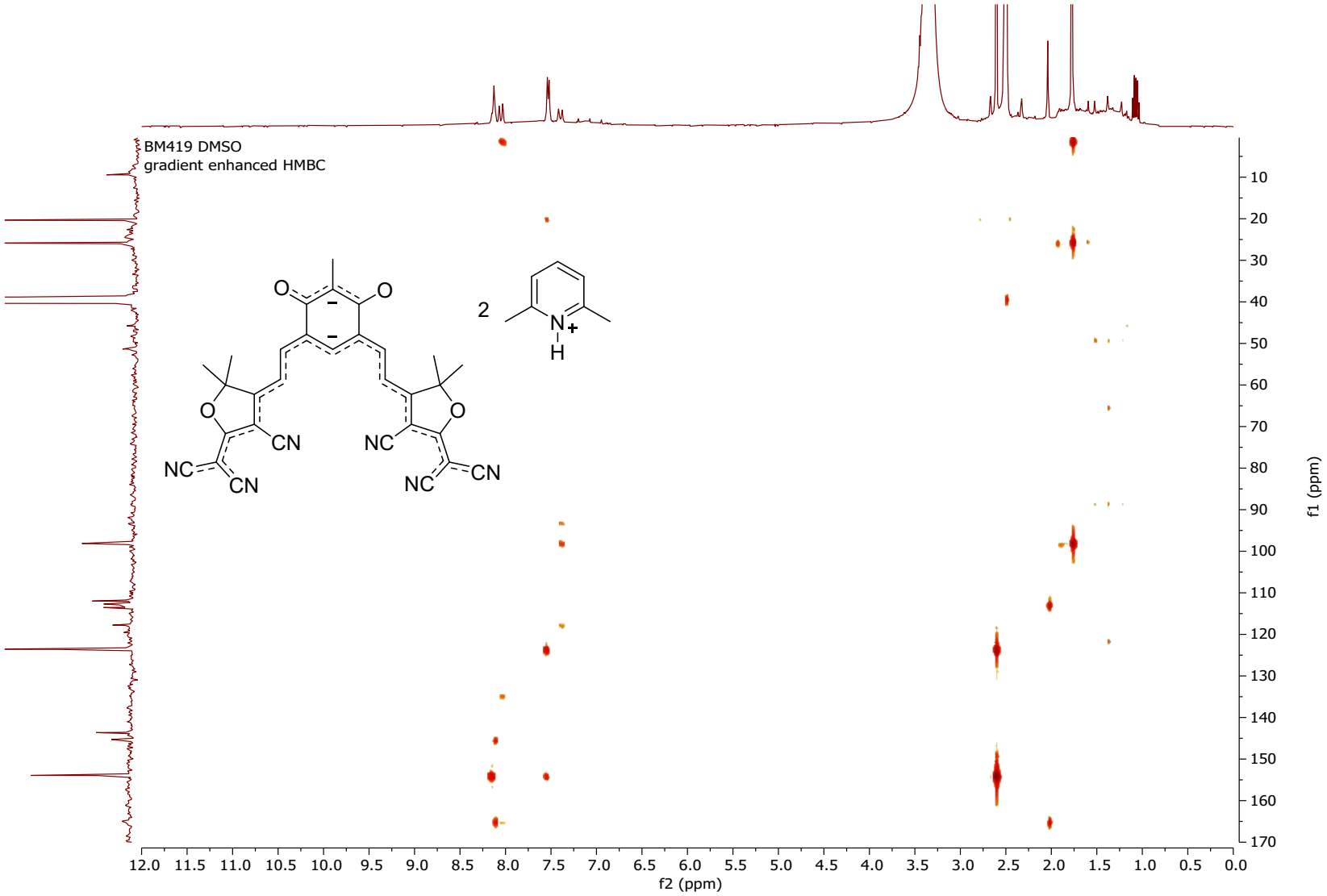

Figure S 27. HMBC NMR (DMSO-d_6) of compound **3b**.

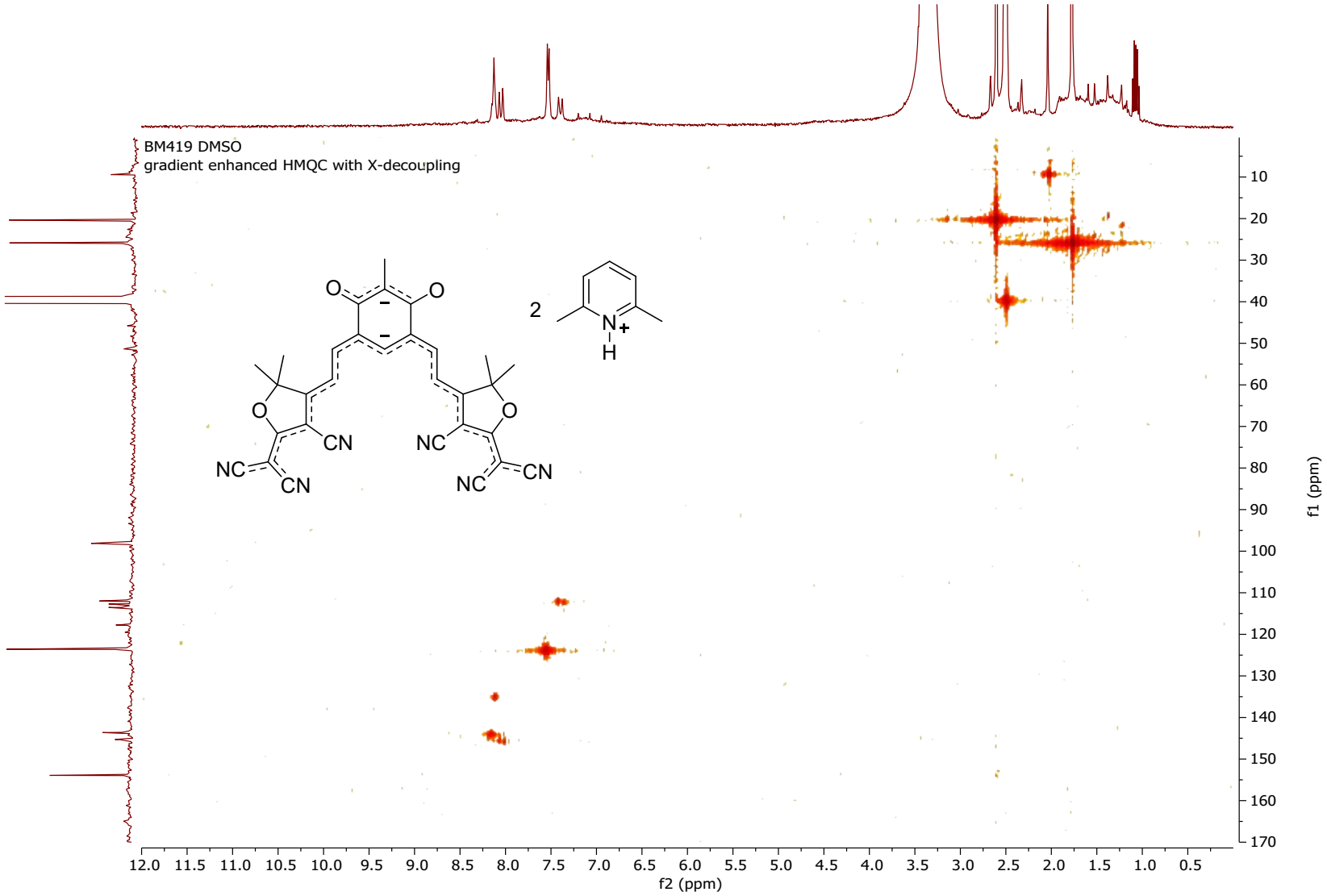

Figure S 28. HMQC NMR (DMSO-d_6) of compound **3b**.

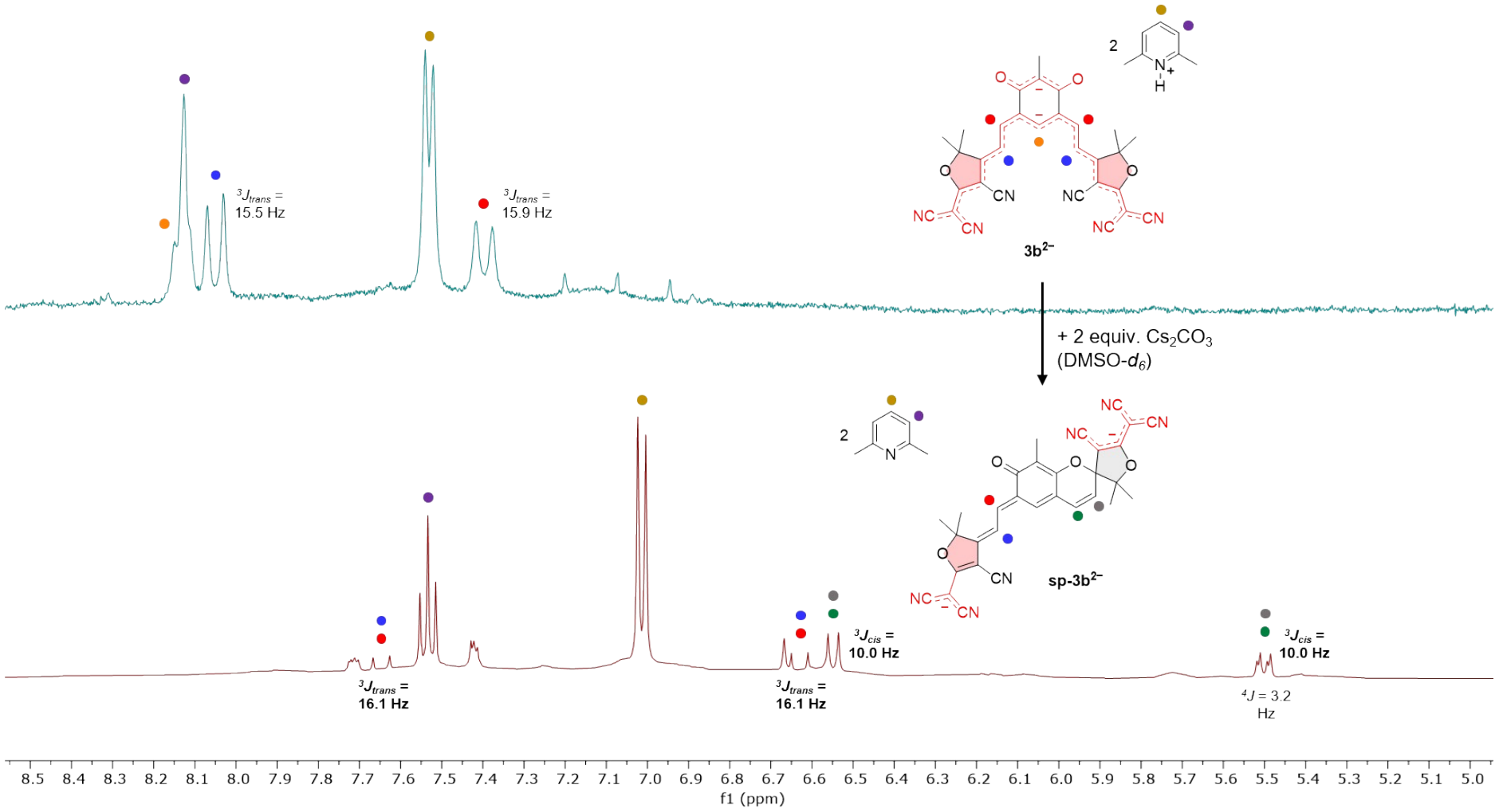

Figure S 29. ^{1}H NMR (400 MHz, DMSO-d_6) of compound **3b** before (top) and after (bottom) addition of 2 equivalents of Cs_2CO_3.

IV. MASS SPECTROMETRY

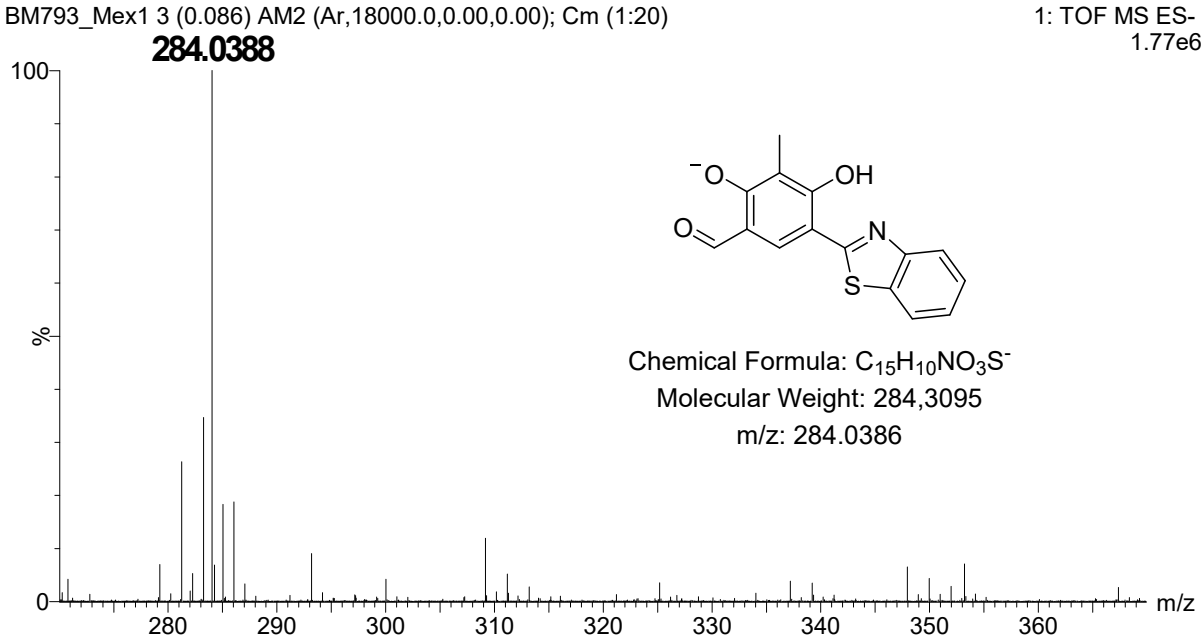

Figure S 30. HRMS spectrum of compound **1a**.

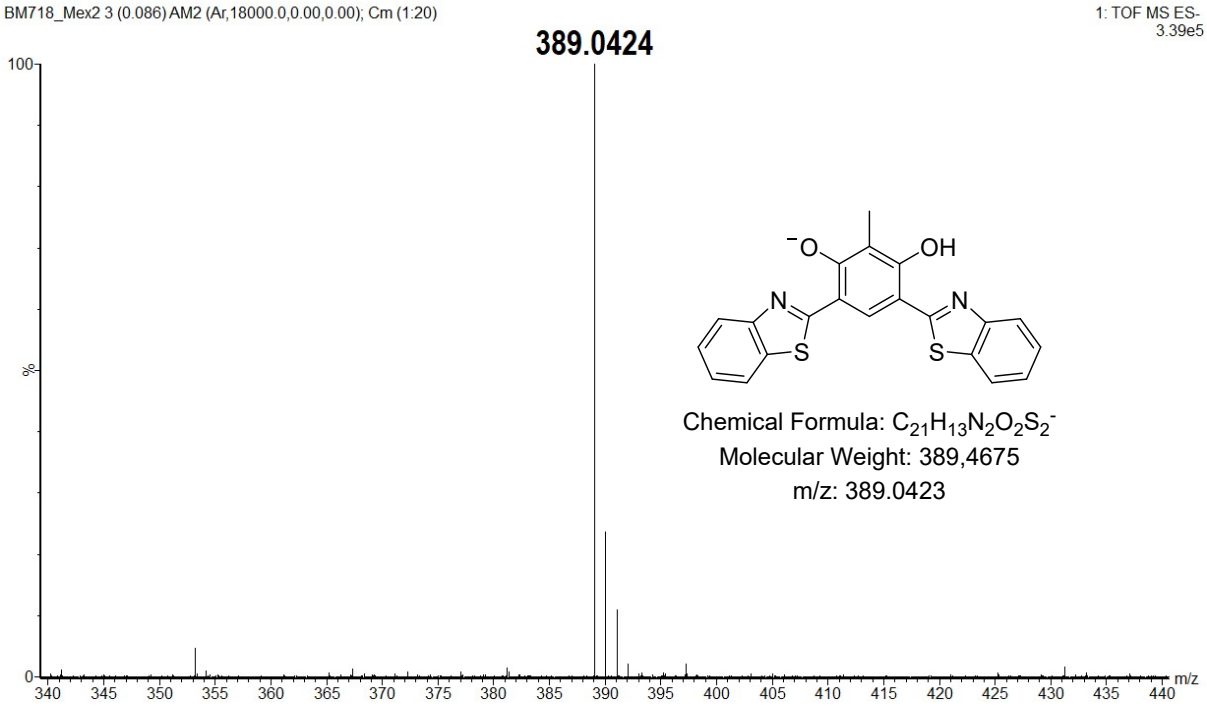

Figure S 31. HRMS spectrum of compound **1b**.

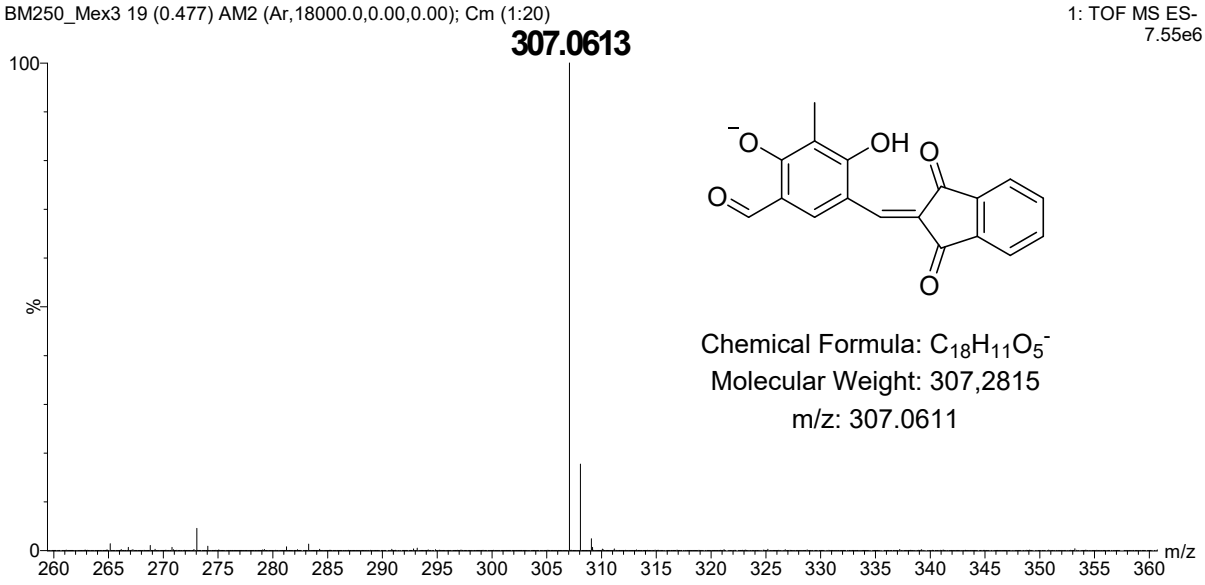

Figure S 32. HRMS spectrum of compound **2a**.

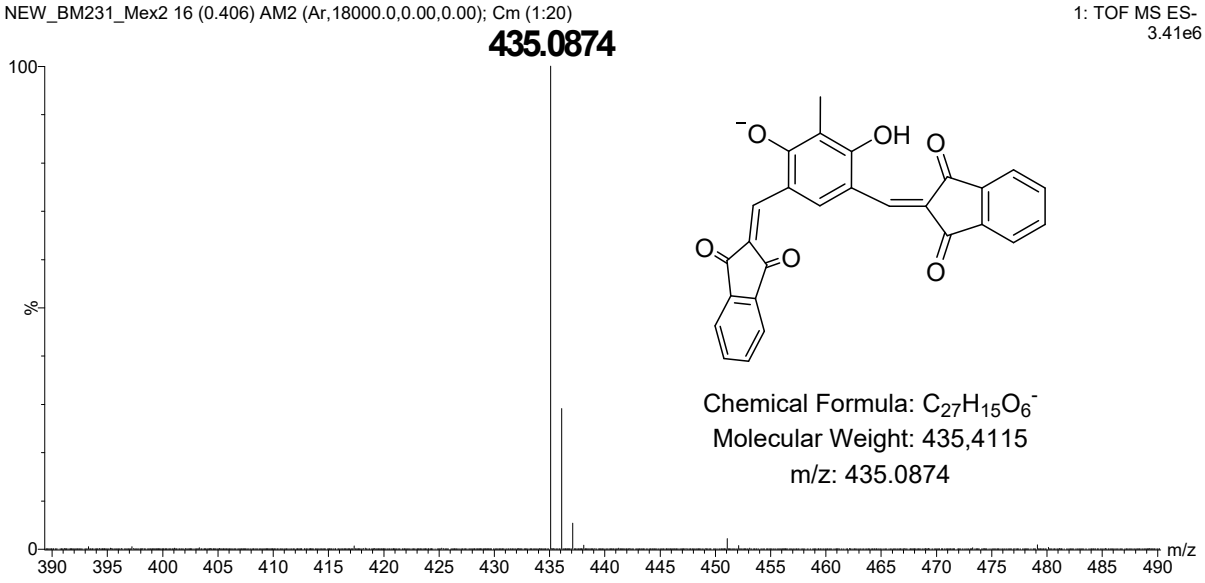

Figure S 33. HRMS spectrum of compound **2b**.

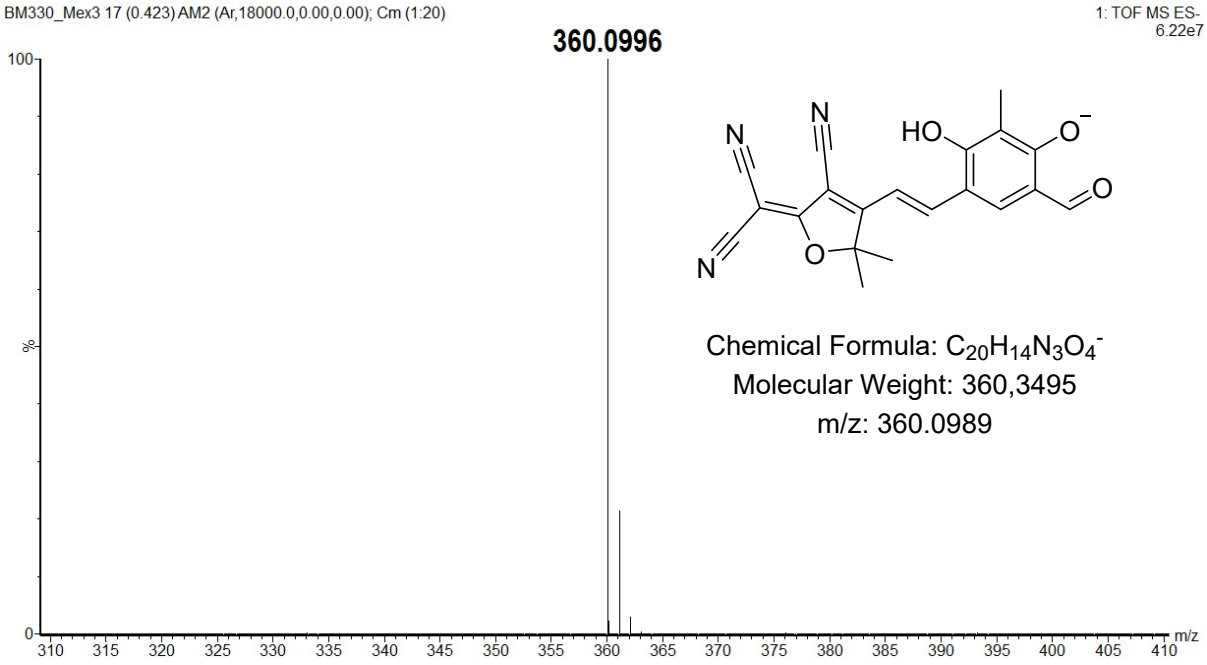

Figure S 34. HRMS spectrum of compound **3a**.

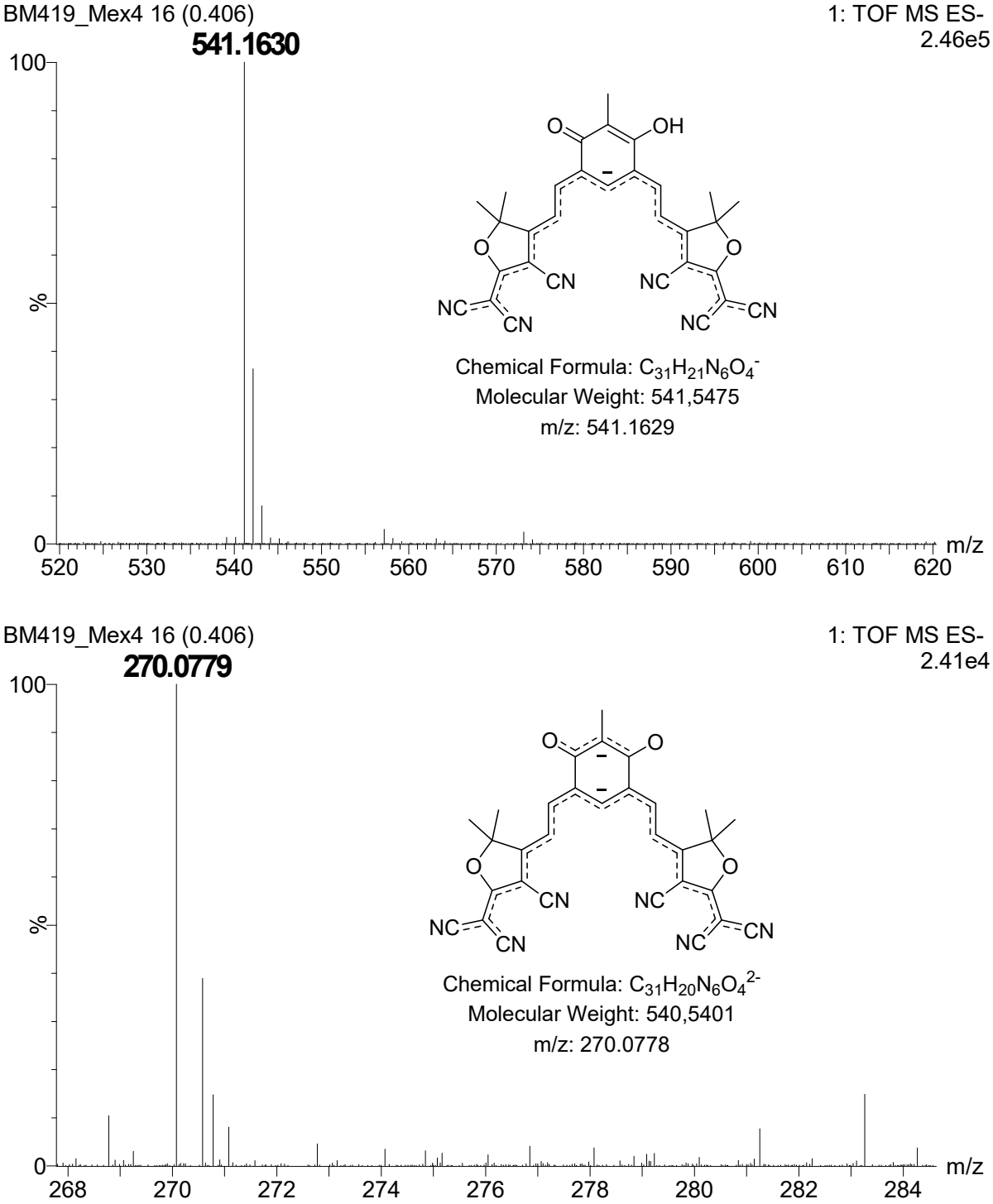

Figure S 35. HRMS spectrum of compound **3b** (top and bottom spectra correspond to a zoom on two different regions).

V. INFRARED SPECTRA

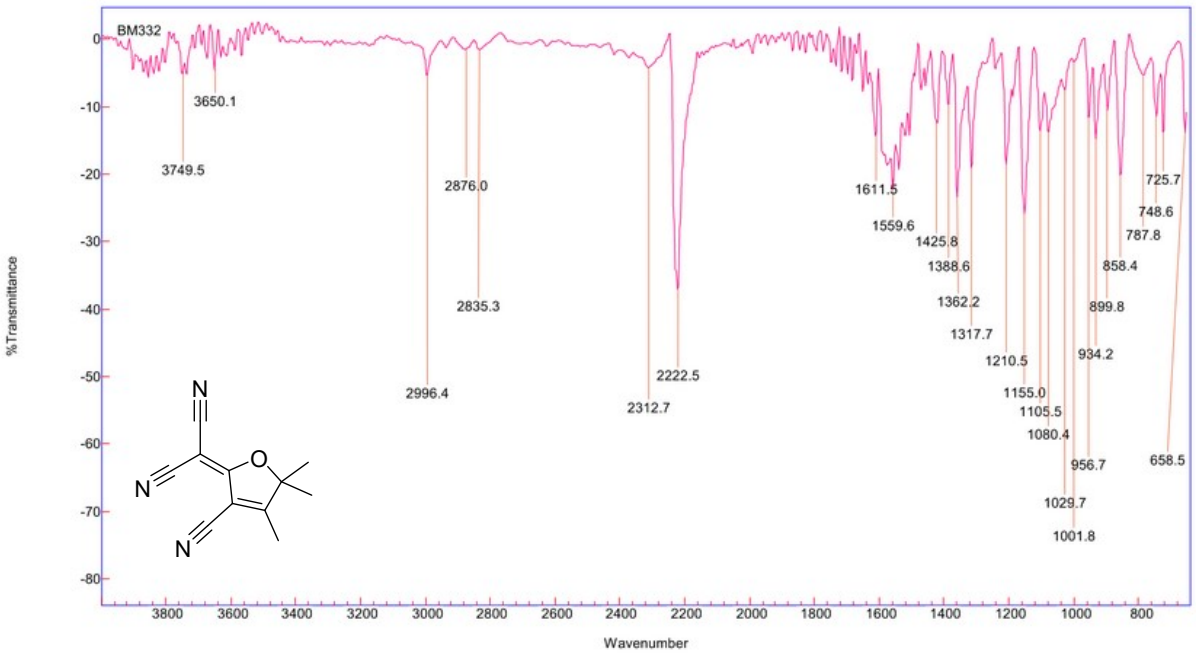

Figure S 36. Infrared spectrum of compound **5** (neat).

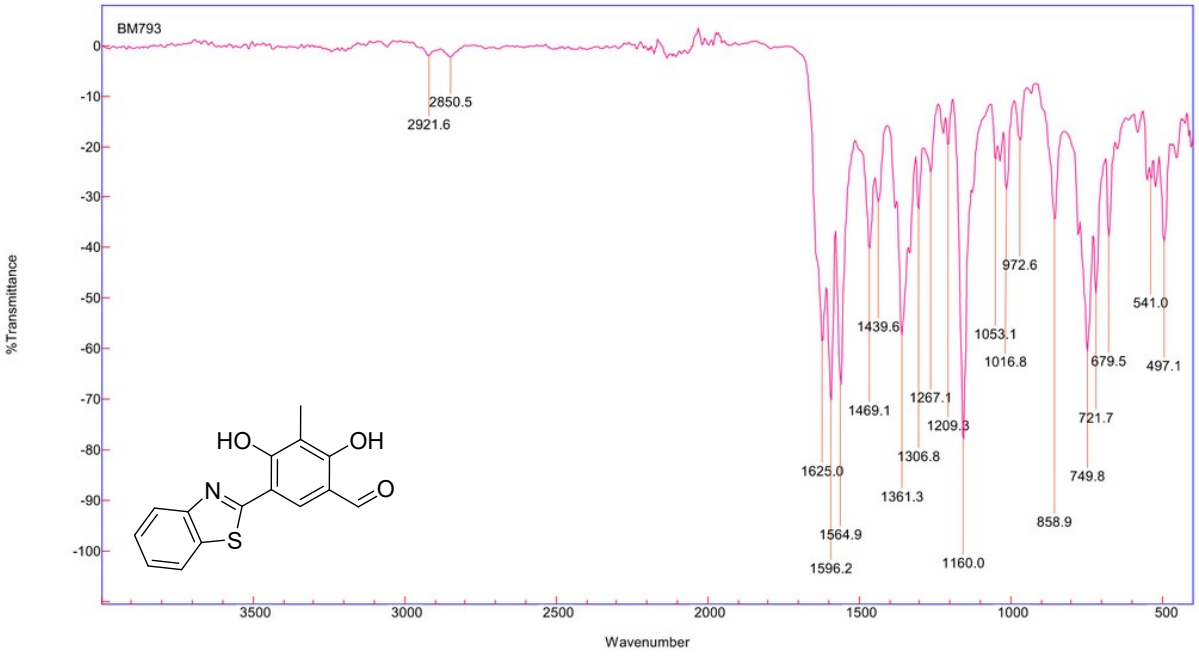

Figure S 37. Infrared spectrum of compound **1a** (neat).

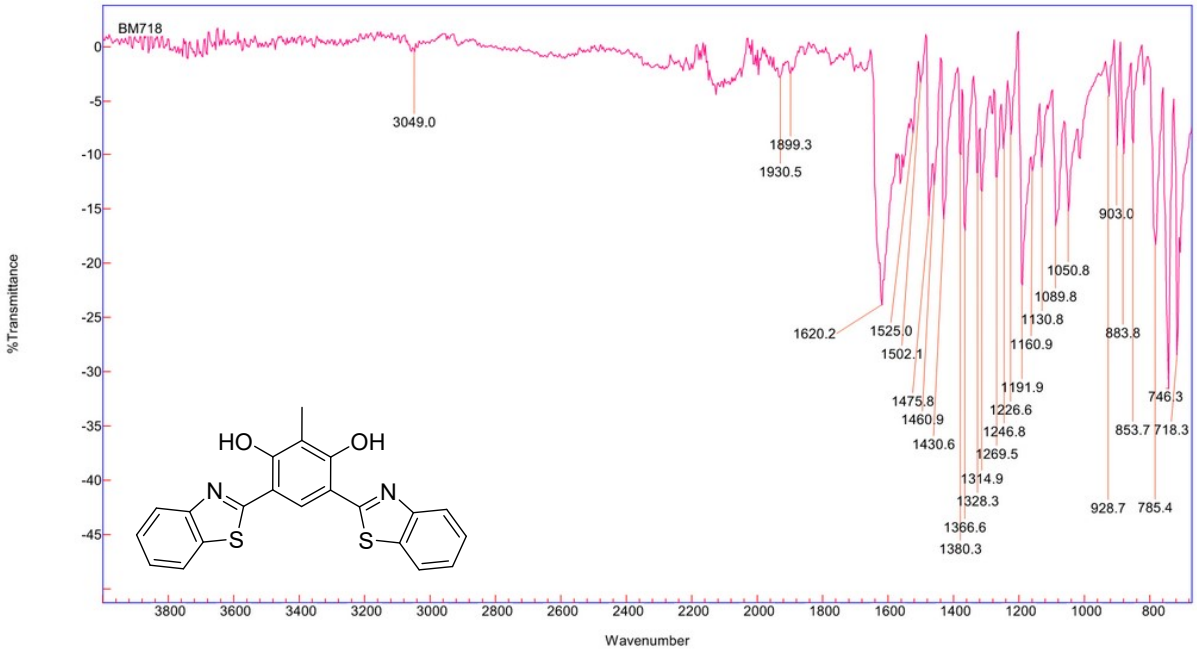

Figure S 38. Infrared spectrum of compound **1b** (neat).

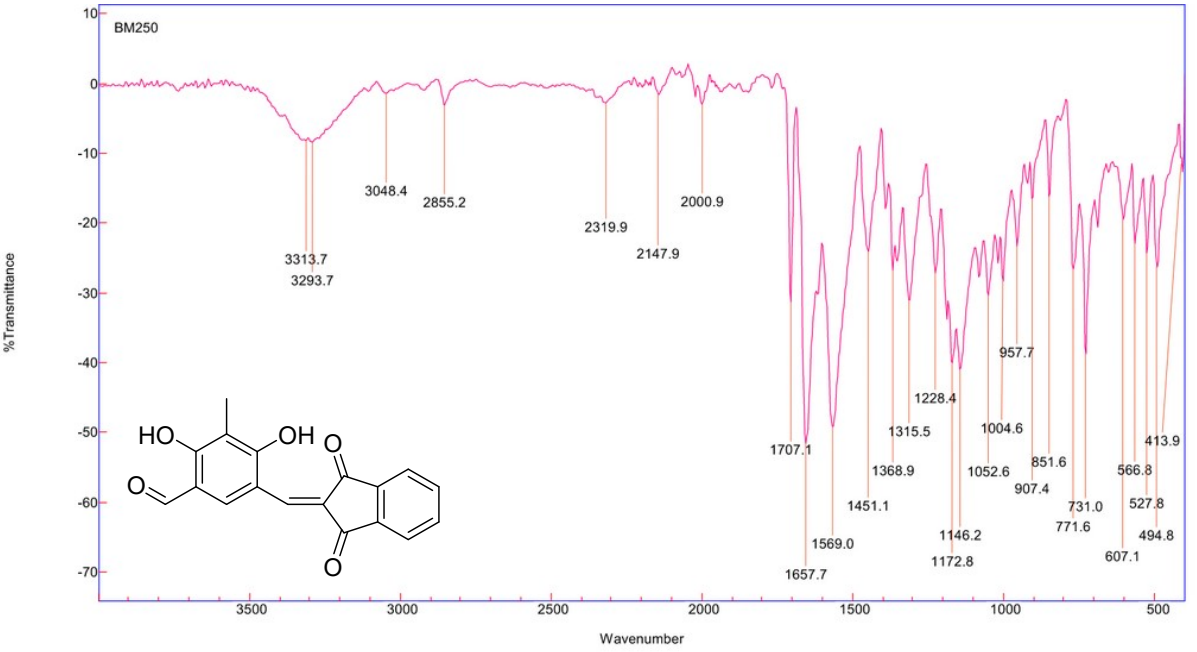

Figure S 39. Infrared spectrum of compound **2a** (neat).

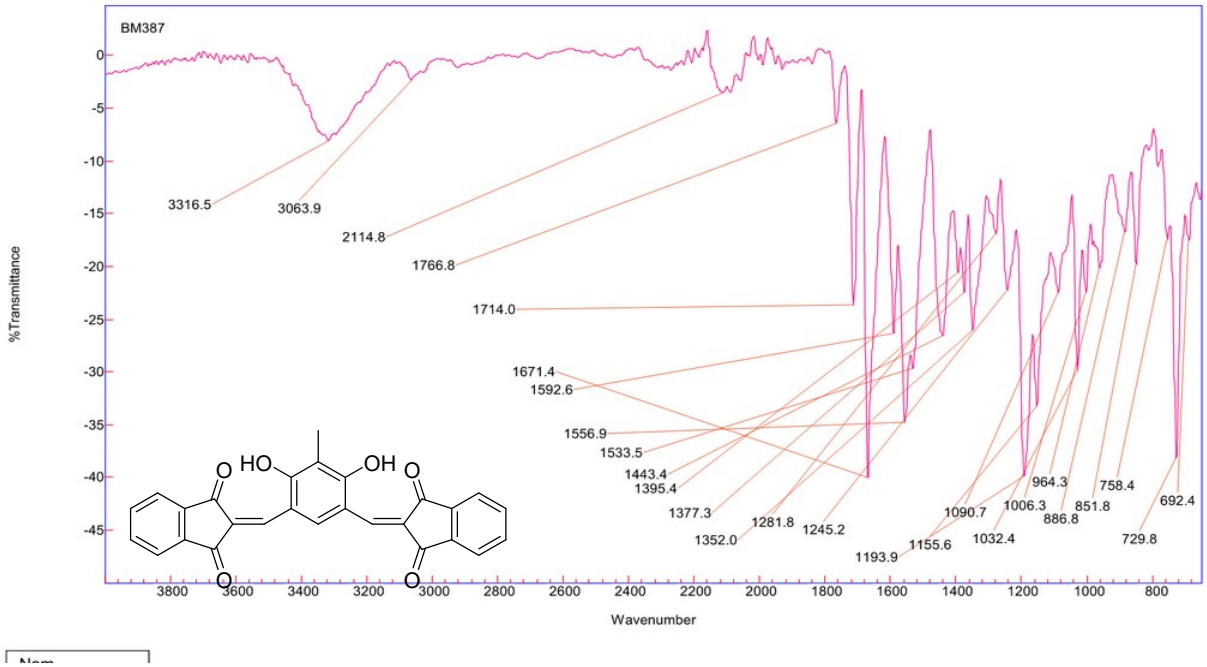

Figure S 40. Infrared spectrum of compound **2b** (neat).

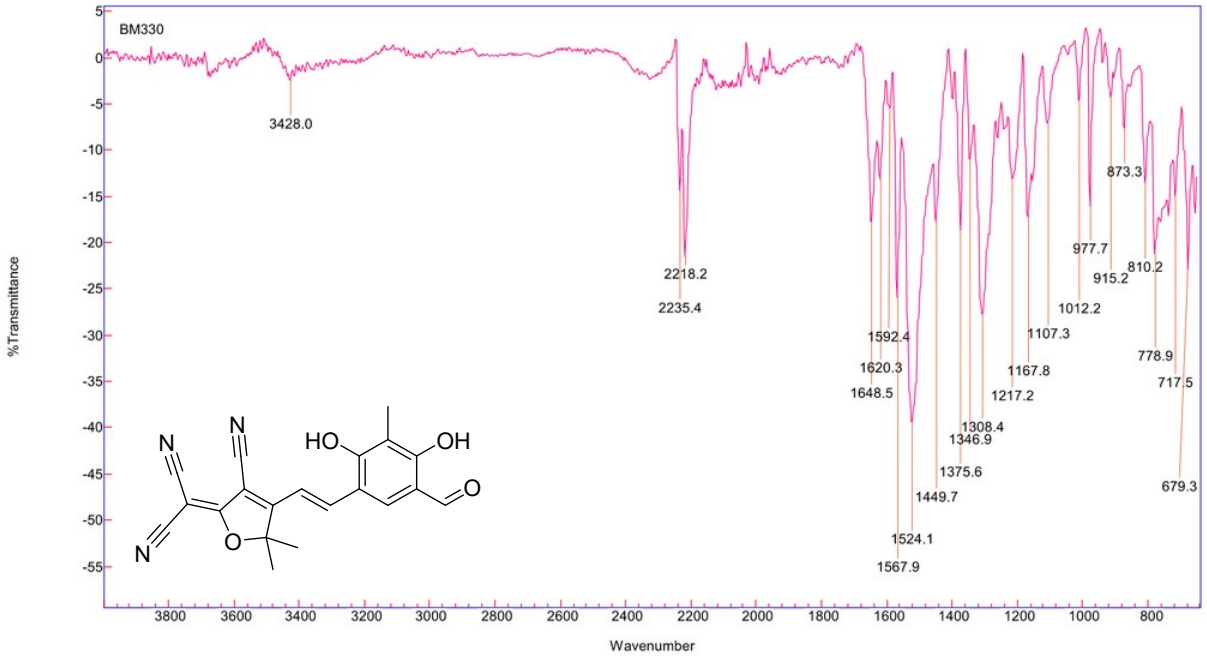

Figure S 41. Infrared spectrum of compound **3a** (neat).

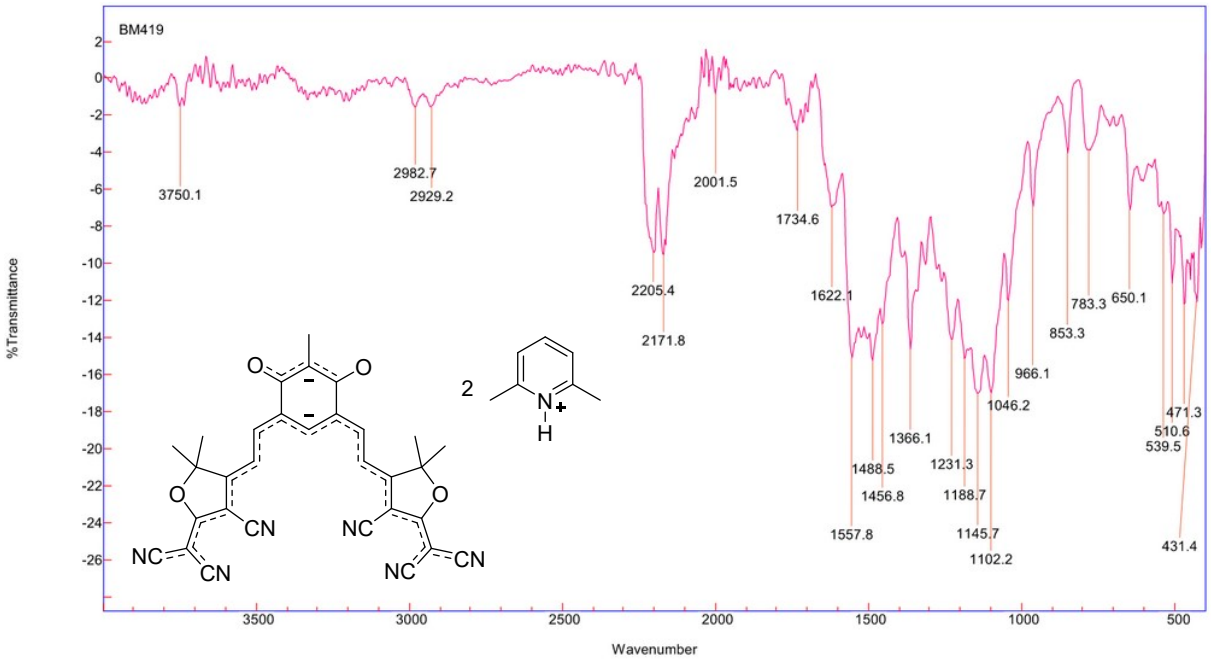

Figure S 42. Infrared spectrum of compound **3b** (neat).

VI. ADDITIONAL PHOTOPHYSICAL DATA

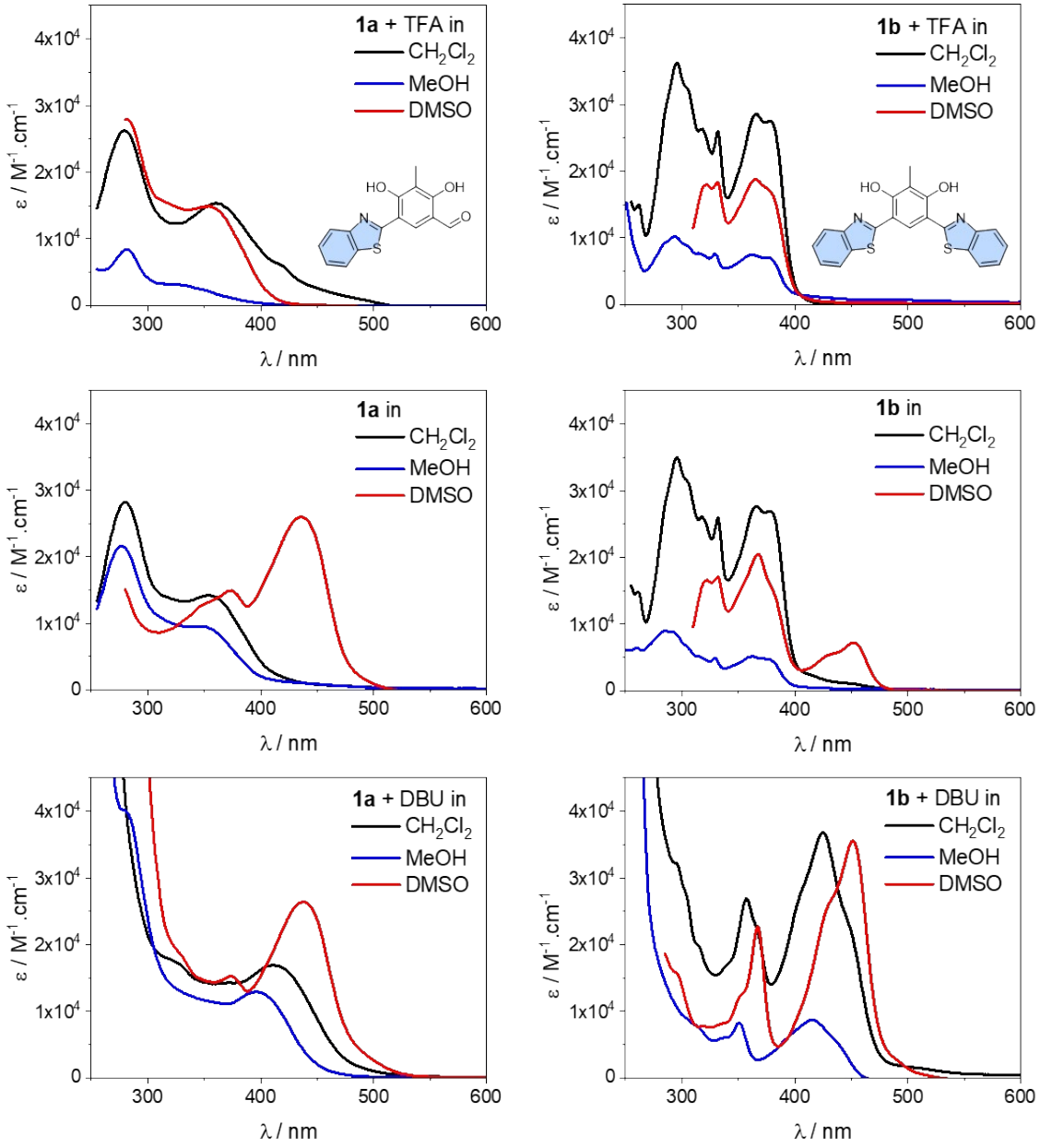

Figure S 43. UV-vis-NIR electronic absorption solvatochromism of **1a** (left column) and **1b** (right column) in acidic (0.1 M TFA), neutral or basic (0.1 M DBU) solvents.

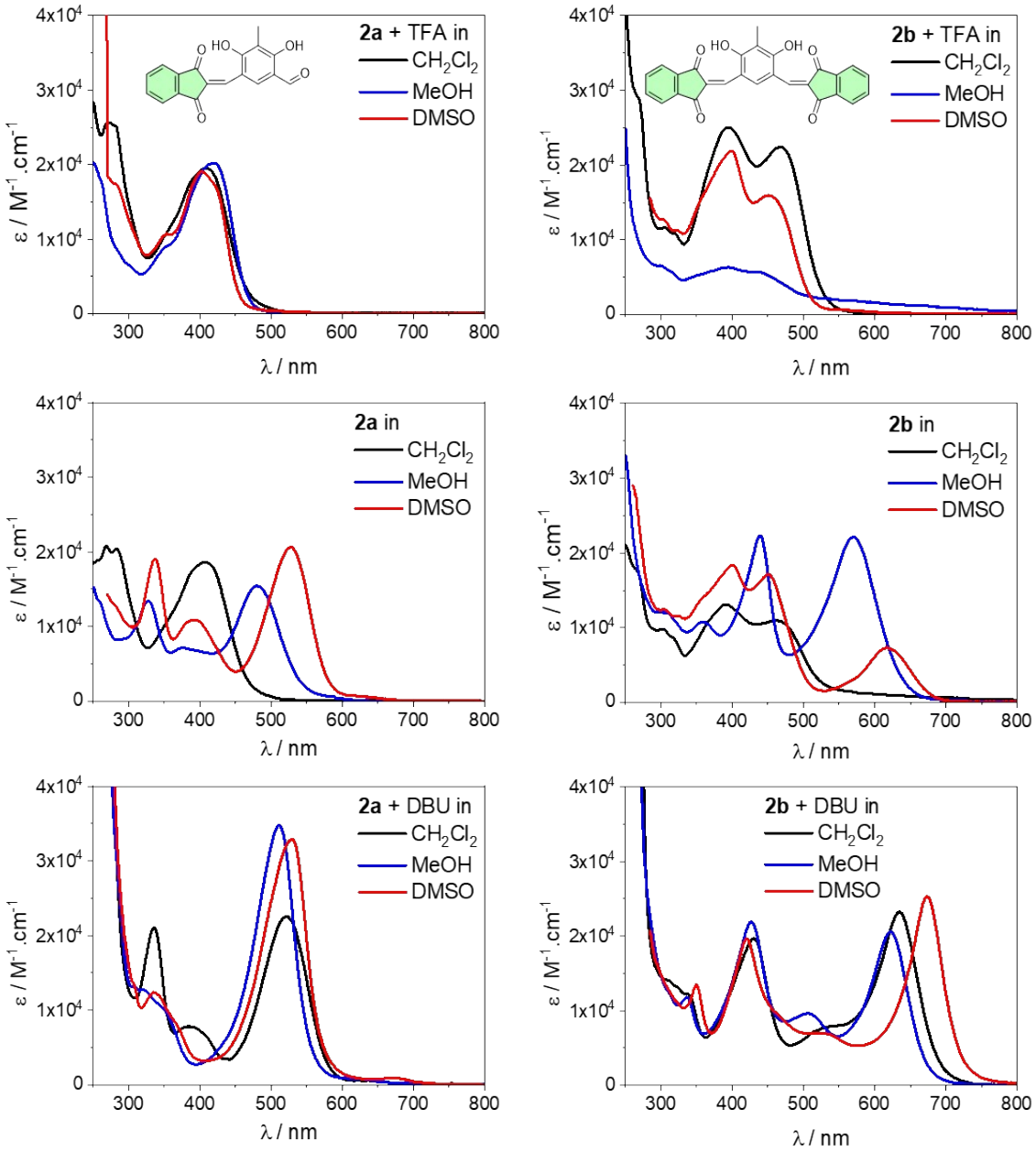

Figure S 44. UV-vis-NIR electronic absorption solvatochromism of **2a** (left column) and **2b** (right column) in acidic (0.1 M TFA), neutral or basic (0.1 M DBU) solvents.

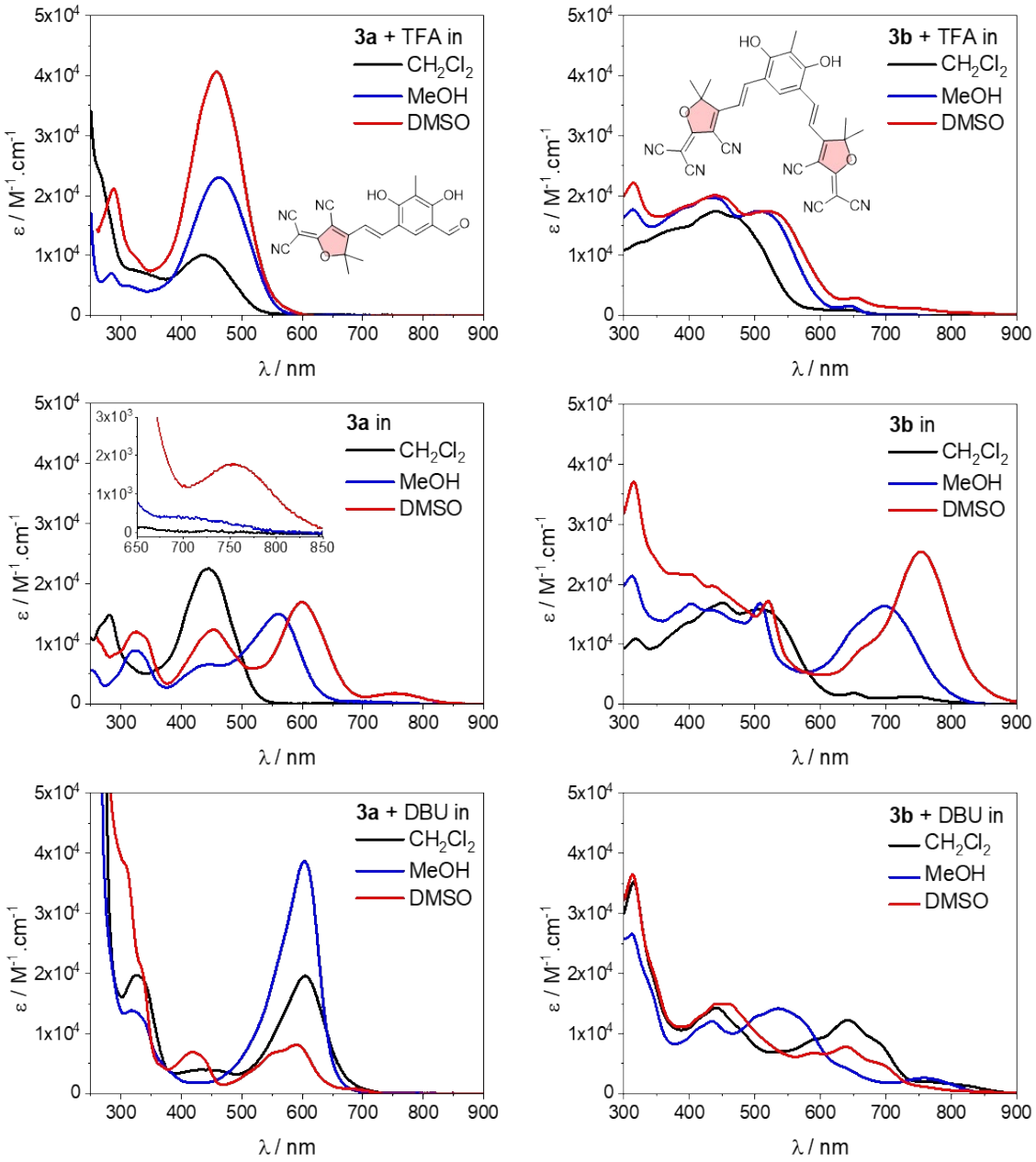

Figure S 45. UV-vis-NIR electronic absorption solvatochromism of **3a** (left column) and **3b** (right column) in acidic (0.1 M TFA), neutral or basic (0.1 M DBU) solvents.

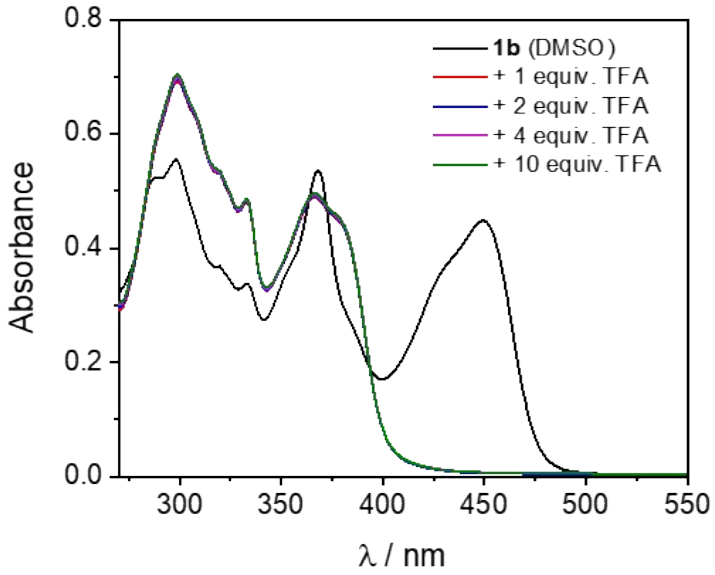

Figure S 46. Evolution of the UV-vis-NIR electronic absorption of **1b** in DMSO (2×10^{-5} M) upon addition titration with TFA.

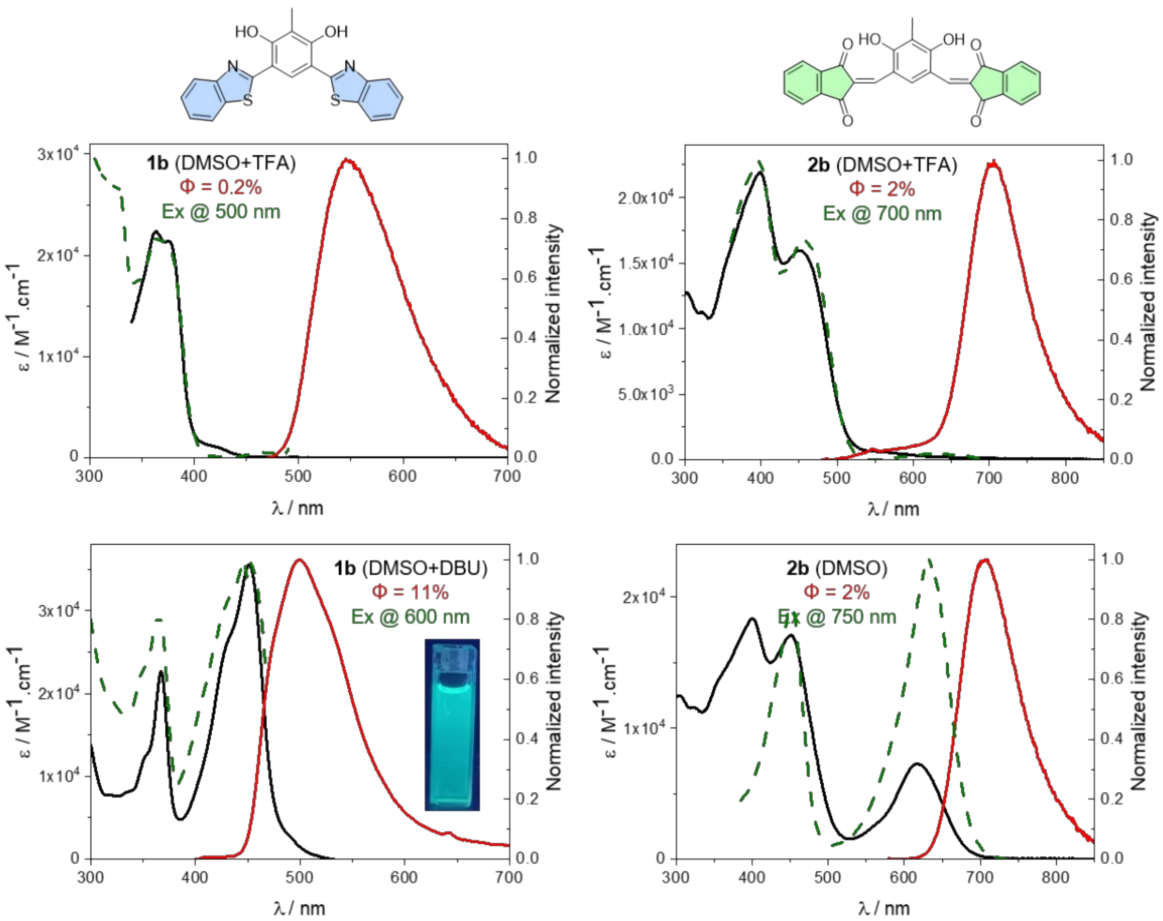

Figure S 47. Electronic absorption (black lines), normalized emission (red lines) and normalized excitation spectra (green dotted lines, with monitoring wavelength specified in green) of the emissive species in DMSO.

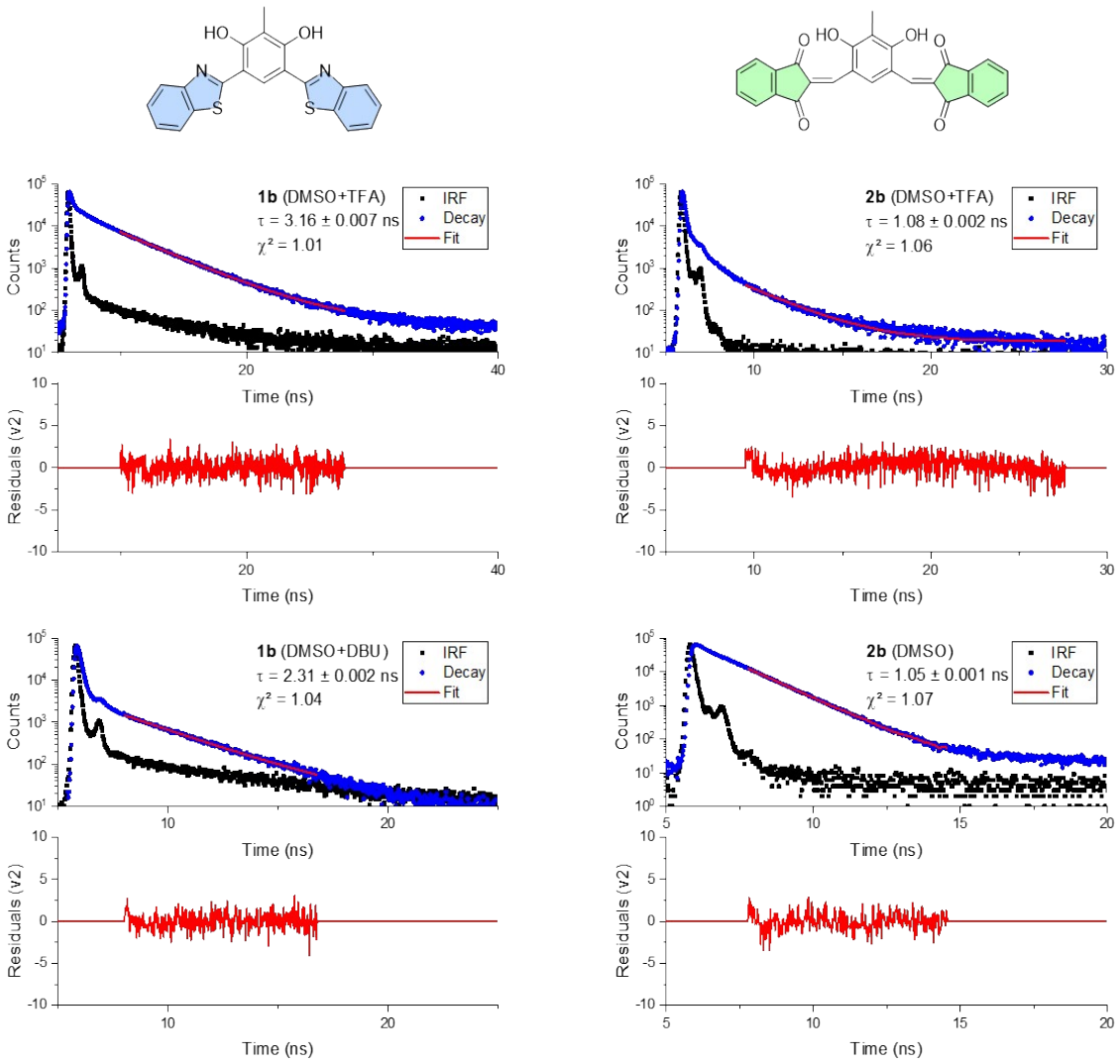

Figure S 48. Time-resolved fluorescence spectroscopy: instrument response function (IRF, black squares), measured fluorescence decay of the compound (blue squares), fit and residuals (red lines). Note: all the measurements were fitted with single exponential decays.

VII. THEORETICAL CALCULATIONS

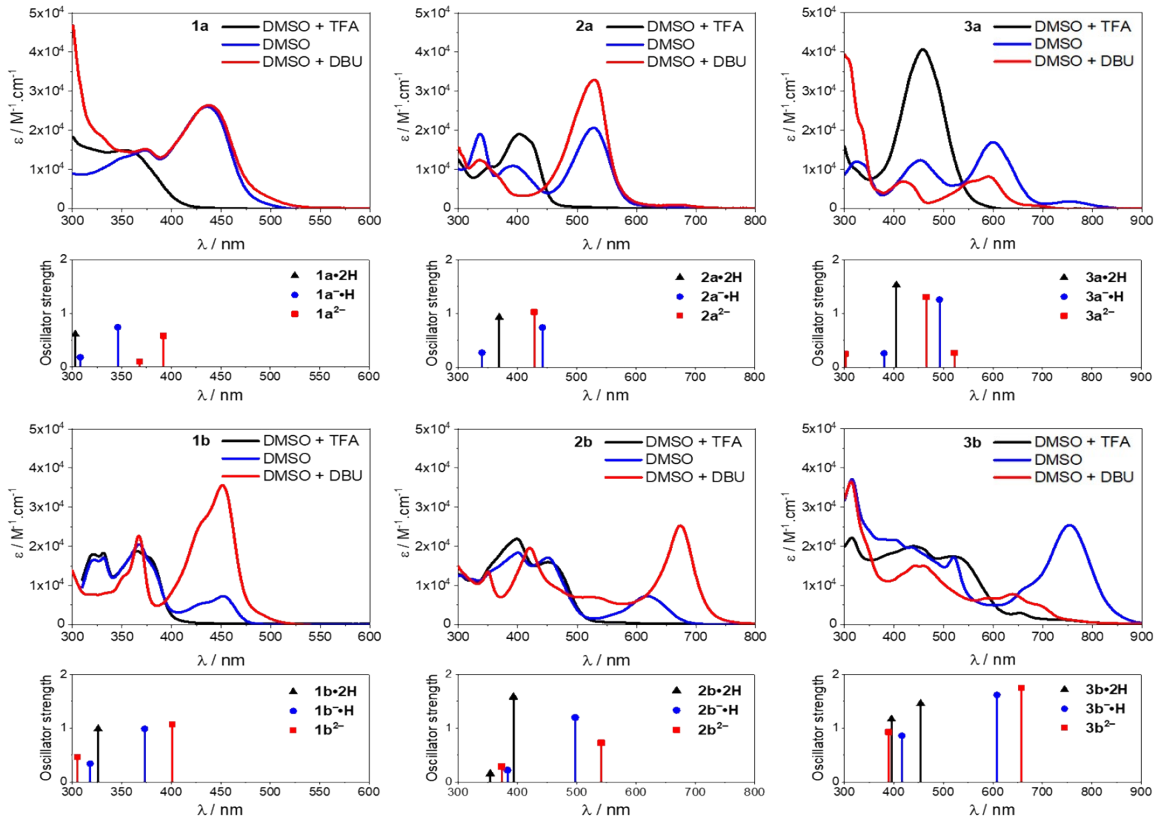

Figure S 49. UV-vis-NIR electronic absorption spectra of mono-condensed (top row) and bis-condensed dyes (bottom row) dissolved at *ca.* 2×10^{-5} M in acidic (0.1 M TFA), neutral or basic (0.1 M DBU) DMSO. Below each experimental UV-vis-NIR computed excitations are presented. These sticks are corresponding to the vertical transitions computed for each relevant protonation state.

Table S 1. Experimental electronic absorption in DMSO and theoretical vertical transition wavelengths computed at cLR[2] level with the corresponding oscillator strength and CC2 corrections (when available) for the most important excited states. TD-DFT energies and oscillator strengths are extracted from the most stable isomers unless differently specified. CC2 corrections (as well as EDD plots, and main orbitals with threshold of isosurface 0.001 and 0.03 respectively, see below) are computed for the most stable isomers.

Experimental			Theoretical			
Dyes	Conditions[a]	λ_{max}^{exp} [nm] (ε [M^{-1}cm^{-1}])	Species	State	$\lambda_{vert-abs}^{theo}$ [nm] (f)[b]	$\lambda_{vert-abs}^{theo}$ [nm][c]
	DMSO/TFA	355 (14700) 282 (28000)	**1a•2H**	1 3 5	303 (0.61) 285 (0.28) 256 (0.75)	315 277
1a	DMSO	436 (26000) 374 (14900)	**1a^{-}•H**	1 2 3	346 (0.74)[d] 308 (0.18)[d] 291 (0.15)[d]	374[d]
	DMSO/DBU	438 (26400) 374 (15200)	**1a^{2-}**	1 2 4	392 (0.58) 368 (0.10) 295 (0.61)	n.d.
	DMSO/TFA	378 (sh, 17000) 364 (18800) 331 (18300)	**1b•2H**	1 2 3	326 (0.99) 294 (0.34) 271 (0.39)	342 304 284
1b	DMSO	452 (7200) 430 (sh, 5400) 367 (20500)	**1b^{-}•H**	1 2 4	373 (0.99) 318 (0.34) 280 (0.39)	409
	DMSO/DBU	451 (35600) 430 (sh, 26400) 367 (22400)	**1b^{2-}**	1 3 5	401 (1.07) 305 (0.47) 291 (0.54)	n.d.
	DMSO/TFA	402 (19000) 350 (sh, 10700)	**2a•2H**	1	369 (0.93)	400
2a	DMSO	527 (20600) 391 (10900) 336 (18900)	**2a^{-}•H**	1 5	442 (0.74) 340 (0.27)	504
	DMSO/DBU	529 (33000) 336 (12300)	**2a^{2-}**	2	428 (1.03)	n.d.
	DMSO/TFA	452 (16000) 398 (21900)	**2b•2H**	1 5	393 (1.58) 354 (0.15)	431 387
2b	DMSO	617 (7400) 452 (17100) 400 (18200)	**2b^{-}•H**	1 2 3	497 (1.20) 383 (0.22) 367 (0.39)	573 378 366
	DMSO/DBU	674 (25400) 534 (7000) 421 (19700)	**2b^{2-}**	1 5 8	541 (0.73) 373 (0.28) 337 (0.52)	n.d.
	DMSO/TFA	459 (40800) 288 (21200)	**3a•2H**	1	405 (1.53)[d]	406
3a	DMSO	755 (1700) 600 (17000) 453 (12400)	**3a^{-}•H**	1 2 5 6	492 (1.26)[d] 380 (0.26)[d] 289 (0.18)[d] 267 (0.19)[d]	557 417
	DMSO/DBU	595 (8300) 420 (7200)	**3a^{2-}**	1 2 6	522 (0.27)[d] 465 (1.31)[d] 302 (0.25)[d]	n.d.
3b	DMSO/TFA	654 (2900) 523 (17300) 441 (20000)	**3b•2H**	1 2 3	454 (1.46)[d] 395 (1.17)[d] 336 (0.29)[d]	467 423

DMSO	754 (25500) 660 (sh, 9100) 521 (17000)	**3b⁻•H**	1 2	608 (1.62)[d] 416 (0.86)	n.d.
DMSO/DBU	690 (sh, 5000) 638 (7800) 591 (6800)	**3b²⁻**	1 4	657 (1.75)[d] 389 (0.93)[d]	n.d.
		sp-3b²⁻	1 2 3	527 (1.42)[d] 391 (0.33)[d] 357 (0.06)[d]	n.d.
		dsp-3b²⁻	1 2 3	297 (0.03) 291 (0.91) 289 (0.11)	n.d.

[a] Pure DMSO or mixture of DMSO + 0.1 M TFA or DBU. [b] Calculated at the cLR² level. [c] Calculated at the cLR² level with CC2 corrections. [d] Computed as the Boltzmann average of the most stable isomers. sh: shoulder. n.d.: not determined.

Table S 2. Theoretical absorption and emission wavelengths extracted from vibrationally resolved spectra computed at cLR²+CC2 level (when available), for neutral and anionic forms. The spectra are obtained from the most stable isomers.

	Absorption	Emission
Species	λ_{abs}^{theo} [nm] (ε [$M^{-1}cm^{-1}$])	λ_{fluo}^{theo} [nm]
1a•2H	317 (24422)	n.d.
1a⁻•H	383 (29142)	n.d.
1b•2H	358 (40635)	n.d.
1b⁻•H	438 (48350)	n.d.
2a•2H	431 (38884)	n.d.
2a⁻•H	530 (36940)	n.d.
2b•2H	466 (69534)	526
2b⁻•H	611 (68802)	n.d.
3a•2H	449 (62557)	n.d.
3a⁻•H	554 (78377)	n.d.
3b•2H	498 (48691)	761
3b⁻•H	790 (39345)	681

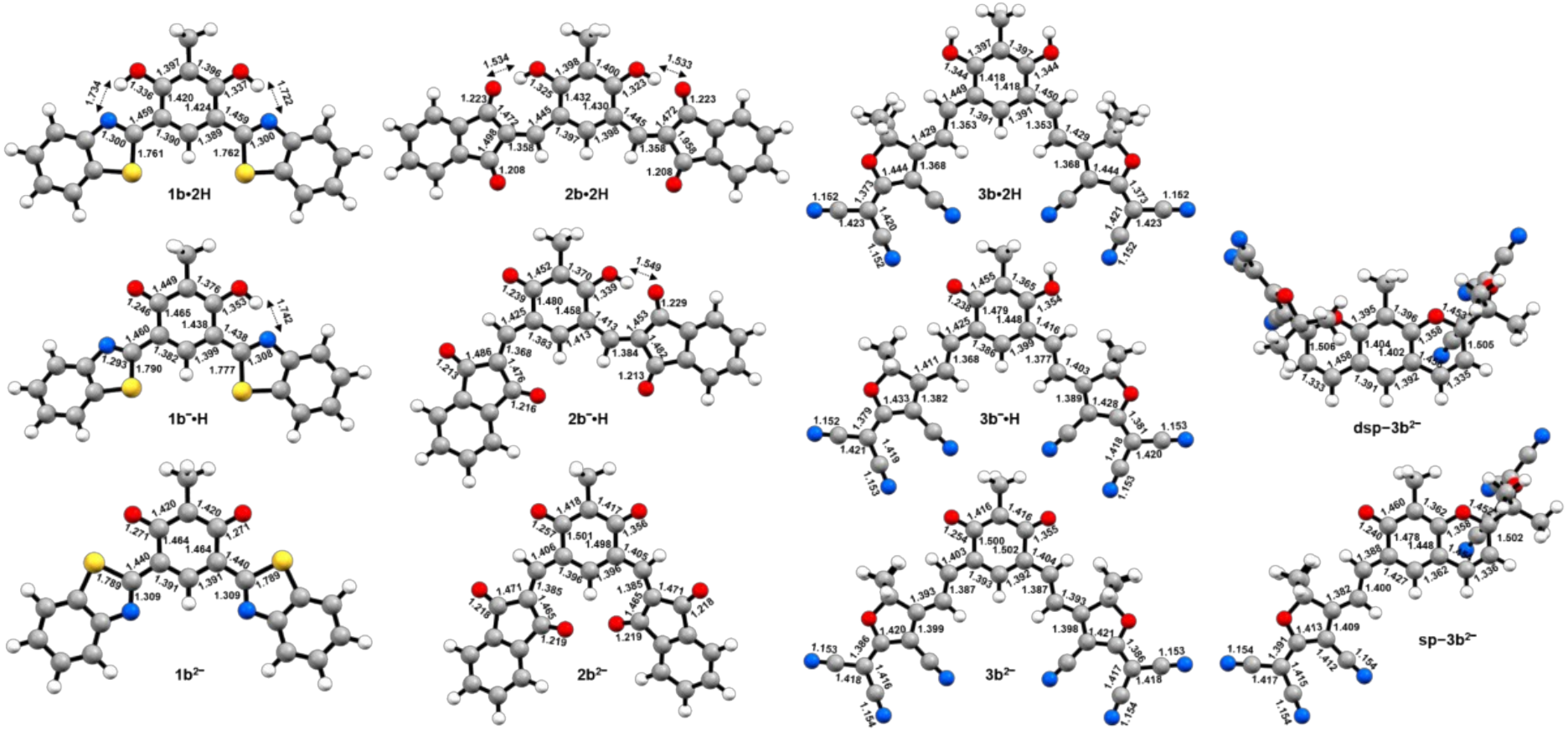

Figure S 50. DFT optimized geometries of the most stable structures.

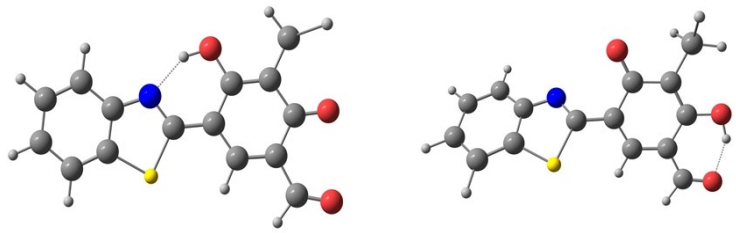

Isomer a
ΔG = 0.10 kcal/mol

Isomer b
ΔG =0.00 kcal/mol

Figure S 51. Schematic representation of the most significant isomers of **1a^{-}•H**.

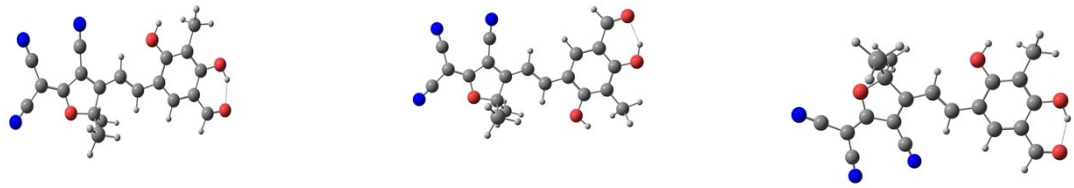

Isomer a
ΔG = 0.00 kcal/mol

Isomer b
ΔG = 0.29 kcal/mol

Isomer c
ΔG = 0.68 kcal/mol

Figure S 52. Schematic representation of the most significant isomers of **3a•2H**.

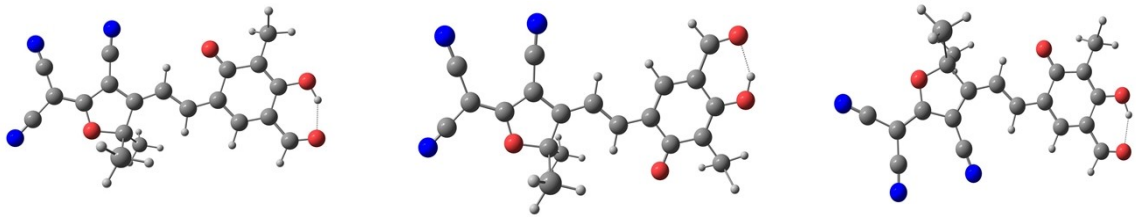

Isomer a
ΔG = 0.21 kcal/mol

Isomer b
ΔG = 0.25 kcal/mol

Isomer c
ΔG = 0.00 kcal/mol

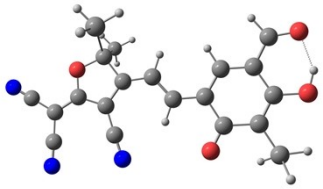

Isomer d
ΔG = 1.25 kcal/mol

Figure S 53. Schematic representation of the most significant isomers of **3a^{-}•H**.

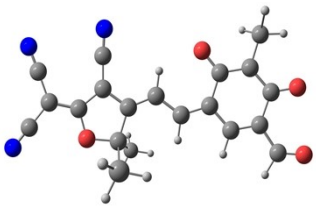

Isomer a
ΔG = 0.89 kcal/mol

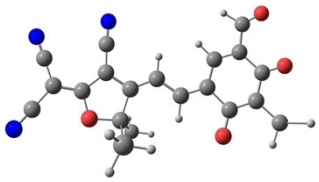

Isomer b
ΔG = 0.48 kcal/mol

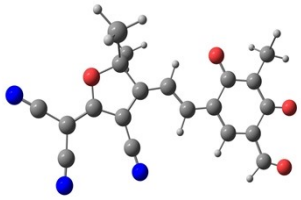

Isomer c
ΔG = 0.00 kcal/mol

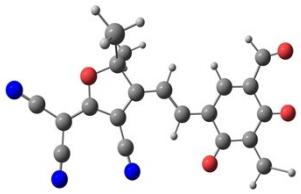

Isomer d
ΔG = 0.97 kcal/mol

Figure S 54. Schematic representation of the most significant isomers of **3a**$^{2-}$.

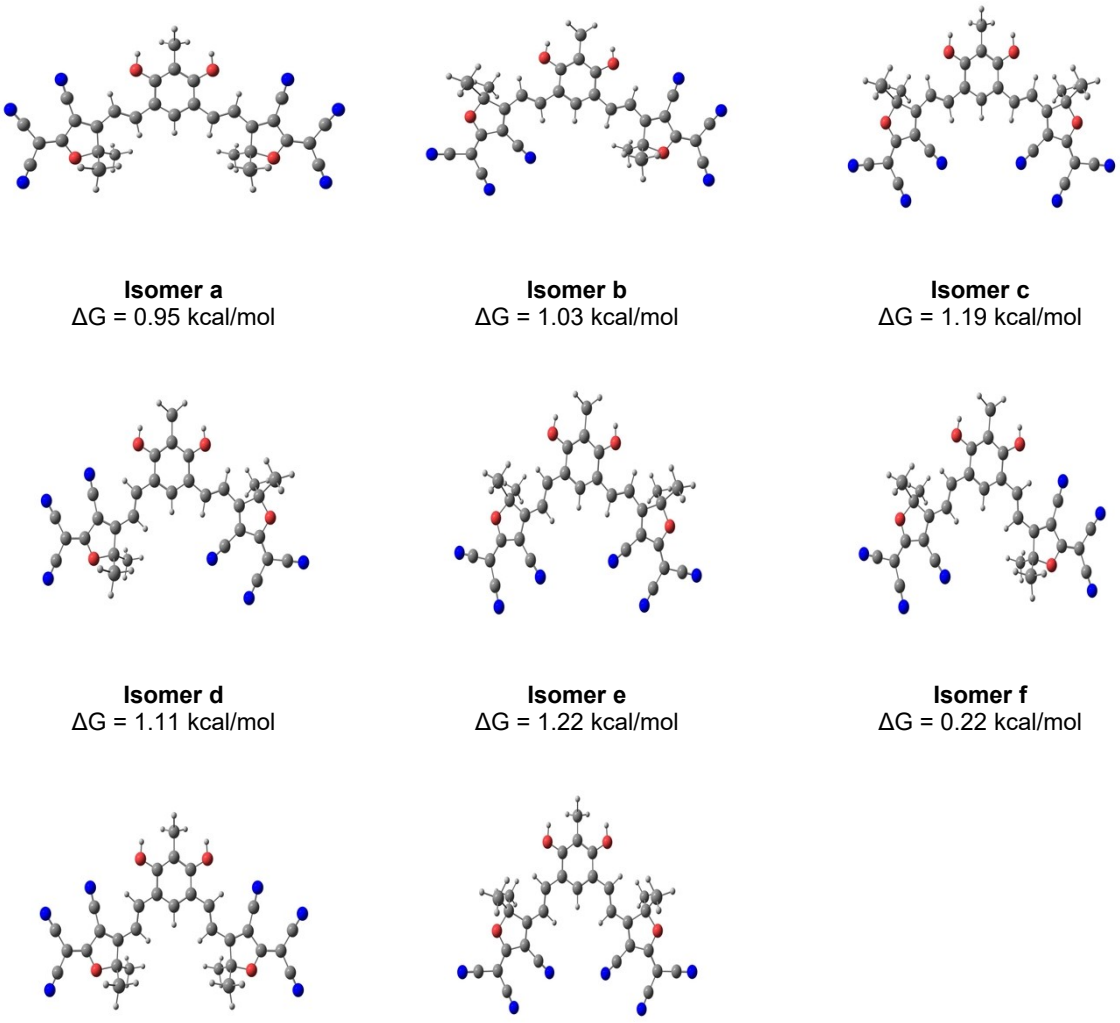

Isomer a
ΔG = 0.95 kcal/mol

Isomer b
ΔG = 1.03 kcal/mol

Isomer c
ΔG = 1.19 kcal/mol

Isomer d
ΔG = 1.11 kcal/mol

Isomer e
ΔG = 1.22 kcal/mol

Isomer f
ΔG = 0.22 kcal/mol

Isomer g
ΔG = 0.94 kcal/mol

Isomer h
ΔG = 0.00 kcal/mol

Figure S 55. Schematic representation of the most significant isomers of **3b•2H**.

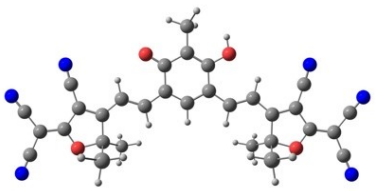

Isomer a
ΔG = 0.42 kcal/mol

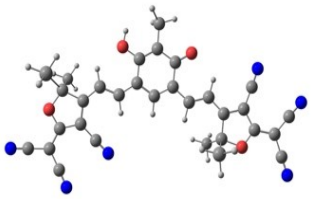

Isomer b
ΔG = 1.55 kcal/mol

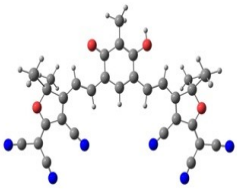

Isomer c
ΔG = 1.72 kcal/mol

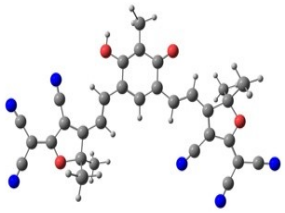

Isomer d
ΔG = 1.78 kcal/mol

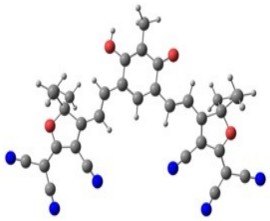

Isomer e
ΔG = 1.35 kcal/mol

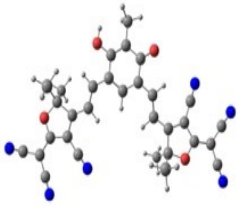

Isomer f
ΔG = 0.56 kcal/mol

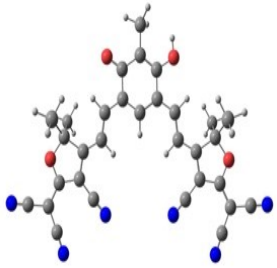

Isomer g
ΔG = 0.00 kcal/mol

Figure S 56. Schematic representation of the most significant isomers of **3b^{-}•H**.

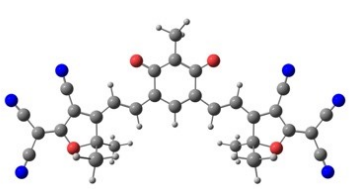

Isomer a
ΔG = 1.75 kcal/mol

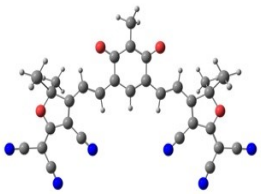

Isomer b
ΔG = 1.64 kcal/mol

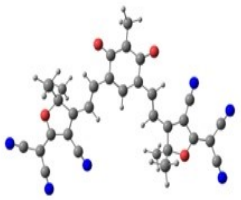

Isomer c
ΔG = 1.12 kcal/mol

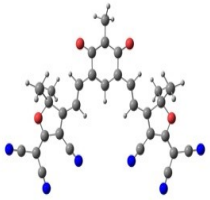

Isomer d
ΔG = 0.00 kcal/mol

Figure S 57. Schematic representation of the most significant isomers of **3b**$^{2-}$.

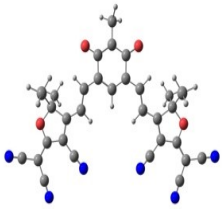

Isomer d
ΔG = 13.6 kcal/mol

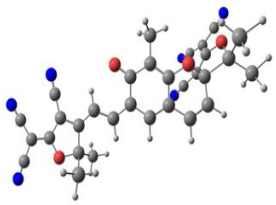

Isomer e
ΔG = 6.5 kcal/mol

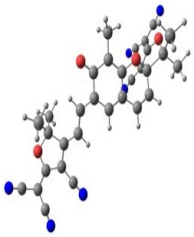

Isomer f
ΔG = 5.2 kcal/mol

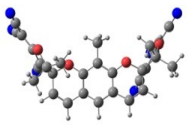

Isomer g
ΔG = 0.00 kcal/mol

Figure S 58. Schematic representation of the most significant isomers of **3b**$^{2-}$ by including the spyrociclic forms. The isomer d corresponds to the most stable analogue from Figure S57.

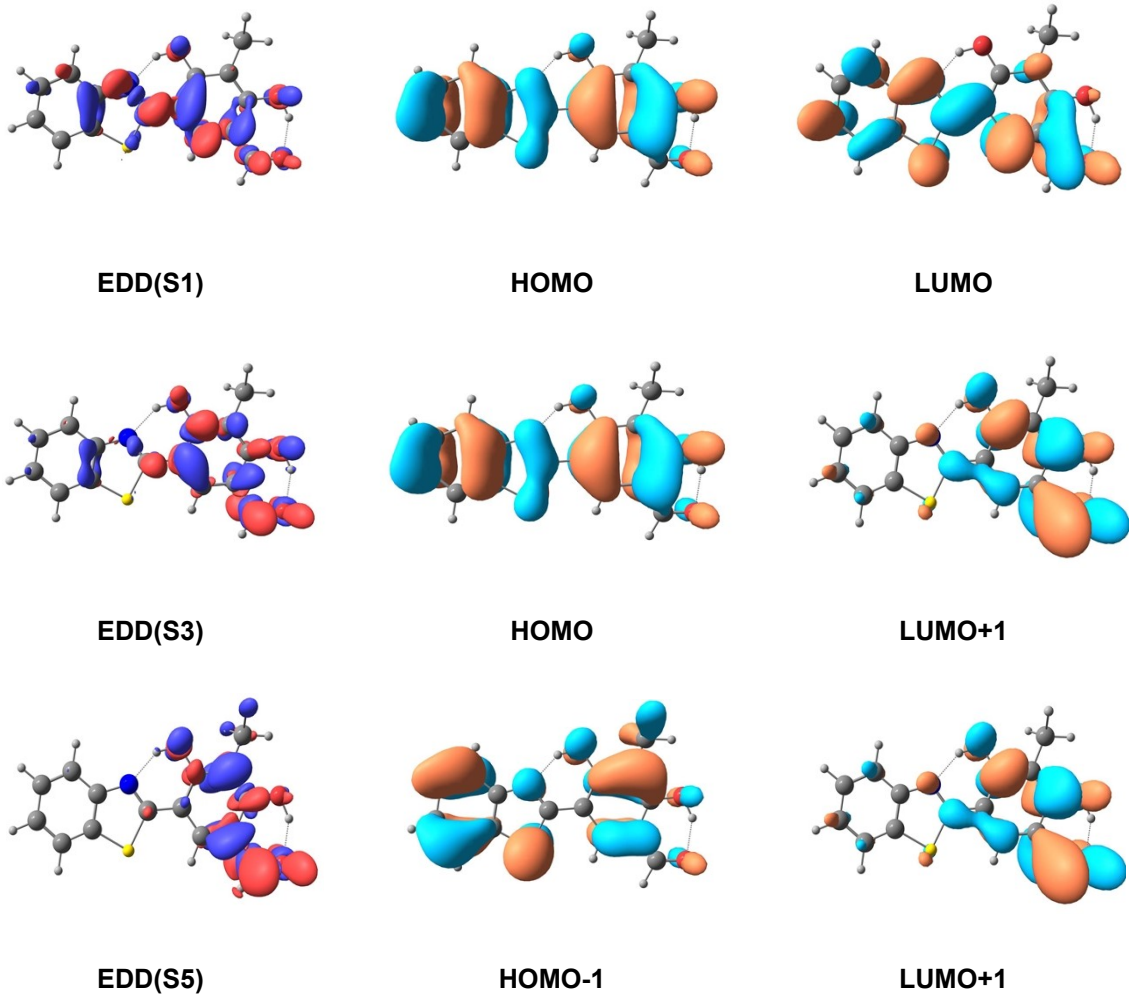

Figure S 45. Electronic density differences (EDD) and corresponding key orbital representations of **1a•2H**.

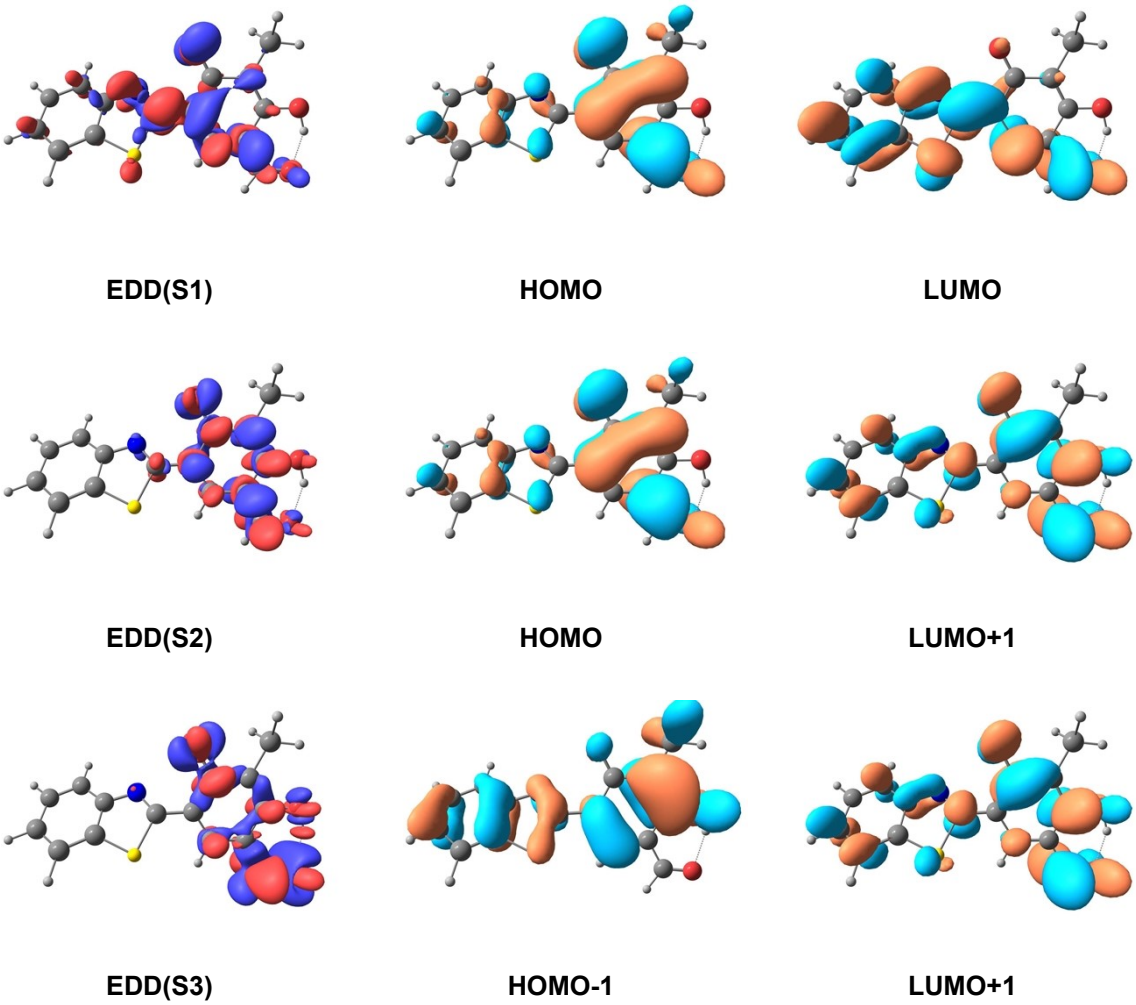

Figure S 59. Electronic density differences (EDD) and corresponding key orbital representations of **1a^{-}•H** (isomer b).

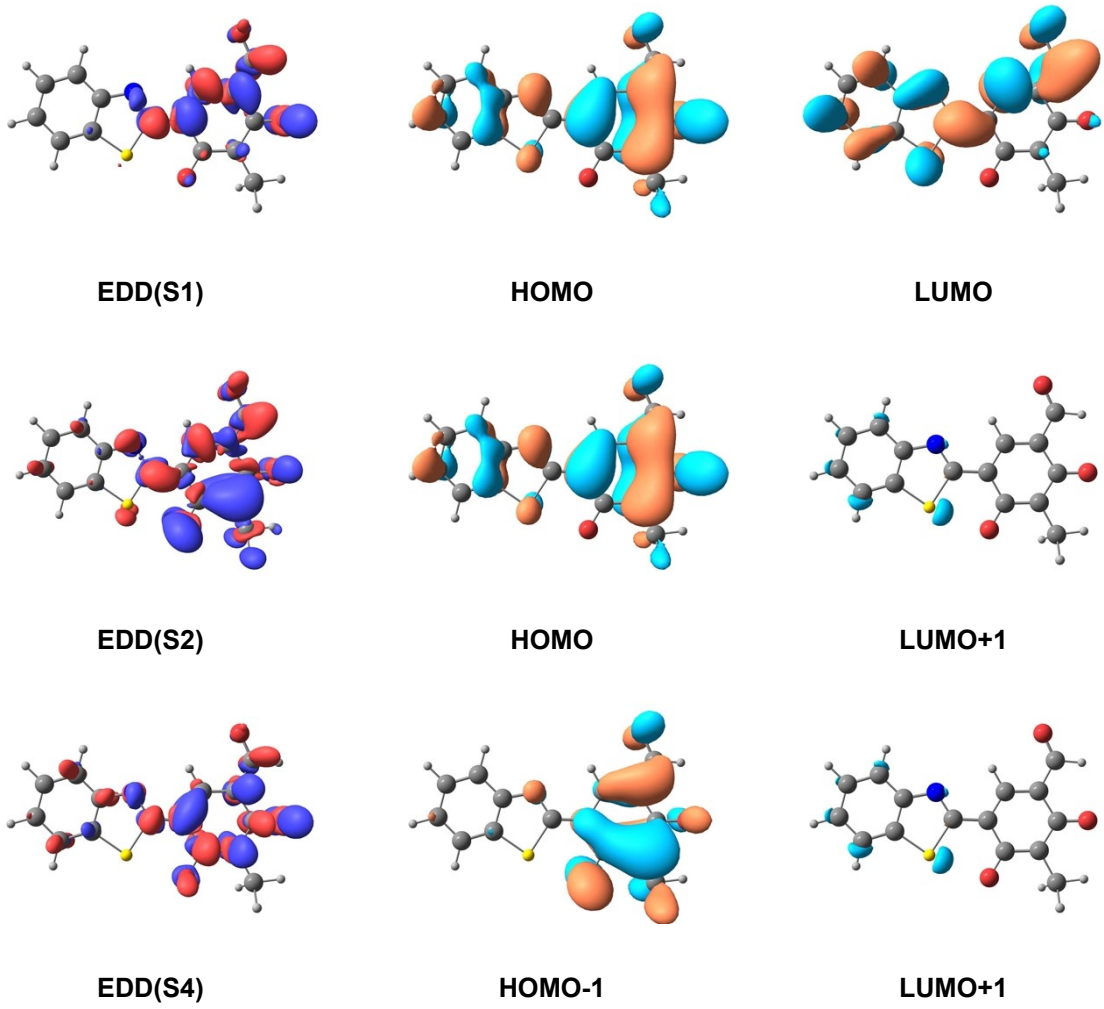

Figure S 60. Electronic density differences (EDD) and corresponding key orbital representations of **1a**$^{2-}$.

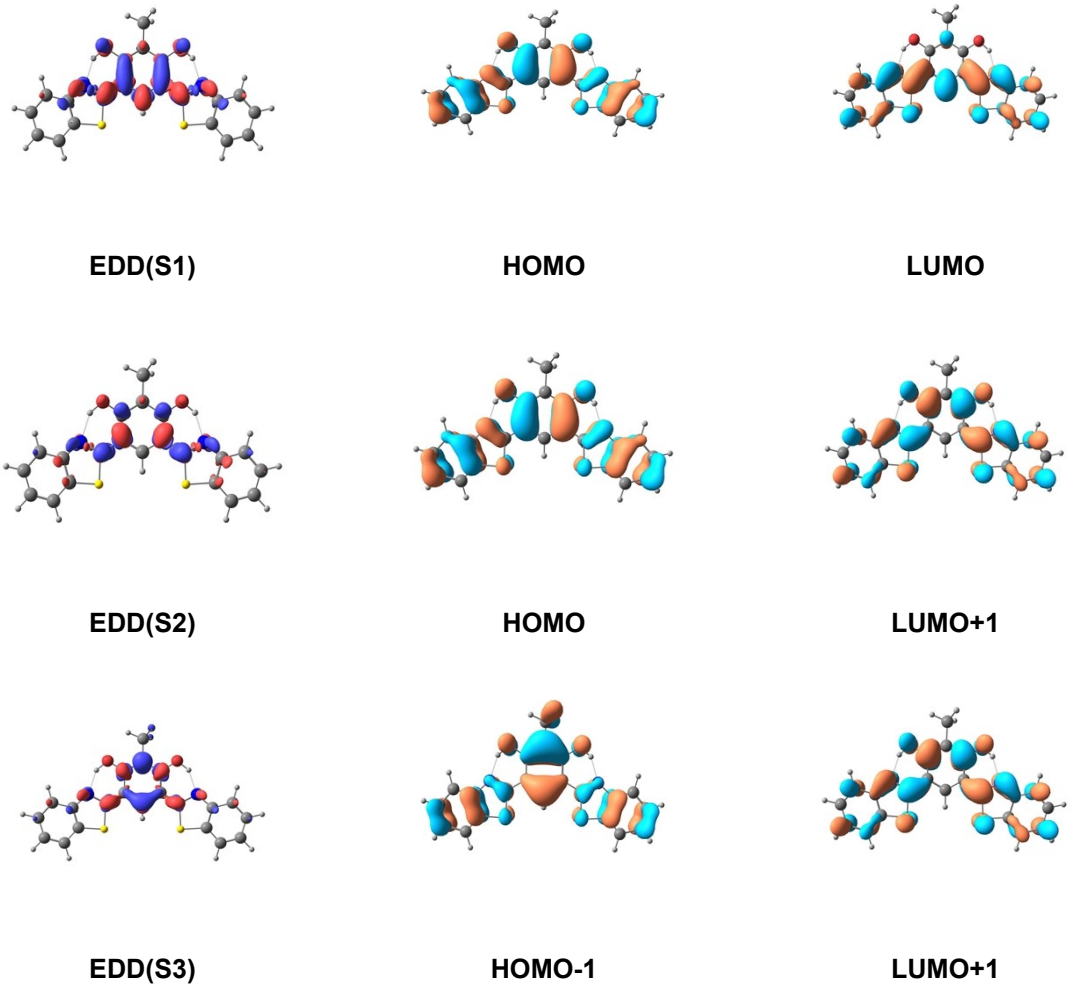

Figure S 61. Electronic density differences (EDD) and corresponding key orbital representations of **1b•2H**.

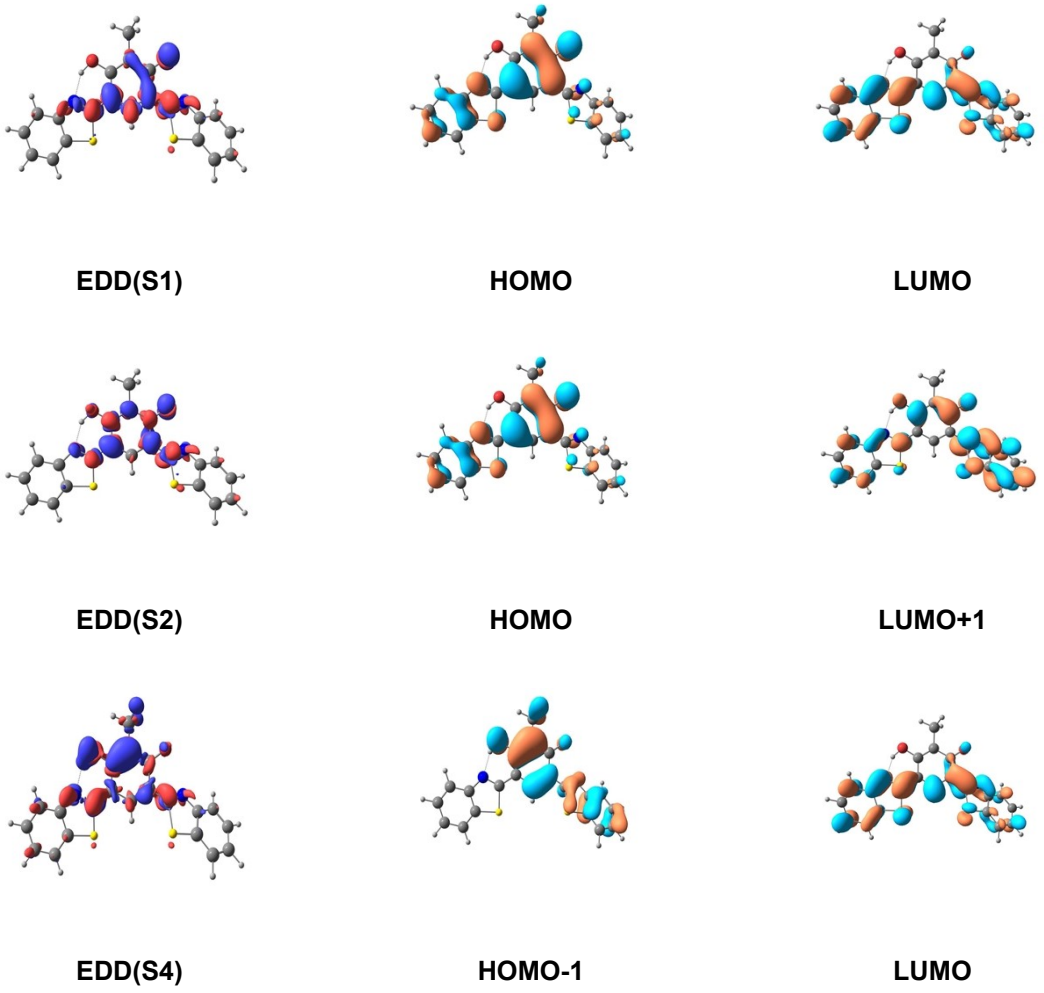

Figure S 49. Electronic density differences (EDD) and corresponding key orbital representations of **1b^{-}•H**.

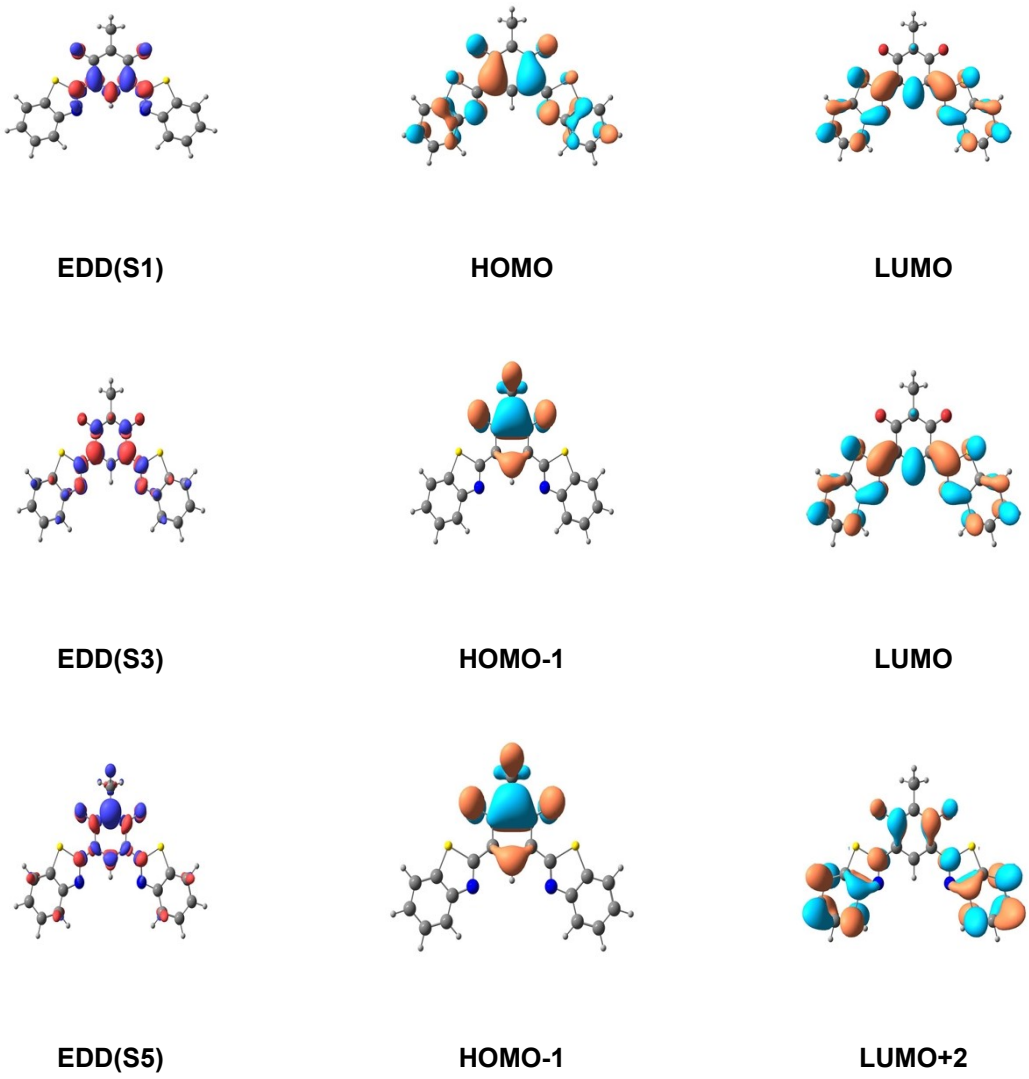

Figure S 50. Electronic density differences (EDD) and corresponding key orbital representations of **1b**$^{2-}$.

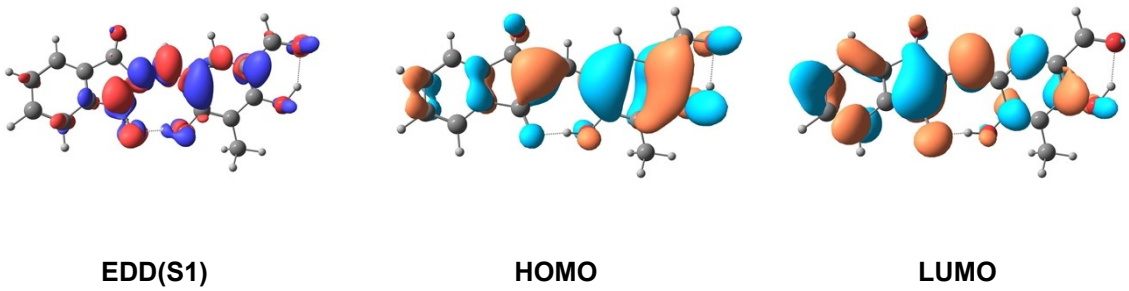

Figure S 51. Electronic density differences (EDD) and corresponding key orbital representations of **2a•2H**.

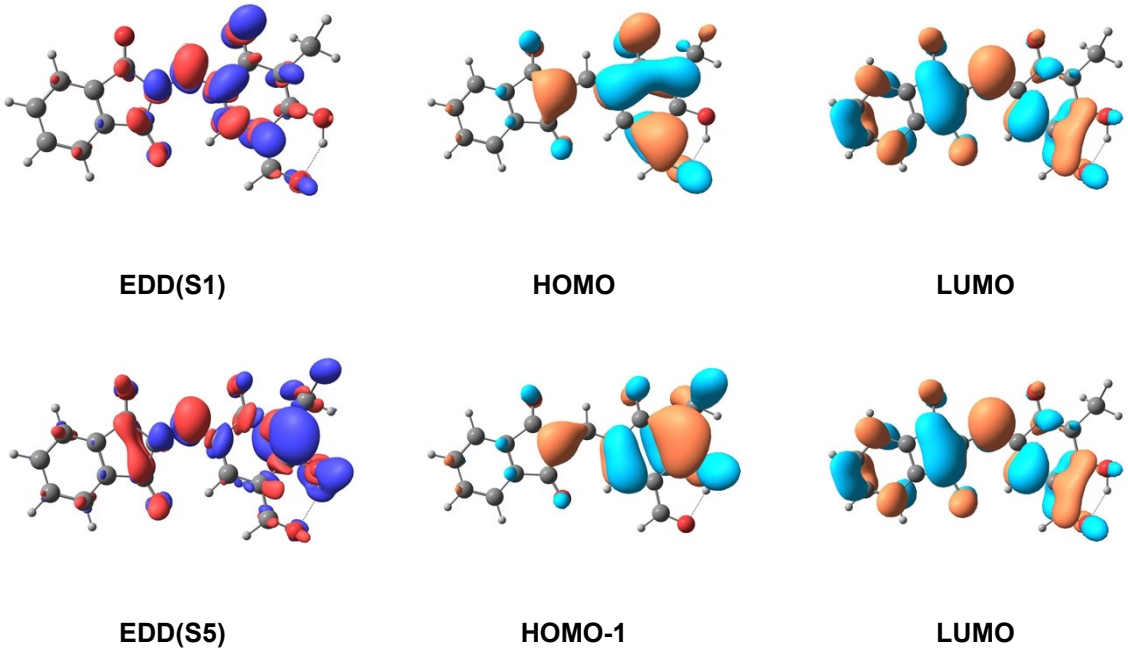

Figure S 52. Electronic density differences (EDD) and corresponding key orbital representations of **2a^{-}•H**.

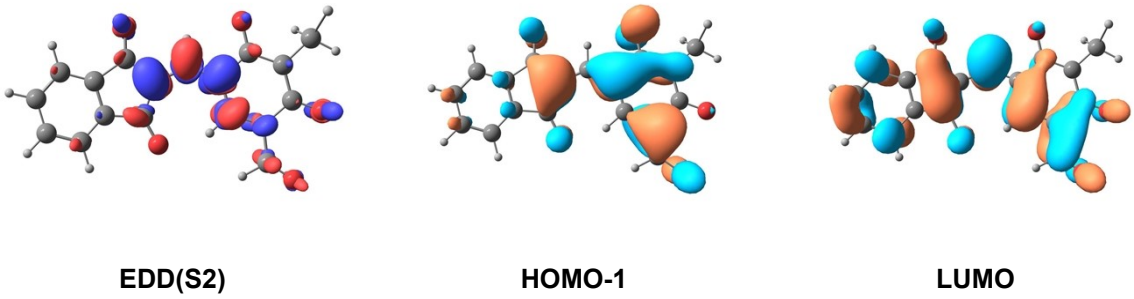

Figure S 53. Electronic density differences (EDD) and corresponding key orbital representations of **2a^{2-}**.

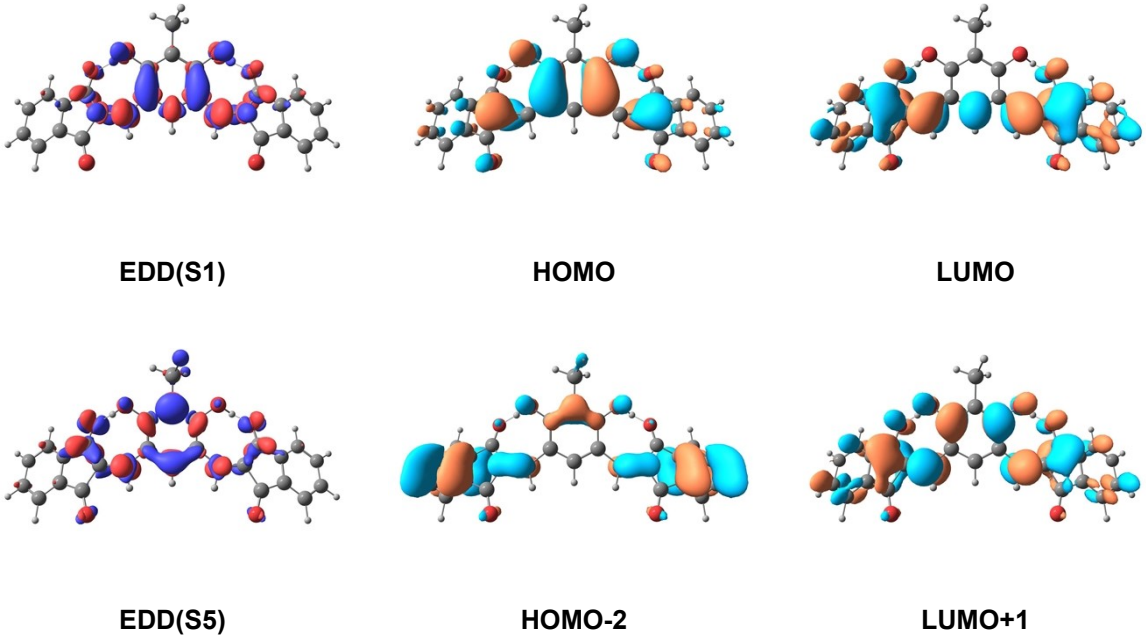

Figure S 54. Electronic density differences (EDD) and corresponding key orbital representations of **2b•2H**.

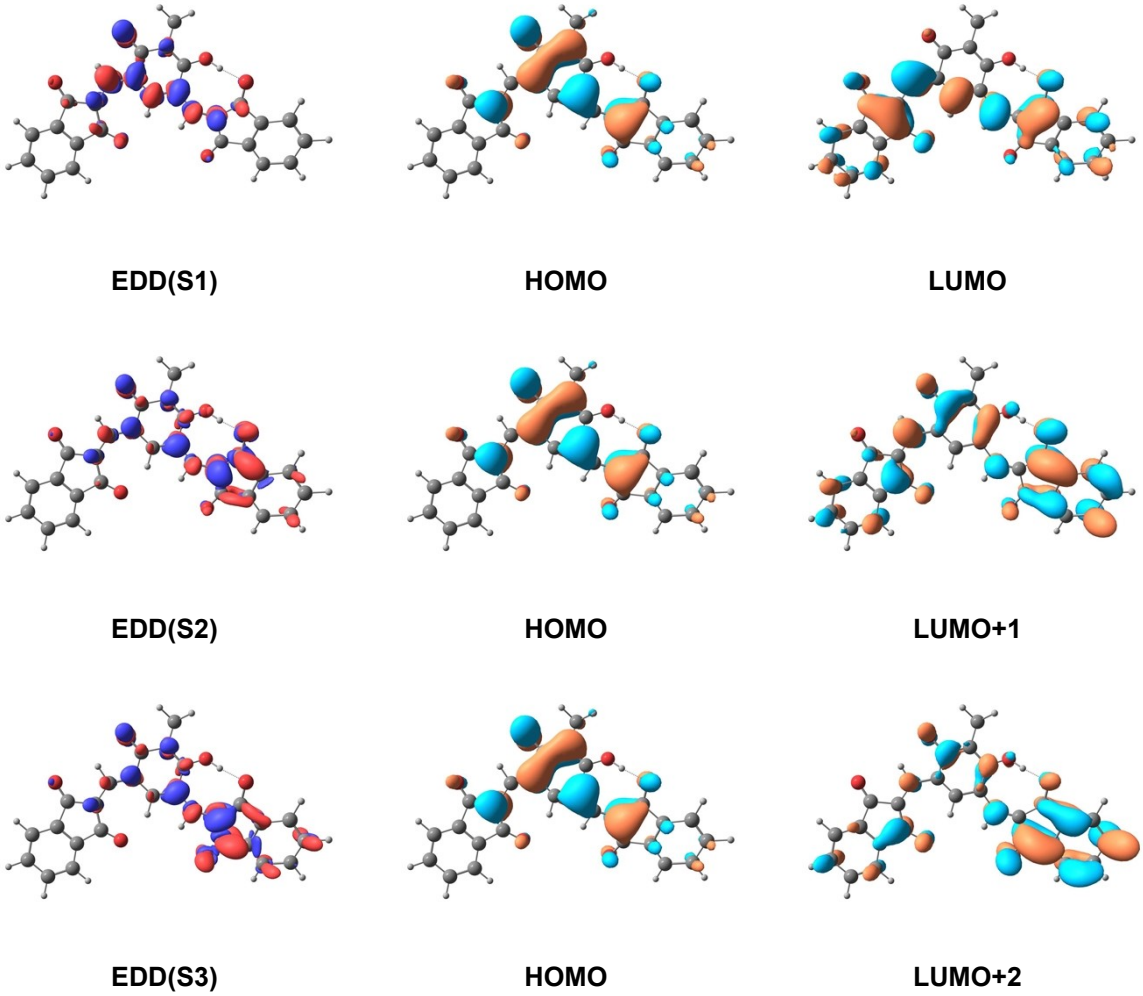

Figure S 62. Electronic density differences (EDD) and corresponding key orbital representations of **2b^{-}•H**.

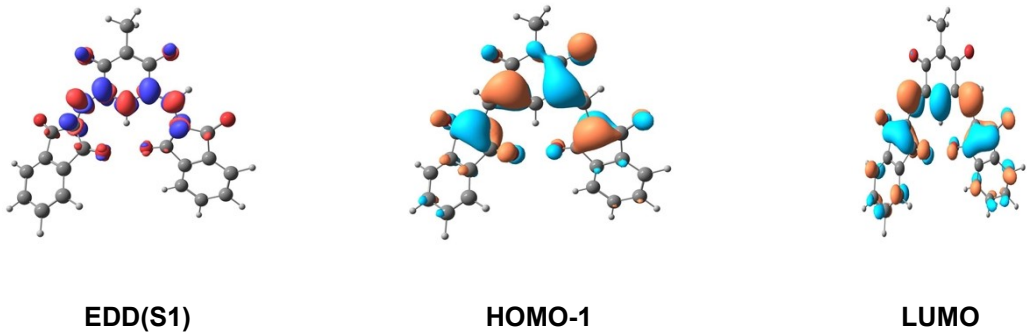

EDD(S1) **HOMO-1** **LUMO**

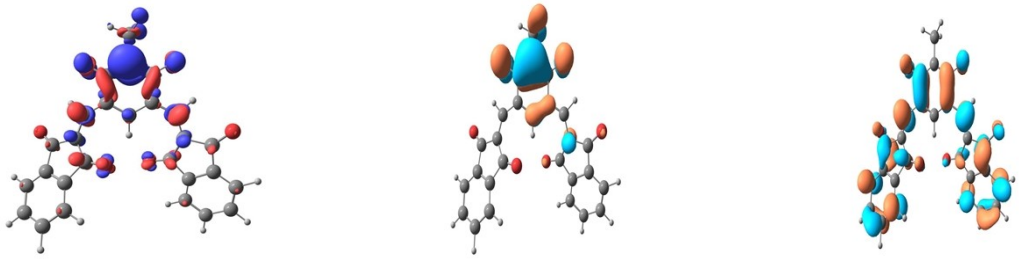

EDD(S5) **HOMO** **LUMO+3**

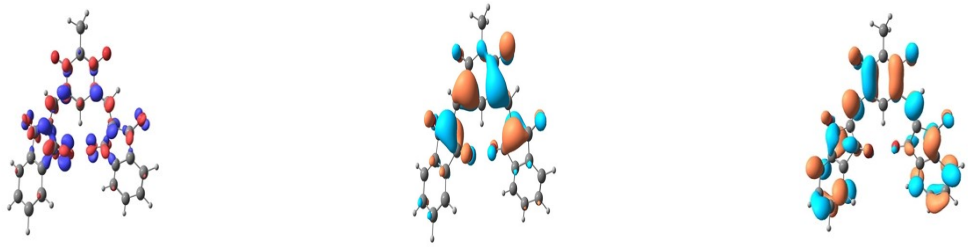

EDD(S8) **HOMO-1** **LUMO+3**

Figure S 63. Electronic density differences (EDD) and corresponding key orbital representations of **2b**$^{2-}$.

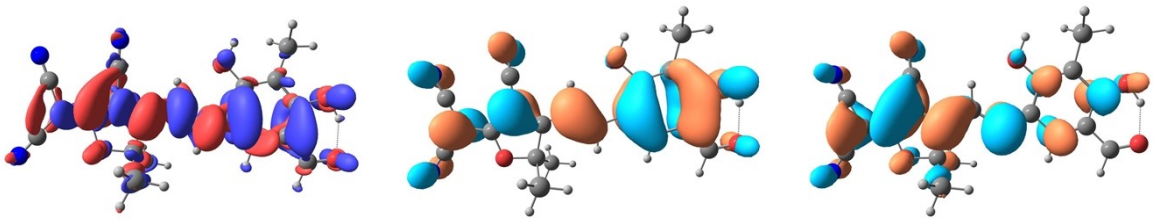

EDD(S1) **HOMO** **LUMO**

Figure S 64. Electronic density differences (EDD) and corresponding key orbital representations of **3a•2H** (isomer a).

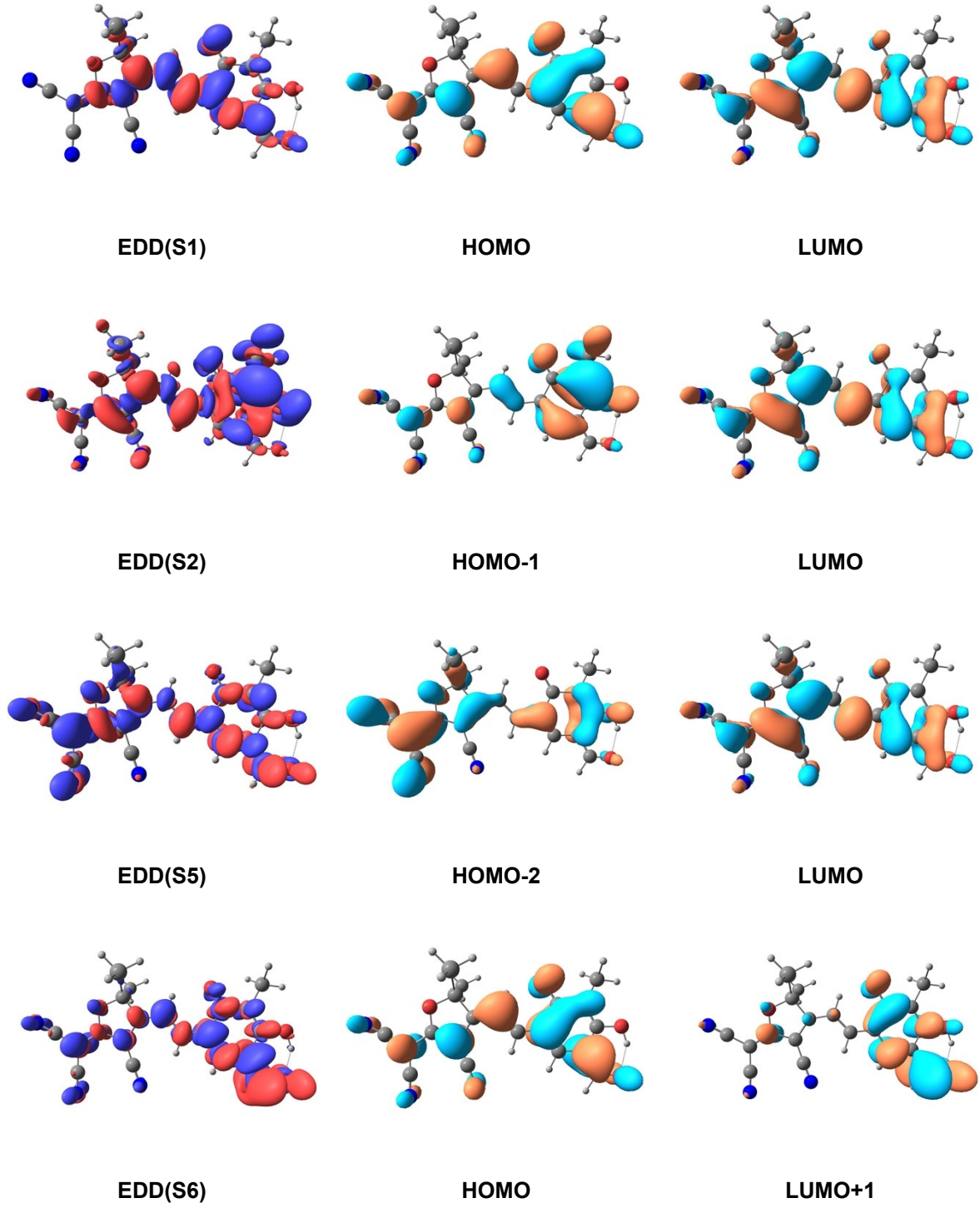

Figure S 65. Electronic density differences (EDD) and corresponding key orbital representations of **3a^{-}•H** (isomer c).

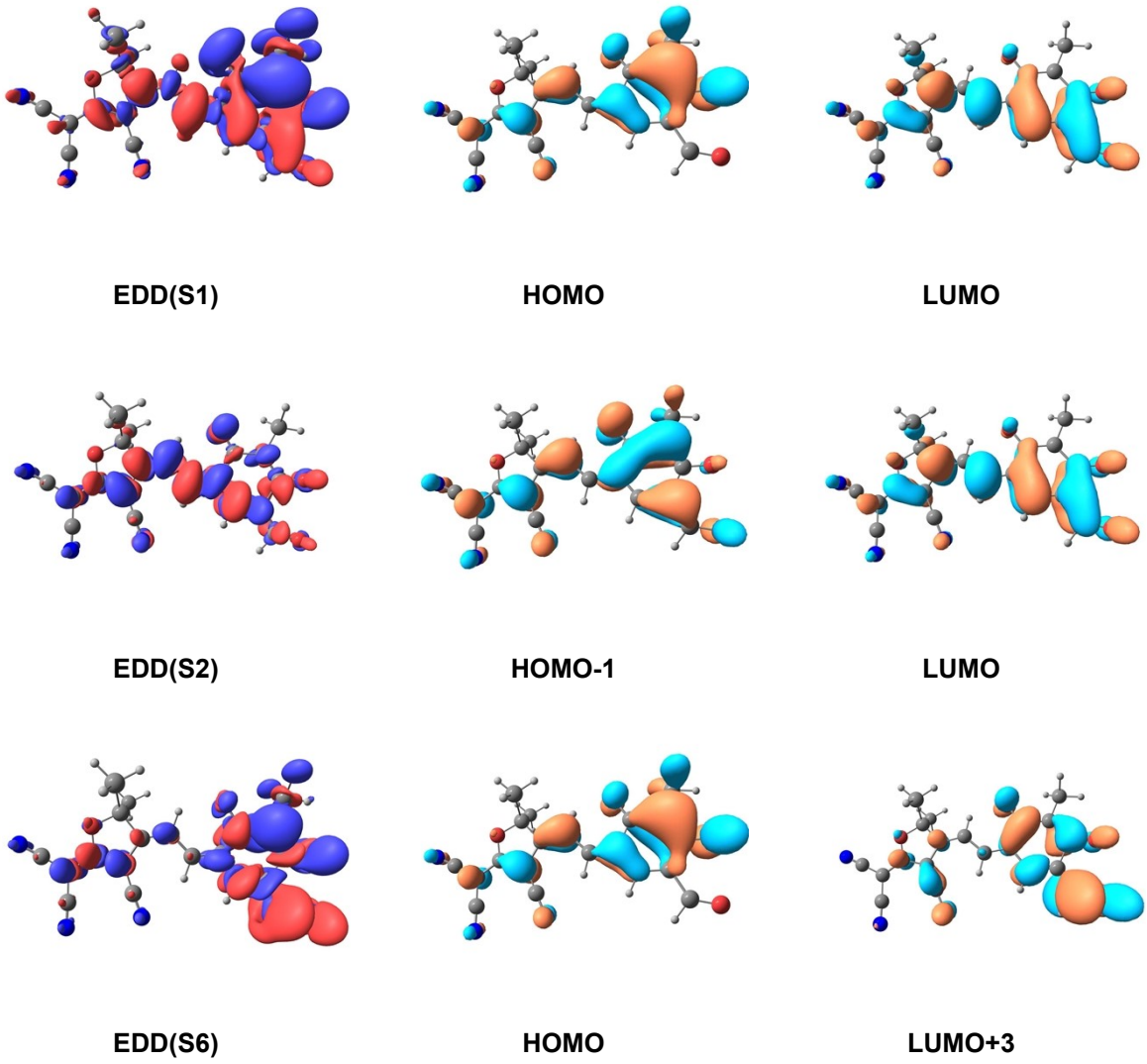

Figure S 66. Electronic density differences (EDD) and corresponding key orbital representations of **3a**$^{2-}$ (isomer c).

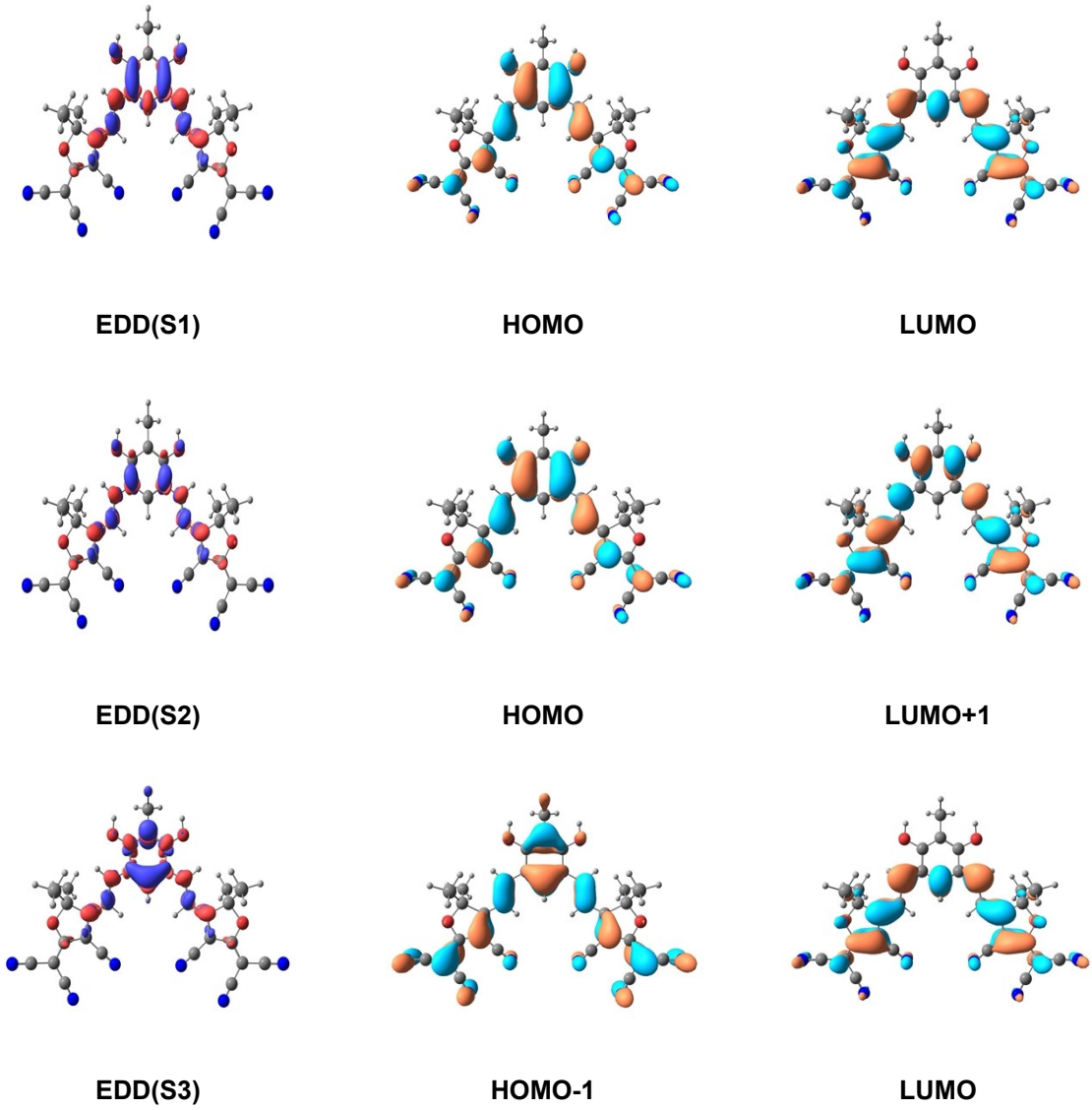

Figure S 67. Electronic density differences (EDD) and corresponding key orbital representations of **3b•2H** (isomer h).

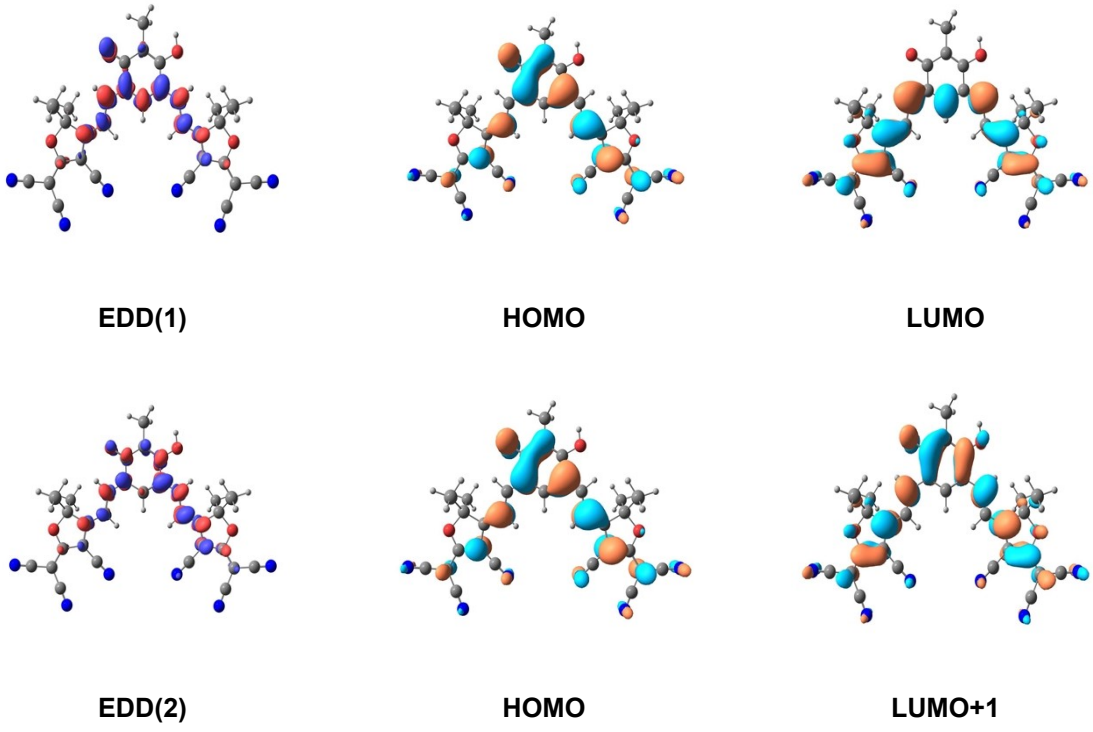

Figure S 68. Electronic density differences (EDD) and corresponding key orbital representations of **3b^{-}•H**.

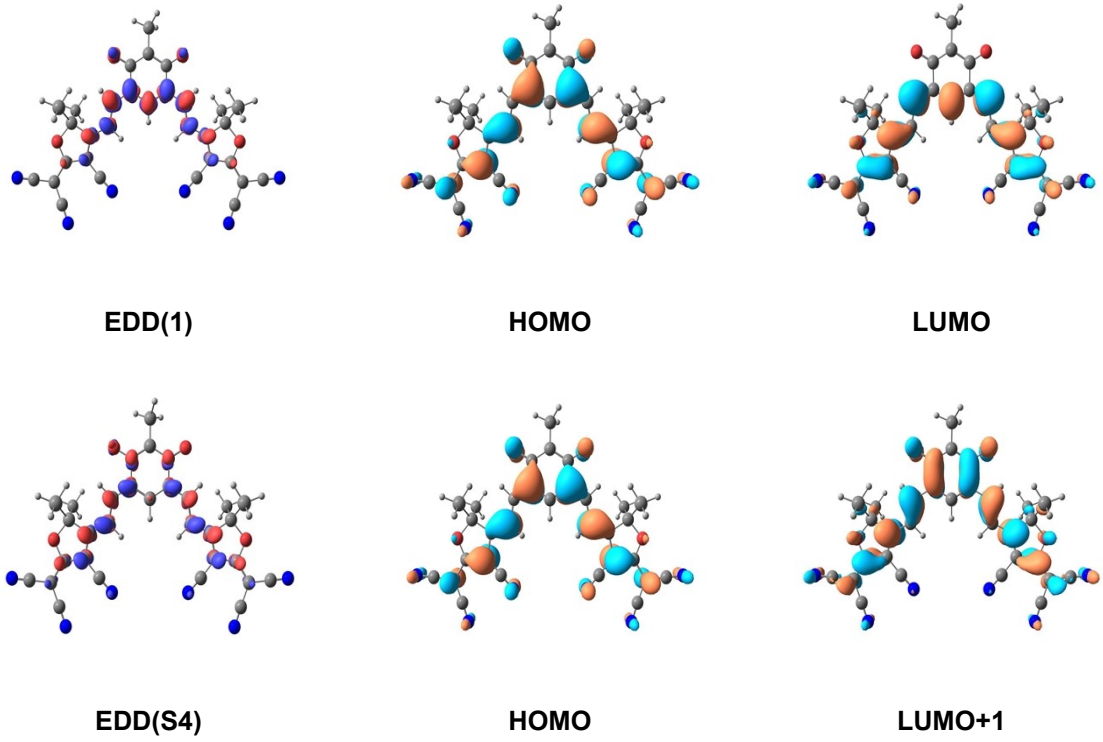

Figure S 69. Electronic density differences (EDD) and corresponding key orbital representations of **3b^{2-}**.

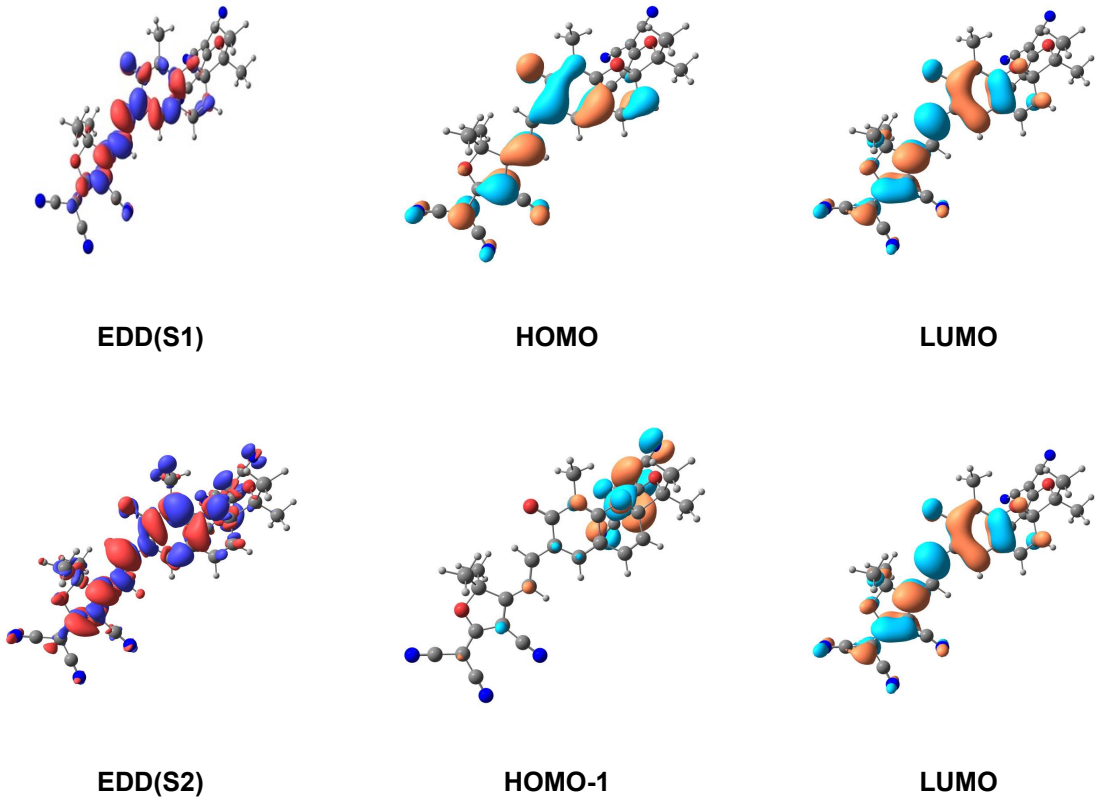

Figure S 70. Electronic density differences (EDD) and corresponding key orbital representations of **sp-3b**$^{2-}$.

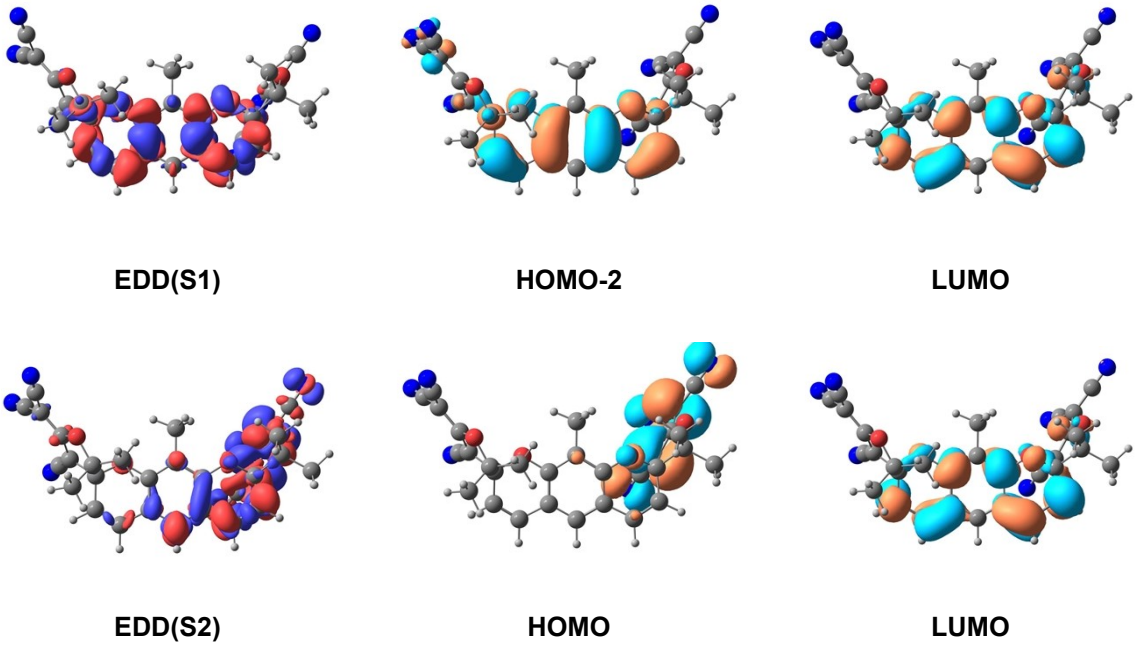

Figure S 71. Electronic density differences (EDD) and corresponding key orbital representations of **dsp-3b**$^{2-}$.

VIII. REFERENCES

1 B. Mourot, V. Mazan, M. Elhabiri, R. Sarkar, D. Jacquemin, O. Siri and S. Pascal, *Chem. Sci.*, 2024, **15**, 1248–1259.

2 A. M. Brouwer, *Pure Appl Chem*, 2011, **83**, 2213–2228.

3 M. J. Frisch et al., Gaussian 16A.03, Gaussian Inc., Wallingford, USA, 2016.

4 Y. Zhao and D. Truhlar, *Theor. Chem. Acc.*, 2008, **120**, 215–241.

5 J. Tomasi, B. Mennucci and R. Cammi, *Chem. Rev.*, 2005, **105**, 2999–3094.

6 C. A. Guido, A. Chrayteh, G. Scalmani, B. Mennucci and D. Jacquemin, *J. Chem. Theory Comput.*, 2021, **17**, 5155–5164.

7 Chemcraft - graphical software for visualization of quantum chemistry computations (version 1.8) https://www.chemcraftprog.com.

8 O. Christiansen, H. Koch and P. Jørgensen, *Chem. Phys. Lett.*, 1995, **243**, 409–418.

9 C. Hättig and F. Weigend, *J. Chem. Phys.*, 2000, **113**, 5154–5161.

10 TURBOMOLE, V7.4.1 2019, a Development of University of Karlsruhe and Forschungszentrum Karlsruhe GmbH, 1989−2007, TURBOMOLE GmbH, since 2007. http://www.turbomole.com.

11 P. von R. Schleyer, C. Maerker, A. Dransfeld, H. Jiao and N. J. R. van Eikema Hommes, *J. Am. Chem. Soc.*, 1996, **118**, 6317–6318.

12 Z. Chen, C. S. Wannere, C. Corminboeuf, R. Puchta and P. von R. Schleyer, *Chem. Rev.*, 2005, **105**, 3842–3888.

13 F. Santoro and J. Cerezo, FCclasses3 (version 1.0 (v3-0.1-177-g4b1514a)) http://www.iccom.cnr.it/en/fcclasses/ 2021.

14 F. J. Avila Ferrer, J. Cerezo, J. Soto, R. Improta and F. Santoro, *Comput. Theor. Chem.*, 2014, **1040–1041**, 328–337.

15 T. Zhang, K. Peng Guo, L. Qiu and Y. Shen, *Synth. Commun.*, 2006, **36**, 1367–1372.